

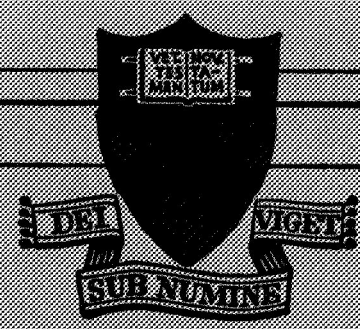
~~PR 10002~~
NASA CR-117040

Prepared for
National Aeronautics
and Space Administration

THE CATHODE REGION OF A QUASI-STEADY
MAGNETOPLASMA DYNAMIC ARCJET

P. J. Turchi
and
R. G. Jahn

Report 940*



PRINCETON UNIVERSITY
DEPARTMENT OF
AEROSPACE AND MECHANICAL SCIENCES

NASA Research Grant NGL 31-001-005
(Supplement No. 8)

Prepared for
National Aeronautics
and Space Administration

THE CATHODE REGION OF A QUASI-STEADY
MAGNETOPLASMA DYNAMIC ARCJET

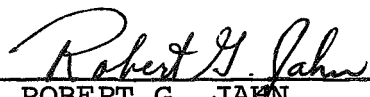
P. J. Turchi
and
R. G. Jahn

Report 940*

Prepared by


PETER J. TURCHI

Approved by


ROBERT G. JAHN
Professor of Aerospace Sciences
and Research Leader

*This report is a reproduction in entirety of the Ph.D. dissertation (AMS 940 T) of Mr. Peter J. Turchi. It is submitted to the sponsor and to the distribution list in this form both as a presentation of the technical material, and as an indication of the academic program supported by this Grant.

Reproduction, translation, publication, use and disposal in whole, or in part, by or for the United States Government is permitted.

October 1970

School of Engineering and Applied Science
Department of Aerospace and Mechanical Sciences
Guggenheim Aerospace Propulsion Laboratories
PRINCETON UNIVERSITY
Princeton, NJ 08540

ABSTRACT

A magnetoplasmadynamic discharge is examined near the cathode of a 2.5 MW, quasi-steady, self-field arcjet. High speed photography shows a concentration of arc luminosity in the cathode region, while detailed measurements with electric and magnetic field probes indicate that 85% of the total arc power is deposited within one base diameter of the cathode surface. Ion energies are shown to be proportional to the voltage drop in the cathode region even though current conduction is accomplished primarily by electrons in a tensor manner. It is found that a high speed plasma flow is delivered to the cathode where it is converted into a useful exhaust jet in a thin, high density layer at the cathode surface. Local measurements of electron temperature and estimates of electron density, made within the discharge and exhaust jet using a twin Langmuir probe technique, indicate a nearly uniform electron temperature of about 1.5 eV throughout the quasi-steady arcjet flow. Theoretical considerations of current conduction and plasma acceleration processes near the cathode are correlated with the experimental evidence and lead to relationships among overall arcjet properties. In particular, ion kinetic energies in the exhaust jet should be comparable to the arc voltage, exhaust velocity and arc impedance should be proportional, and the influence of insulator ablation should become important when the input mass flow is fully ionized by the arc.

CONTENTS

	<u>Page</u>
Title Page	i
Abstract	ii
Contents	iii
List of Illustrations.	v
Nomenclature	vi
Chapter	
1	INTRODUCTION 1
	Nature of the Problem. 1
	Approach to the Problem. 2
	The Cathode Region 3
	Subdivisions of the Cathode Region 3
	Organization of the Thesis 5
2	THE EXPERIMENTAL ATTACK. 6
	The Experimental Facility. 6
	The Experimental Program 7
	Photography. 7
	Surface Phenomena. 13
	Magnetic Field Distribution. 17
	Voltage Distribution 20
	Langmuir Probing 22
3	THE CATHODE PLASMA 36
	Ionization Level 36
	Debye Length 41
	Electrical Conductivity. 43
	Electron-Ion Collision Frequency 44
	Equilibration Times. 45
	Distribution of Resistive Heating. 47
	Heavy-Particle Interactions. 49
	Magnetic Interactions. 51
	Summary. 54
4	DISCHARGE STRUCTURE. 56
	Voltage Distribution 56
	Overall Discharge Structure. 58
	Current Conduction 61
	The Electric Field 63
	Electron Motion. 64
	Ion Motion 65
	The Cathode Plasma Revisited 70
	Electron Pressure Gradients. 72
	Summary. 73

CONTENTS

		<u>Page</u>
Chapter 5	THE CATHODE SURFACE LAYER	75
	Nature of the Flow Problem.	75
	MGD Analysis Including Pressure Gradients	77
	Approximate Equations for the Surface Layer Flow.	78
	Solution of the Cathode Surface Layer Flow.	81
	Boundary Layer Considerations	84
	Discussion of the Cathode Tip and Jet	85
	Model for the Emission Layer.	88
	EXPERIMENTAL CONCLUSIONS.	103
6	FUNDAMENTALS OF MPD DISCHARGE STRUCTURE	107
	Origin of the Conduction Pattern.	107
	Faraday's Law for an MPD Discharge.	107
	Magnetic Reynolds Number Based on u_e	112
	Solution of the Current Pattern	113
	Meaning of R_{me}	116
	Distortion of the Current Pattern by Plasma Convection.	118
	Interaction of the Plasma Flow with the Current Pattern.	119
	Physical Hierarchy of an MPD Discharge.	120
7	GENERAL CONSIDERATIONS.	124
	Voltage-Current Relation in a Self-Field Plasma Thruster	124
	Heavy-Particle Kinetic Energy	126
	MPD Arcjet Exhaust Velocity	128
	Electromagnetic Thrust Efficiency of a Self-Field MPD Arcjet.	129
	\bar{R}_m Revisited.	130
	Electrothermal Contributions to MPD Arcjet Performance	133
	Losses at the Cathode	134
	Review and Concluding Discussion.	136
	REFERENCES.	142

LIST OF ILLUSTRATIONS

<u>Figure</u>		<u>Page</u>
1-1	Delineations of the cathode region	4
2-1	Accelerator schematic.	8
2-2	17.5 kA current pulse on two different time scales	9
2-3	Color photographs of arc	11,12
2-4	Photographs of tungsten cathode.	15
2-5	Magnified view of cathode tip.	16
2-6	Field probe data records	18
2-7	Enclosed current contours; $t = 100 \mu\text{sec}$	19
2-8	Floating potential probes.	21
2-9	Constant floating potential contours, $t = 100 \mu\text{sec}$	23
2-10	Langmuir probe circuits.	25
2-11	Langmuir probe data records.	26
2-12	Langmuir probe characteristic at $Z = 30 \text{ cm}$, $r = 0$.	27
2-13	Langmuir probe electron current variation with probe voltage	29
2-14	Computed kT_e <u>vs.</u> highest current to probe.	31
2-15	kT_e during quasi-steady operation.	33
2-16	Electron temperatures and densities from twin probe data	34
3-1	Characteristics of the cathode plasma.	42
4-1	Plasma potential <u>vs.</u> radial position	57
4-2	Current streamlines and equipotentials	59
4-3	Conductivities and electron densities computed from field data	69
4-4	Ion flow in cathode region	71
5-1	Details of cathode surface layer	76
5-2	Cathode surface layer flow	82
5-3	Comparisons with hypersonic near wake flows.	86
5-4	Schematic of emission layer model.	91
5-5	Cathode surface temperature <u>vs.</u> electron temperature.	97
5-6	Current conduction and power deposition in the emission layer.	99
7-1	Current patterns in self-field plasma thrusters. .	132

NOMENCLATURE

\vec{B}	magnetic field strength [W/m^2]
\vec{E}	electric field measured in the laboratory [V/m]
I	current to probe tip [A]
J	total arc current [A]
K	heat conductivity [$\text{W}/\text{m} \text{ } ^\circ\text{K}$]
L_a	distance for which $R_{me} = \sigma_{iu} L = 1$
M	Mach number
\vec{F}_{iA}	drag force between ions and atoms [Nt/m^3]
P	pressure [Nt/m^2]
Q	collision cross section [m^2]
Rey	Reynolds number (from fluid mechanics)
R_m	magnetic Reynolds number
T_H	temperature of heavy particles [$^\circ\text{K}$]
V	voltage [V]
Z	partition function (Chap. 3); impedance (Chap. 7)
a	speed of sound [m/sec]
h	thickness of cathode surface layer [m]
h	enthalpy [m^2/sec^2]
\vec{j}	current density [A/m^2]
k	Boltzmann's constant = $1.38 \times 10^{-23} \text{ J}/^\circ\text{K}$
m	particle mass [kg]
n	particle density [$/\text{m}^3$]
q	heat or energy flux [W/m^2]
r	radial position
\dot{s}	entropy production rate (per unit area) [$\text{W}/\text{m}^2/^\circ\text{K}$]
t_{eq}	time for equipartition between ions and electrons
u	velocity [m/sec]; u_c plasma speed normal to cathode from convective zone
v_{th}	thermal speed $(8kT/\pi m)^{1/2}$
z	axial position

NOMENCLATURE

α	degree of ionization
γ	ratio of specific heats
δ	compressible boundary layer thickness
$\bar{\delta}$	incompressible boundary layer thickness
ϵ_i	ionization potential [eV]
χ	thermal diffusivity [m^2/sec]
λ_{AB}^c	mean free path of particle A before encountering particle B and experiencing transfer or chemical event C
Λ	plasma parameter
ν	collision frequency
ν_μ	kinematic viscosity
ρ	mass density
$\sigma = 1/\eta$	electrical conductivity [mho/m] = [resistivity, ohm-m] $^{-1}$
ϕ_w	work function [eV]
Ω	Hall parameter

Subscripts

e	electron	;	H	heavy-particle
i	ion			
A	atom			
	parallel to current density \vec{j}			
⊥	perpendicular to \vec{j} ; parallel to $\vec{j} \times \vec{B}$			
W	wall conditions			

CHAPTER 1

INTRODUCTION

Our purpose here is to understand the physical processes involved near the cathode of a magnetoplasmadynamic arcjet. Interest in such processes derives from a desire to achieve logical guidelines for the design of an optimum electric thruster of this type for space applications. We shall be particularly concerned with the mechanics of current conduction and plasma acceleration in the vicinity of the cathode, and the transfer of electrical energy to the plasma in this region.

Nature of the Problem

A magnetoplasmadynamic arcjet involves, as its name implies, the production of a directed plasma flow by an arc discharge in a magnetic field. The history, development, and characteristics of such devices has been the subject of extensive review by several authors.¹⁻⁵ Briefly, this type of plasma accelerator is distinguished from the thermal arcjets or plasma-jets, that preceded it, by higher current and lower particle density operation and by significantly improved performance. The association of these characteristics suggests that some more efficient electromagnetic interactions become important at high-current, low-density conditions, although the MPD arc may still reflect its electrothermal ancestry and should thus be considered a hybrid form of electric thruster.

As such, the details of its operation can be quite complex. The thermal arcjet itself is difficult to describe because of the vigorous energy transport processes associated with

an arc discharge. To this, we now add the complications of an electromagnetic body force distribution which depends on the velocity and conductivity of the ionized gas, and we also include the possibility of noncontinuum flow conditions. On one hand, we have the two-dimensional acceleration of a non-equilibrium, ionized gas. On the other, we must deal with the nonlinear mechanics of charged particles in the electric and magnetic fields of the discharge. These extreme points of view have taken the form of simplified models for MPD arcjet operation. In the latter case, for example, electrostatic acceleration of ions provides the basis for both current conduction and plasma acceleration, while the self-magnetic field acts to deflect the ions downstream, thereby protecting the cathode surface from excessive bombardment.^{6,7} In the former case, the current conduction mechanism is not specified and pressure gradients are invoked to obtain axial thrust from the radial component of the $\vec{j} \times \vec{B}$ force in the discharge.⁴

Approach to the Problem

To understand the interplay of the various physical processes involved, we may follow two approaches. The arc could be operated over a range of externally controlled conditions, such as total current and input mass flow rate. Measurements of other arcjet properties such as thrust, exhaust velocity, and total arc voltage could then be used to deduce the mechanics of plasma acceleration and current conduction. The results of such endeavors are discussed in the previously cited review articles. The other approach is to analyze a particular typical arcjet operation in detail, directly obtaining the structure of the discharge flow by measurement within the arc chamber of the current density distribution, electric and magnetic field distributions and electron densities and temperatures. Understanding of the interrelationships between these quantities and their connection to overall arcjet parameters may then be generalized to other operating conditions. This is the approach we shall follow here.

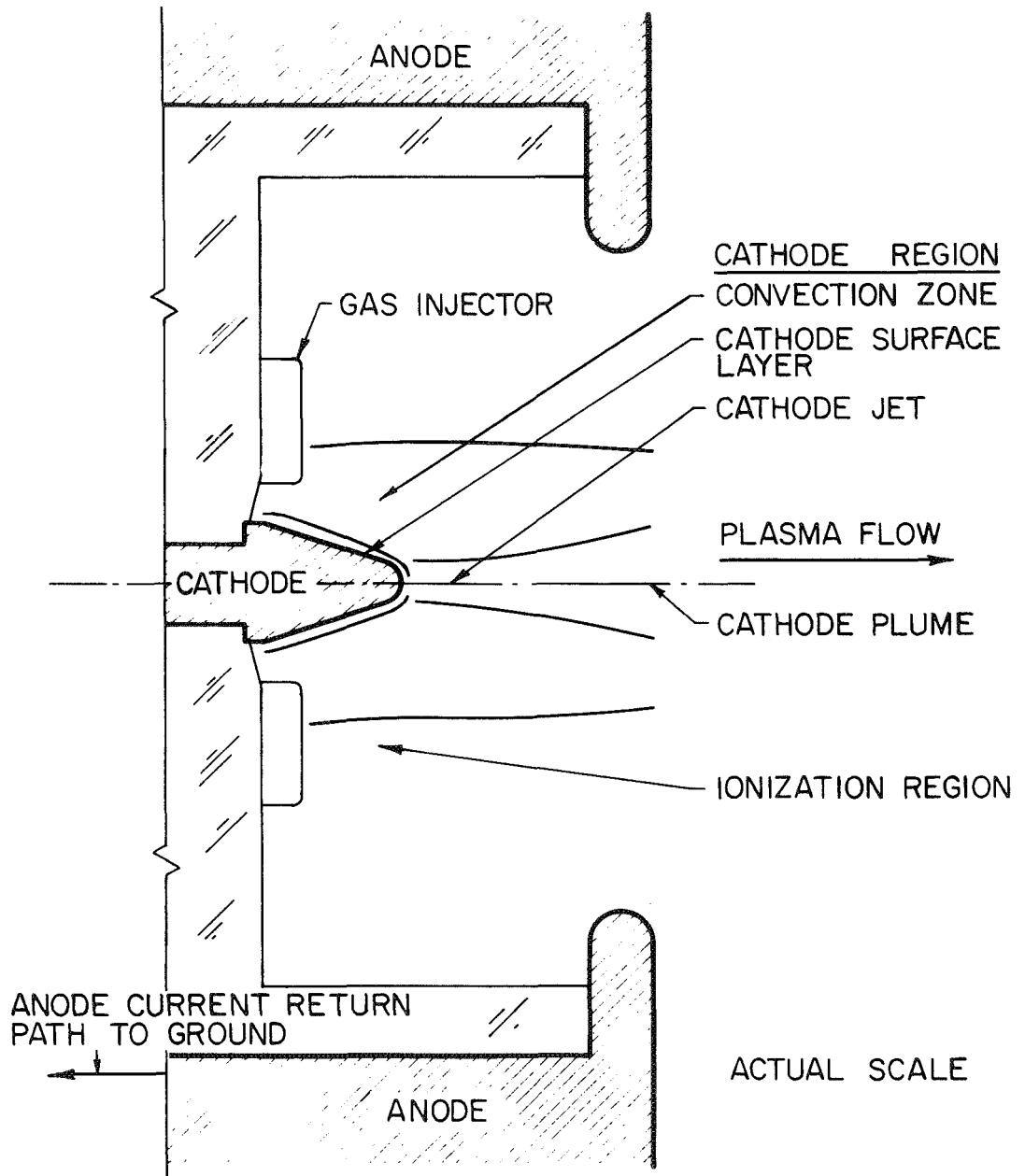
The Cathode Region

In a coaxial geometry, the current density and magnetic field strength are both greatest near the central electrode. The electromagnetic interactions with the plasma flow will therefore be most intense in this region, both from the standpoint of the $\vec{j} \times \vec{B}$ force exerted in the gas, and in terms of ion and electron Hall parameters. In addition, higher current densities suggest that ohmic heating (ηj^2) may be greatest in this region (depending of course on the variation of gas conductivity). Thus, since the cathode is normally the central electrode in an arcjet, we have chosen to concentrate our efforts there so as to encounter fully the various processes characterizing an MPD arcjet. We shall therefore limit our concern to the discharge and plasma flow within one base diameter of the cathode surface. This is defined as the cathode region.

Subdivisions of the Cathode Region

To simplify a very complicated problem, we shall divide the cathode region into zones or layers in which either the situation is dominated by physical processes that can be described locally by our experimental evidence, or the geometry is such that a knowledge of overall properties is adequate to determine the characteristics of the discharge and plasma flow. We expect that the subdivisions shown in Fig. 1 are sufficient to delineate portions of the cathode region in which different physical phenomena are important.

In the convective zone, plasma particles are accelerated by electromagnetic forces to create a plasma flow near the cathode. It is in this region that particles are convected to the cathode surface layer where various interactions with the cathode surface are important. In this surface layer, we are concerned with the deflection of the plasma flow to the cathode, conduction across the cathode-plasma interface, and energy transfer and erosion by ion bombardment of the cathode. Just downstream of the cathode tip is the cathode jet which



DELINEATIONS OF THE CATHODE REGION

AP 25 R 4654 70

FIGURE 1-1.

receives the plasma flow both from the cathode surface layer and from the convective zone, and channels this flow into the arcjet exhaust. (Beyond the cathode region, the MPD discharge circuit is completed through a region of gas ionization, in which plasma acceleration may also occur.)

Organization of the Thesis

To aid the reader, we now indicate the order and purpose of the various sections of the thesis. Immediately following this introduction, the experimental program and its more direct results are described. In subsequent chapters (Chaps. 3, 4, and 5), the data are analyzed in detail to establish the nature of the working fluid, the current conduction and plasma acceleration processes in the convective zone, and the energy deposition and flow deflection in the cathode surface layer and jet. Following Chap. 5, the experimentally obtained physical picture of the cathode region in our quasi-steady MPD arcjet is reviewed.

The fundamental basis for the structure of an MPD discharge is delineated in Chap. 6. There, the interactions between the plasma flow and the current conduction pattern are considered and the relation of the arc voltage to the ion kinetic energy is discussed. In Chap. 7, we apply our understanding of the physical processes involved in the cathode region to MPD arcjet operation and performance.

CHAPTER 2

THE EXPERIMENTAL ATTACK

Experiments inside MPD arcjets have long been prohibited by the small volume of the arc chamber and the violence of arc operation. Understanding of MPD processes has thus been limited to inferences made from a knowledge of various terminal properties such as total voltage, current, thrust, etc.,¹⁻⁷ supplemented by optical measurements of arc luminosity distribution, and species existence and temperature.^{8,9} Our purpose here is to improve this situation by a series of detailed measurements within a high power, large radius, quasi-steady arcjet.

The Experimental Facility

By operating an arcjet with a short pulse of high current, we are able to avoid the experimental difficulties of poor, interior access and instant probe destruction. Higher currents allow us to scale the arc chamber dimensions to maintain the intensity of MPD operation in a larger volume. Thus, for a cylindrical system, a factor of 10 increase in current from 2000 A to 20,000 A permits a similar change in chamber diameter from 1 cm to 10 cm. At the same time, the short duration of the current pulse limits energy transfer to modest amounts even at the higher power levels involved, allowing small, uncooled probes to survive within the arc chamber. The design philosophy of the quasi-steady arcjet and details of the construction of the facility used here are discussed at length by Clark.⁵

Briefly, our apparatus consists of a 5-in. diam, 2-in. high chamber in which a diffuse arc forms between a conical

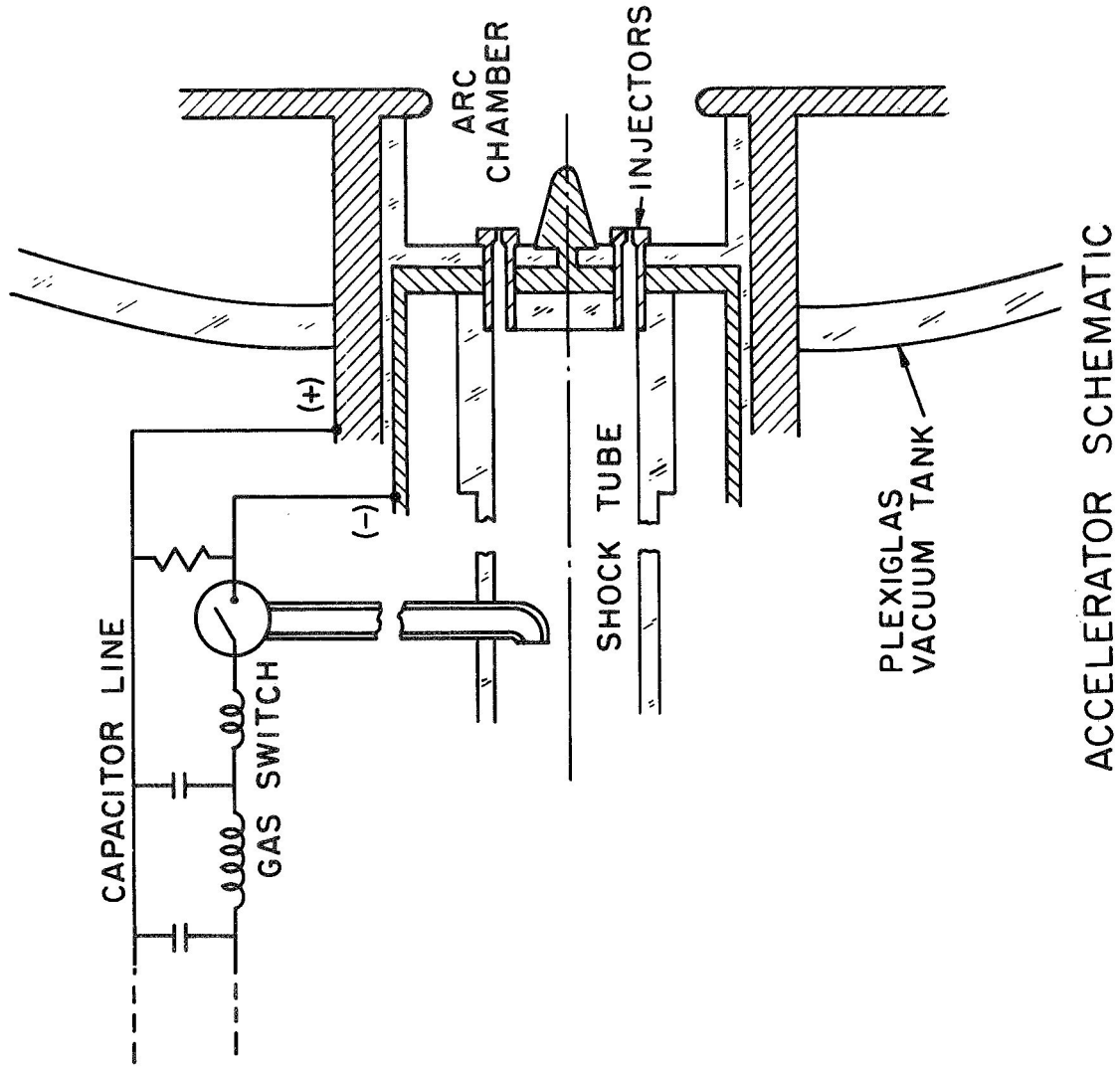
tungsten cathode and a coaxial aluminum anode (see Fig. 2-1). The arc operates in the experiments discussed here, at 17,500 A, with a constant argon mass inflow of 5.5 g/sec, and exhausts into a Plexiglas vacuum vessel maintained at 2×10^{-5} Torr, during the time of interest. Current is supplied by a capacitor bank arranged as an LC-ladder network to provide a flattopped current pulse for 165 μ sec. (See Fig. 2-2; subsequent discharges are due to the gross impedance mismatch between the network and discharge, and need not concern us). Argon flows into the arc chamber through six choked orifices from a high pressure reservoir created at the driven-section endwall of a vacuum shock tube. The current pulse is delivered to the chamber when the mass flow has attained a steady level. Some 30 μ sec after discharge initiation, total voltage, current, magnetic field distribution, and overall arc appearance achieve a steady state which is maintained until the current decreases at the end of the pulse. Recent experiments¹⁰ indicate that this situation is representative of quasi-steady operation with current pulses an order of magnitude longer in duration than that used here.

The Experimental Program

In attempting to mount a balanced attack on our problem, we utilize many techniques, but avoid pursuing any particular measurement beyond our limited knowledge of either the diagnostic situation or the relationship of the measured quantity to arc processes. Such an organic approach is quite appropriate in view of the profligate lack of simplicity involved in the experimental problem, since we cannot hope to obtain a completely unambiguous quantitative result from any of our diagnostic tools. We now describe the experiments and their more immediate results.

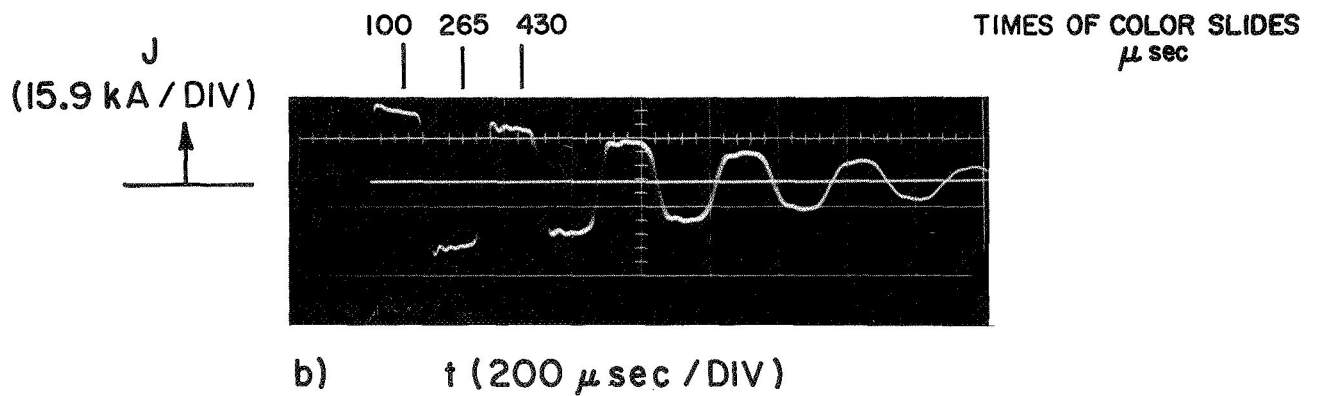
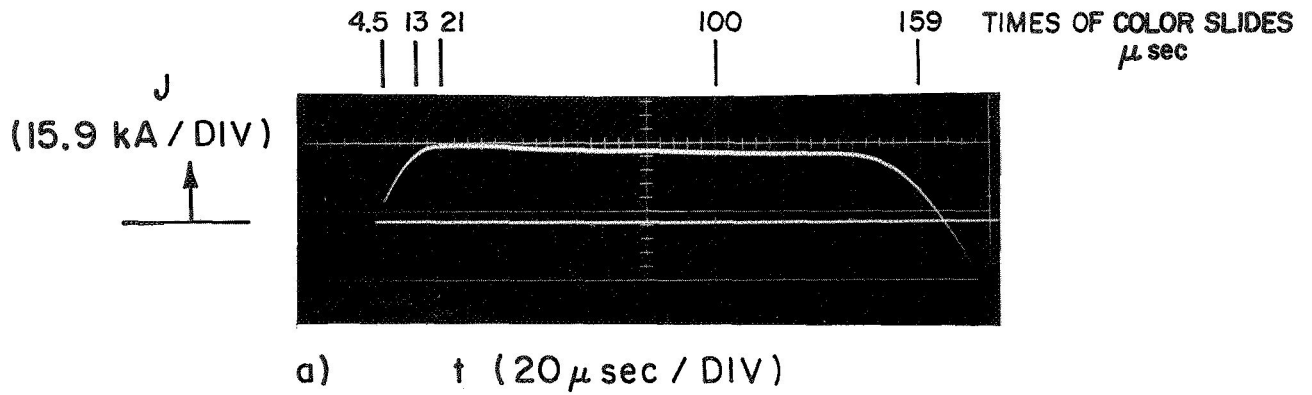
Photography

Qualitative information on the nature of the arc in the cathode region is provided by color photography through a



ACCELERATOR SCHEMATIC

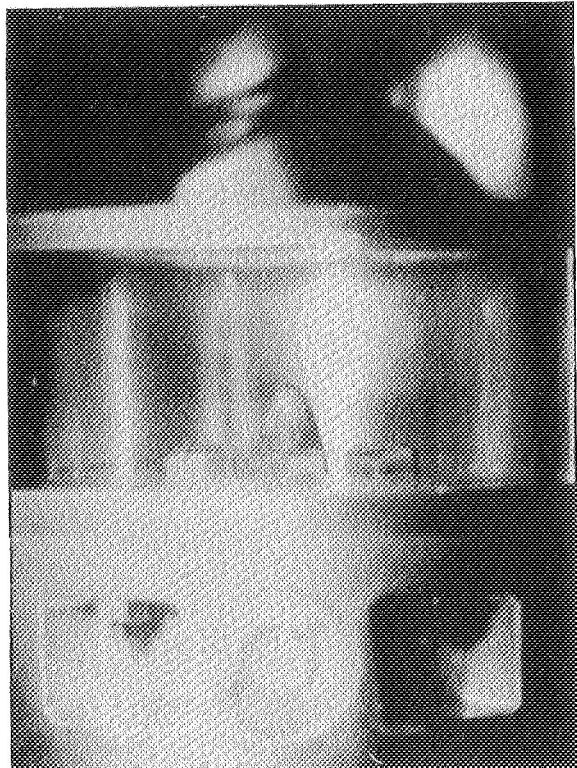
FIGURE 2-1



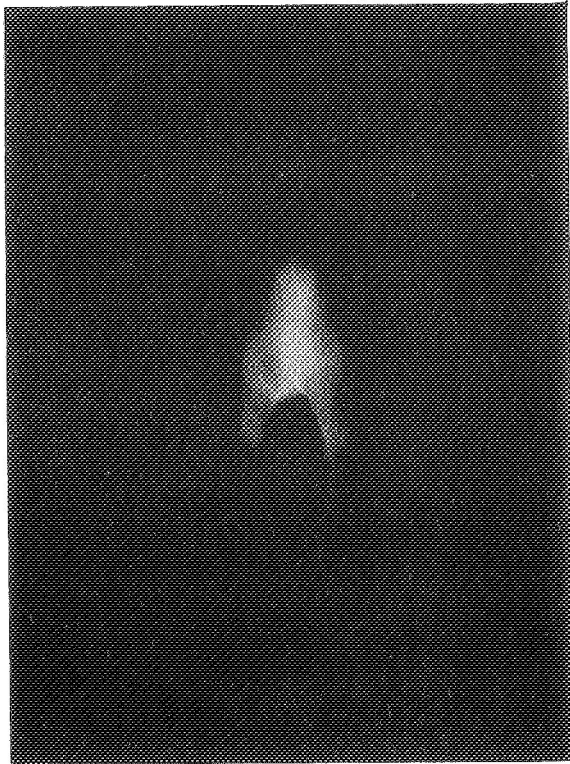
17.5 kA CURRENT PULSE ON TWO DIFFERENT
TIME SCALES

high speed Kerr-cell system. A quarter of the anode current return path was removed at the arc chamber allowing the entire discharge region to be viewed through the glass ring insulator (Fig. 2-3a). Color slides were obtained using High Speed Ektachrome Daylight Film (with standard development; ASA 160) in a 35 mm, single lens, reflex camera (Honeywell Pentax; 50 mm f.l.). The Kerr-cell shutter was triggered at a known time in the current pulse and remained open for 5 μ sec. Bleedthrough of light from the high intensity region at the cathode tip, checked by photographing the arc with the Kerr cell closed, was unnoticeable at the exposure setting used (f/4.7). The figures shown are enlargements made on Polaroid Type 58 color film and satisfactorily represent the original slides. Black and white photographs obtained in the same manner with a 4 x 5 Speed Graphex camera, using Polaroid 3000 film, show the same luminosity distributions but do not, of course, provide as clear a delineation of plasma radiations as the color slides. The sequence of photos shown are representative of the various phases of arc operation.

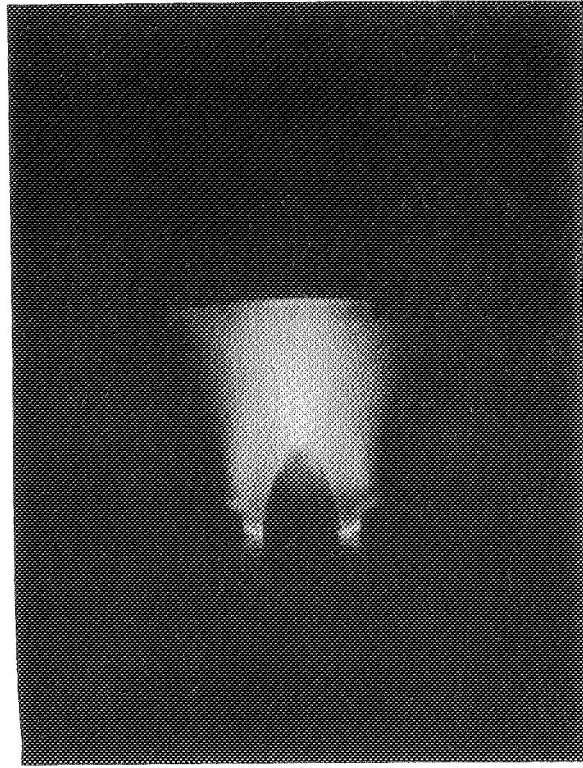
As the current to the arc chamber increases, we observe the motion of cathode spots and the transition of cathode current attachment from a spot to diffuse mode (Figs. 2-3b,c,d). After 20 μ sec (Fig. 2-3d), the luminosity pattern has nearly achieved the quasi-steady situation shown at a representative time in Fig. 2-3e, 100 μ sec after discharge initiation. In later photos, the luminosity pattern becomes less constricted and diminishes in intensity as the current returns to zero (6 μ sec after Fig. 2-3f). When the current reverses, the central electrode becomes the anode and a radically different pattern is obtained. Figures 2-3g and 2-3e are both obtained 100 μ sec into their respective current pulses, but are quite dissimilar. Yet, at the same time into the third current pulse, when the central electrode is again the cathode, we regain normal operation (Fig. 2-3h). The pattern is now less bright and less constricted since the maximum current level is somewhat lower than that of the initial pulse.



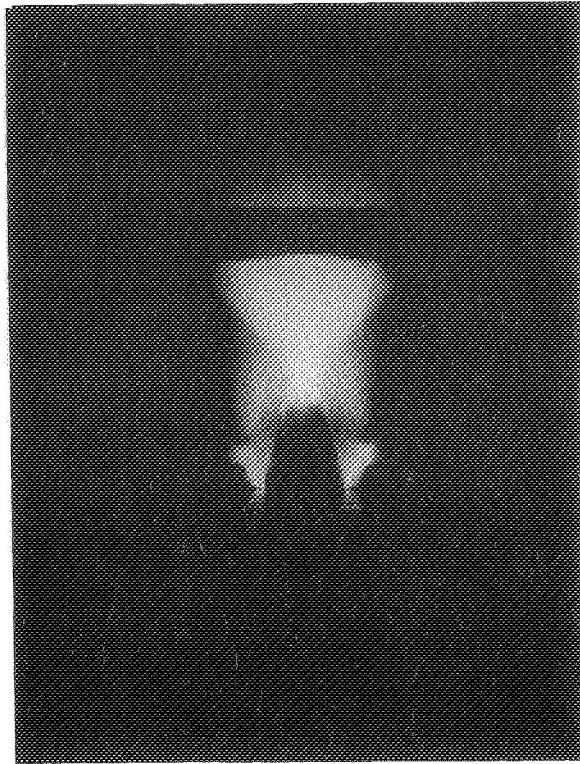
a) ARC CHAMBER THRU SIDEWALL WINDOW



b) DISCHARGE INITIATION $t = 4.5 \mu\text{sec}$



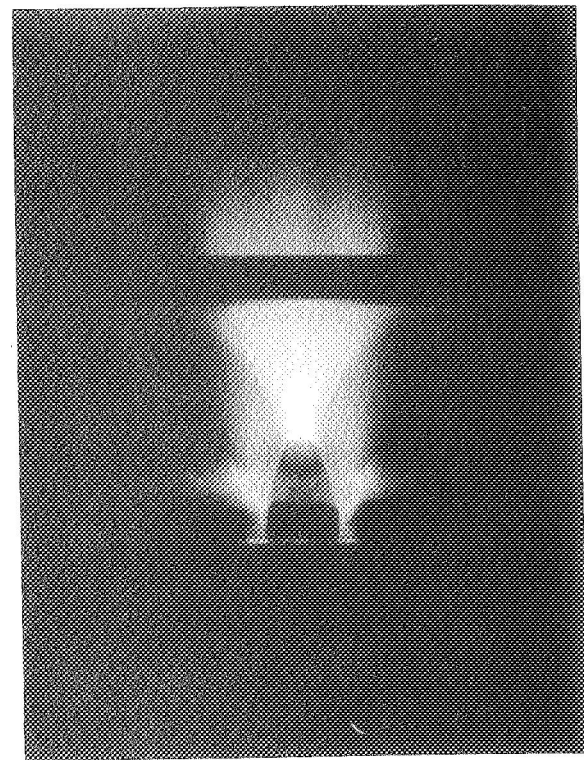
c) DISCHARGE INITIATION $t = 13 \mu\text{sec}$



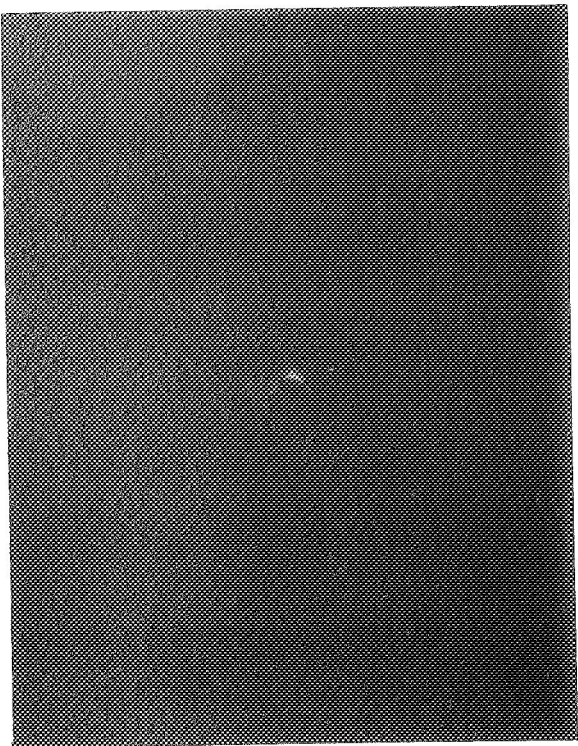
d) DISCHARGE STABILIZATION $t = 21 \mu\text{sec}$

PHOTOGRAPHS OF ARCJET OPERATION

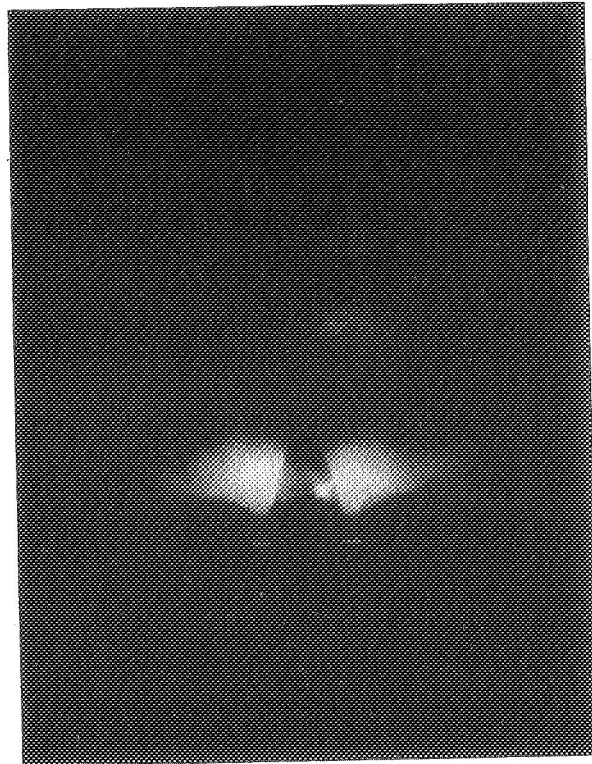
FIGURE 2-3



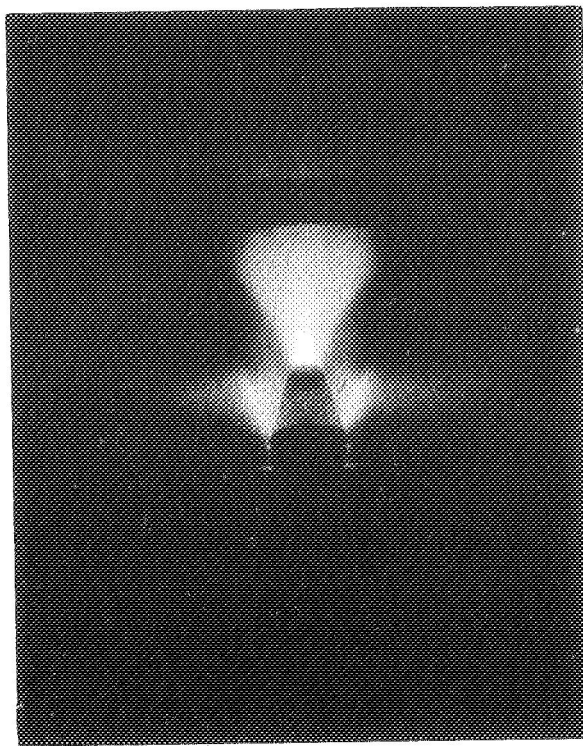
e) QUASI-STEADY OPERATION $t = 100 \mu\text{sec}$



f) CURRENT TURN OFF $t = 159 \mu\text{sec}$



g) CURRENT REVERSAL $t = 265 \mu\text{sec}$



h) RETURN TO NORMAL OPERATION $t = 430 \mu\text{sec}$

PHOTOGRAPHS OF ARCJET OPERATION

FIGURE 2-3

The colors observed in the discharge may be used to indicate various physical phenomena. For example, correlation with spectroscopic evidence¹¹ indicates that green is associated with molecular carbon (C_2) radiation in our discharge, while blue-white is characteristic of bremscontinuum. Thus, we would expect to find molecular carbon in a region extending from the cathode-insulator junction (see Fig. 2-3e). This indicates ablation of the Plexiglas insulator [$n(C_5H_8O_2)$], and the presence therefore of hydrogen and oxygen in the plasma, in addition to molecular and atomic carbon.

Our photographic work also yields some information on the cathode surface. With the possible exception of a small area at the tip, the cathode surface appears dark. This indicates that most of the cathode surface does not achieve incandescent temperatures during the time of our experiment, even though the surface current densities exceed $10^7 A/m^2$. That incandescence should be observable was verified by successfully photographing the filament of a 35 W spot lamp, using the same 5 μ sec shutter Kerr-cell system. Spectroscopic photographs confirm these results, showing bright continuum at the cathode tip, but darkness everywhere else on the surface.

The importance of the photographic work is that it provides a time-resolved, general look at the interior of an MPD arcjet. Discharge mode, arc intensity distribution and polarity effects are immediately seen, and significant evidence is obtained about processes such as insulator ablation and cathode emission.

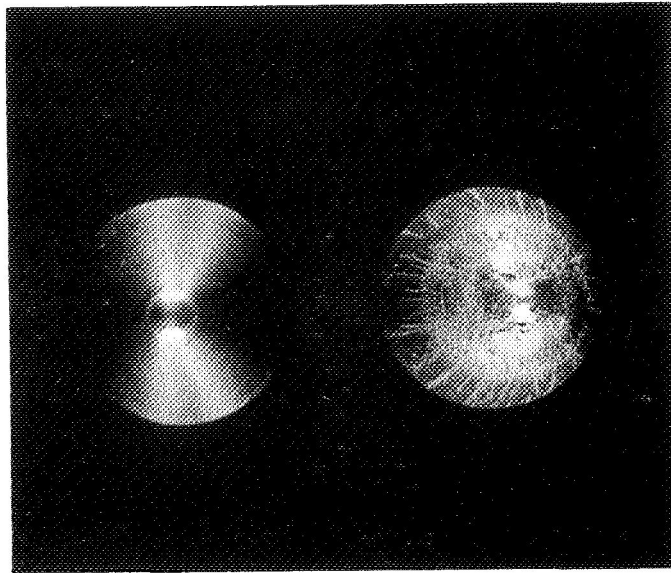
Surface Phenomena

Insulator Ablation. A dial indicator was applied to the initially flat Plexiglas backplate used in the photographic studies. After some 50 firings, a shallow, conical region had been ablated approximately 0.002-in. deep at the cathode-insulator junction and extending out to the radius of gas injection. Measurement of the ablation depth of the backplate normally

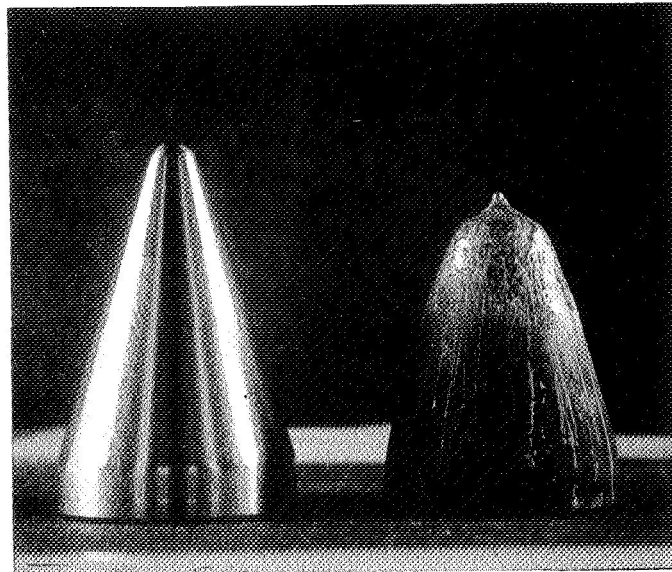
used, after over 3,000 firings at various current and mass flow conditions, yields a comparable value of mass lost per shot. This ablated region is shown in our diagrams of the arc chamber as a conical volume at the base of the cathode. Computations based on the volume of Plexiglas ablated, averaged over the total discharge duration including reverse current pulses, give a mass flow of insulator material of 0.9 g/sec, which is an appreciable fraction of the input argon mass flow (5.5 g/sec in our case). More important, however, is the influx of low mass ions to the plasma, since each Plexiglas group ($C_5H_8O_2$) may be expected to provide up to eight hydrogen ions. This may have important implications for any process, diagnostic or arc, that involves the random flux of positive charge to a surface.

Cathode Surface. After several hundred firings, the cathode was removed for close examination. It is immediately evident that the cathode tip has experienced considerable violence since the initially smooth, large radius cone end has developed a sharp peak at the tip center, surrounded by a rather flattened area. (See Fig. 2-4; note that the unused cathode on the left has a higher base than the used cathode had initially. Also, the used cathode had been filed to smoothness a few times earlier in its history, so we cannot compare the two for erosion due to the discharge.)

The drawing in Fig. 2-5 was made while viewing the cathode with a 3X stereomicroscope. We see that the surface extends with increasing slope from the darker areas of the cathode to form a peak 0.1-in. high, surmounted by a globule 0.04-in. in diameter. The surface appears to have been molten along the sides of the peak as slight folds are observed. These indicate flow away from the end of the cathode and thus opposite to the free stream plasma flow. Occasionally, a red, hot spark will be ejected from the arc chamber during or perhaps slightly after the discharge. We may surmise that this results when the cathode tip deforms to the extent that the globule is freed from the peak. Processes then return to



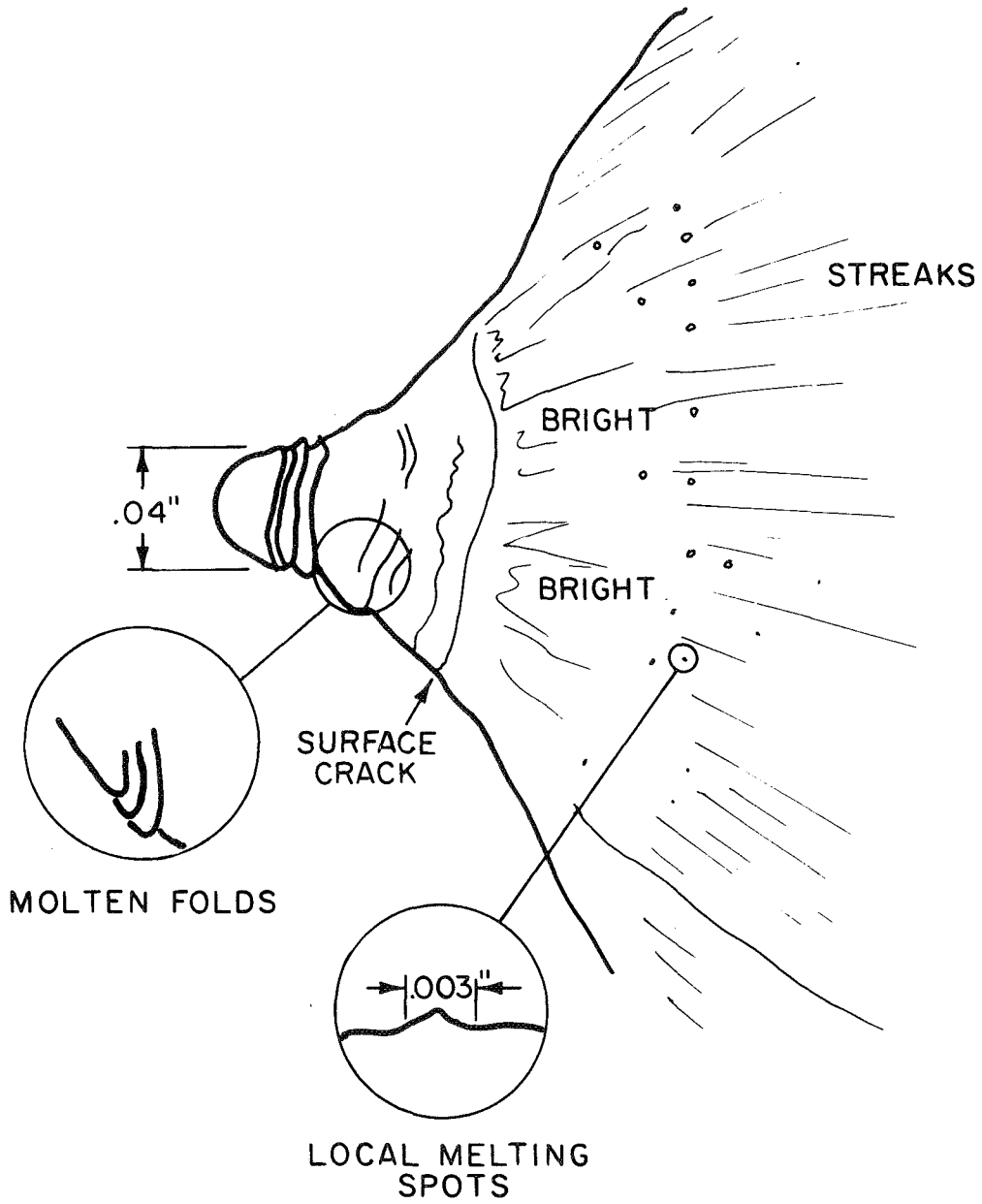
a) TOP VIEW



b) SIDE VIEW

PHOTOGRAPHS OF TUNGSTEN CATHODE

FIGURE 2-4



MAGNIFIED VIEW OF CATHODE TIP

AP 25 12 4604 70

FIGURE 2-5

normal (spark-free) until the mechanical stability of the peak formation is again lost. Although the current density at the base of the cathode is comparable to that at the cathode tip, no melting is apparent there.

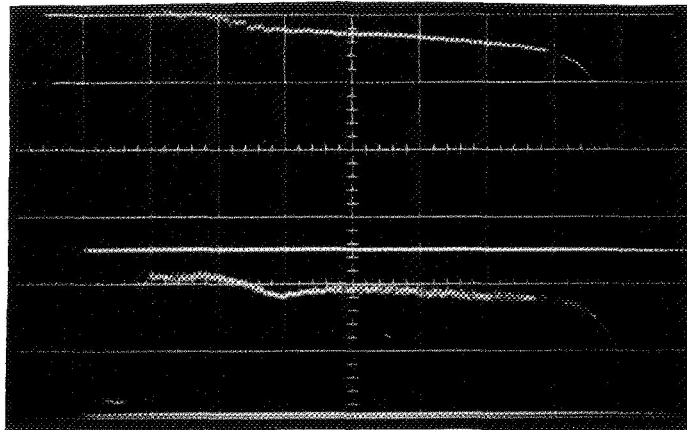
Magnetic Field Distribution

By measurement of the magnetic field distribution within an MPD arcjet, we may obtain both the current flow pattern and the distribution and direction of the $\vec{j} \times \vec{B}$ body force. In a quasi-steady discharge, this is accomplished quite simply by use of a small coil of wire placed at the point of interest.⁵ As the discharge pattern forms and stabilizes, a current is generated in the coil proportional to the local rate of change of magnetic field. Electronic integration of this signal then allows us to monitor the local magnetic field on an oscilloscope (see Fig. 2-6a). Calibration is accomplished in a situation nearly identical to that in which the probe is used by placing the coil at a position in the arc chamber where the magnetic field is known, i.e., at a position enclosing the total discharge current.

The result of a survey of the magnetic field in the cathode region of the discharge is displayed as a plot of enclosed current contours in Fig. 2-7. Constant fractions of the total discharge current flow between these streamlines and the arcjet centerline. This figure was obtained by graphing the enclosed current at over 40 points in the cathode region versus both radial and axial position. The locations at which a specified current is enclosed were then cross plotted to provide a contour. The error boxes are due to finite probe size, shot-to-shot reproducibility, and experimental precision, and indicate the area around each point of the contour at which the particular current may be enclosed. In obtaining enclosed current from the local magnetic field measurement, we make use of the azimuthal symmetry of the discharge. This symmetry is indicated by the quasi-steady character of our signals (no rotating spokes, for example, are suggested) and was confirmed

$t = 20 \mu\text{sec} / \text{DIV}$

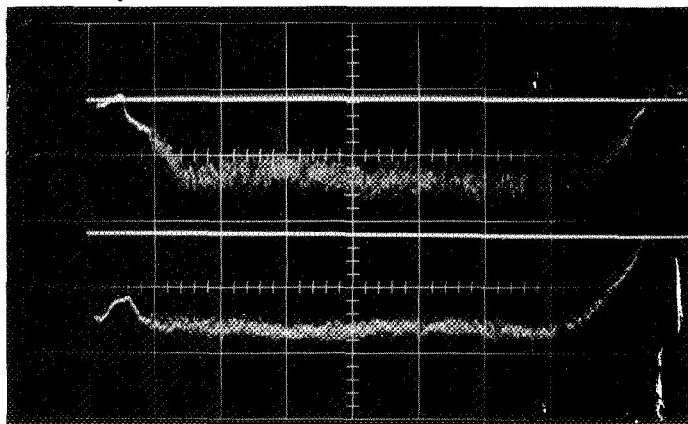
I 3681

 $B_1 .005 \text{ v} / \text{DIV}$ $B_2 .005 \text{ v} / \text{DIV}$

a) MAGNETIC FIELD PROBE

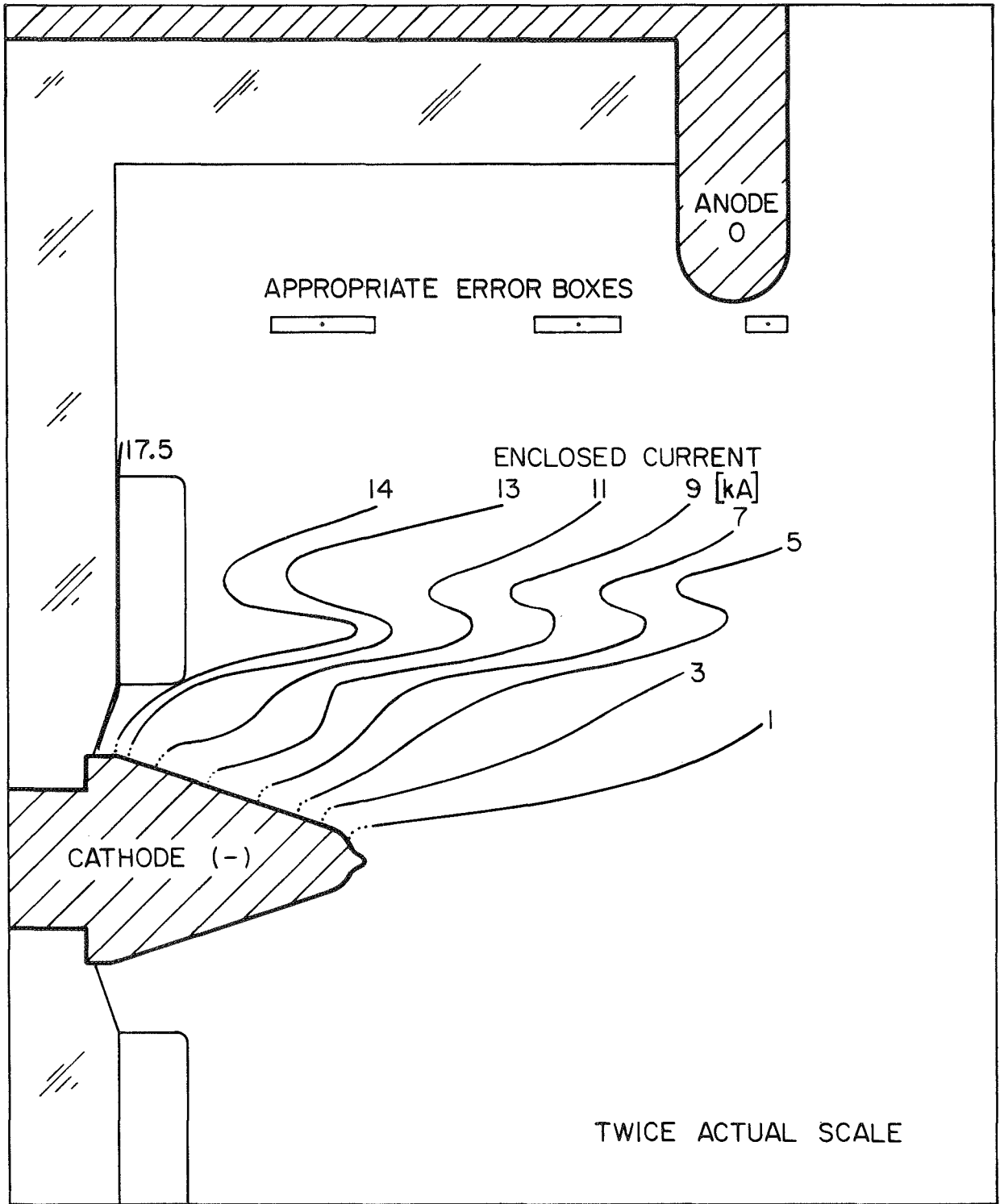
 $t = 20 \mu\text{sec} / \text{DIV}$

I 3887

 $V_1 - V_2 20 \text{ v} / \text{DIV}$ $V_2 50 \text{ v} / \text{DIV}$

b) FLOATING POTENTIAL PROBES

FIELD PROBE DATA RECORDS



AP 25 R 4648 70

ENCLOSED CURRENT CONTOURS, $t=100 \mu \text{ sec}$

FIGURE 2-7

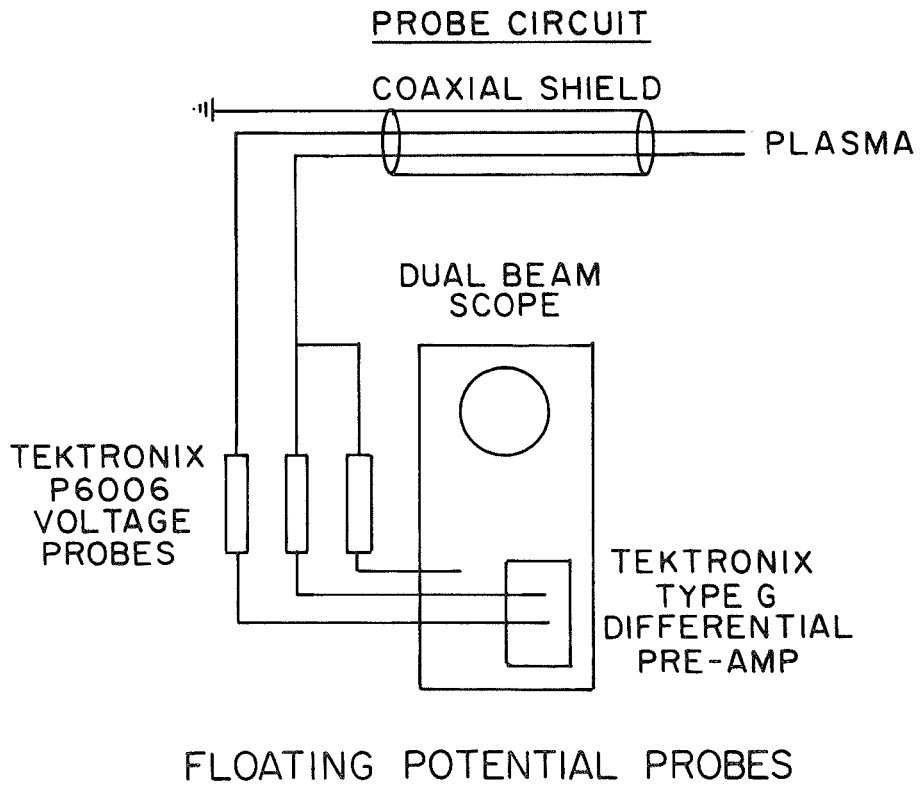
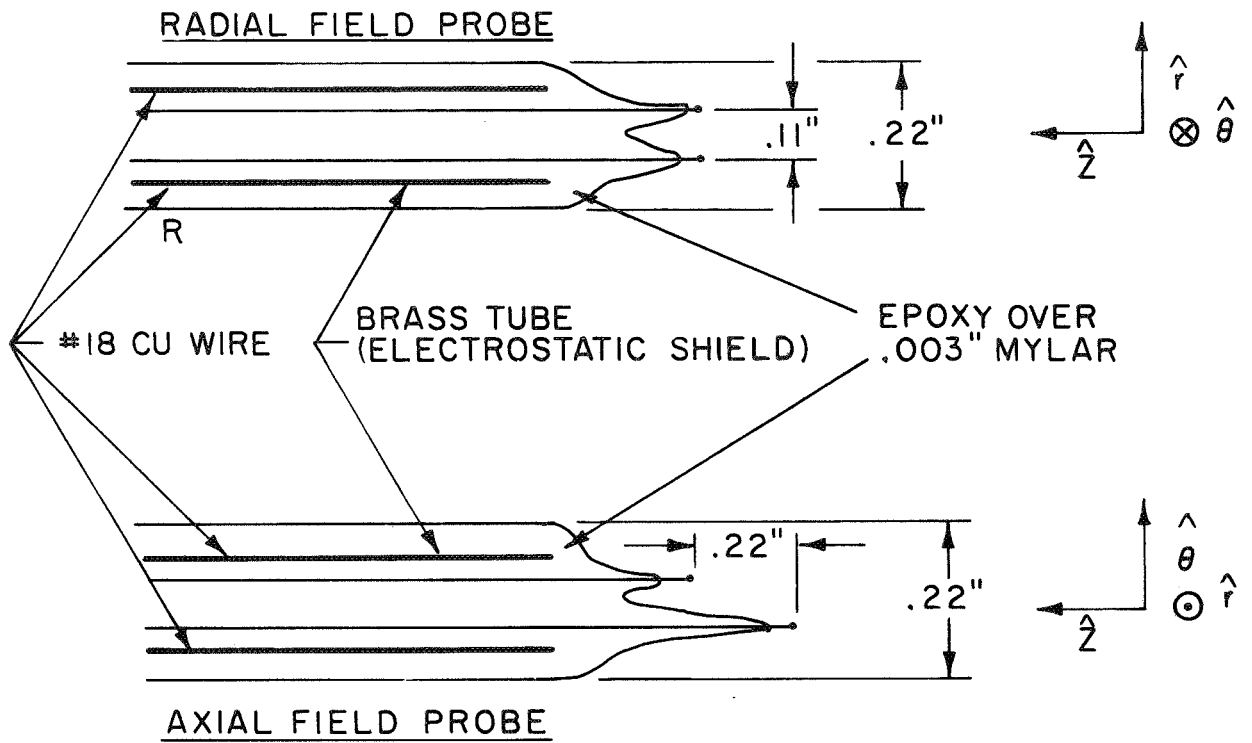
by rotation of the probes 90° out of the usual plane of measurement. The same level and distribution of magnetic field was obtained even though our azimuthal position relative to the hexagonally arranged gas injectors was different.

We call attention at present to some of the more immediate features of the current flow pattern. We note that 25% of the total current travels in a layer adjacent to the insulator wall, with the remainder of the current distributed in a diffuse manner throughout the cathode region. At the cathode surface, the current density is rather uniform. It is highest at the cathode tip (5×10^7 A/m²), somewhat lower at the base of the cathode (4×10^7 A/m²) and lower still along the intervening slope (1.5×10^7 A/m²). Another, rather interesting, aspect of the pattern is the double inflection of the current streamlines at the radius of gas injection. Even when the pattern is smoothed to achieve gentle curves through the error boxes, this feature is still present.

Voltage Distribution

The voltage distribution within the discharge is determined by use of floating electrostatic probes. These measurements accurately reflect the plasma potential distribution if the electron temperature and plasma flow properties do not vary greatly over the distance of interest. From the potential distribution, we may obtain local components of the electric field in the discharge and, with reference to the current distribution, we may also delineate regions of significant electrical energy deposition.

To minimize the effects of total voltage fluctuation from shot-to-shot, we employ two floating probes at nearby positions, separated in either the radial or axial direction. The probe system used here consisted of two #18 copper wires, insulated with Mylar and epoxy, and coaxially shielded in the same support tube (Fig. 2-8). The wire ends were exposed to the plasma as nearly spherical tips, separated by 0.11 in. in the case of the radial field probe, and 0.22 in. for the



AP 25 & 4645 70

FIGURE 2-8

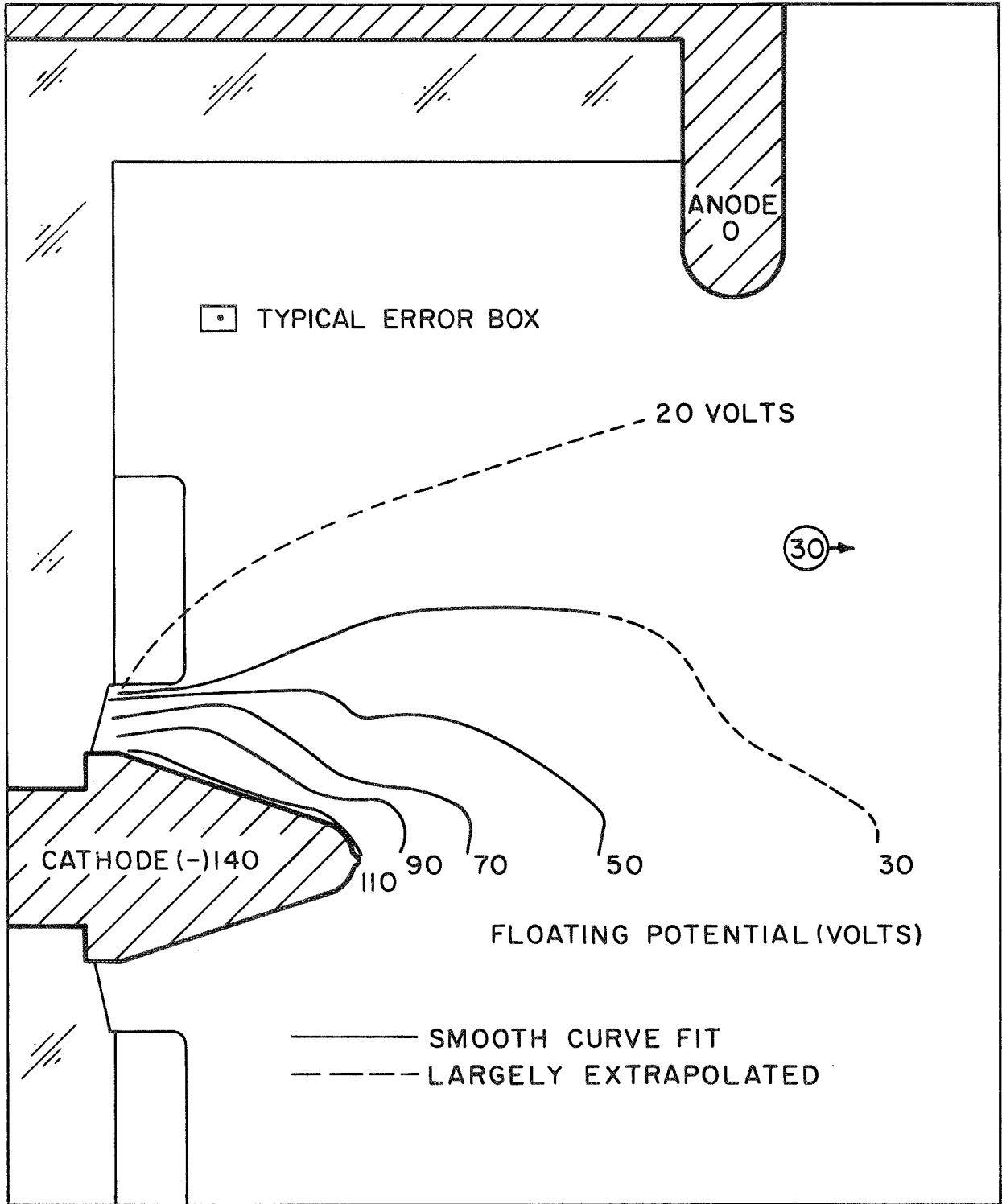
axial field probe. Voltages were monitored by three Tektronix P6006 voltage probes, using a Tektronix Type G differential pre-amp to obtain the voltage difference between tips (see Fig. 2-6b). By simultaneously recording the voltage of one probe and the voltage difference between probes, we obtain the floating potential at two points in the plasma and the average electric field between them. This procedure was applied at over 50 locations in the cathode region, providing over a hundred measurements of floating potential.

Plots of floating potential versus radial and axial position were then used to obtain the locations of particular voltage values. The resulting equipotential contours are shown in Fig. 2-9. The error boxes are again due to finite probe size, shot-to-shot reproducibility, and experimental precision, and again indicate the range of points through which a given contour could be drawn. The voltage level of each line may be corrected by a factor depending on the electron temperature and the appropriate ion speed and mass. Both these corrections tend to decrease given voltage values by up to 10 V. (The electrode voltages need no correction, so the cathode fall voltage may be 10 V more than indicated in Fig. 2-9.)

We note immediately from these contours that the bulk of the arc voltage, and thus electrical power, is provided within one (base) diameter of the cathode surface, confirming the importance of the cathode region to MPD arc processes. A detailed analysis of the electromagnetic structure of the discharge in the cathode region is presented in Chap. 4. We must first determine some of the electrical and mechanical properties of our plasma.

Langmuir Probing

Time-resolved local measurements of electron temperature and estimates of electron density are obtained by Langmuir probe techniques. Briefly, a Langmuir probe consists of a wire inserted into a plasma and exposed there as a surface of known



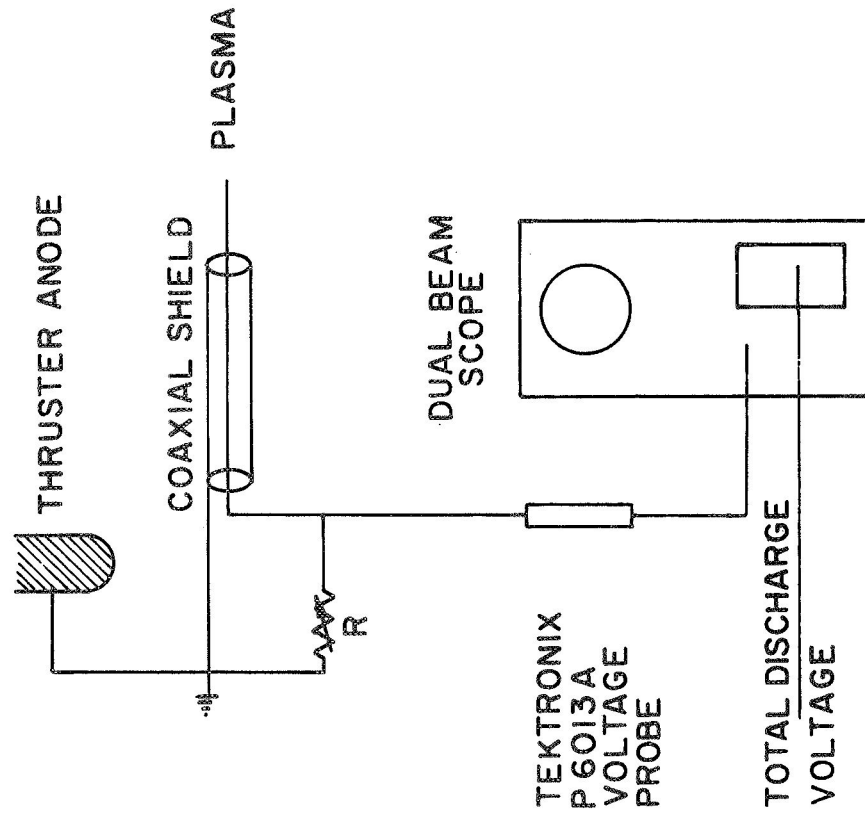
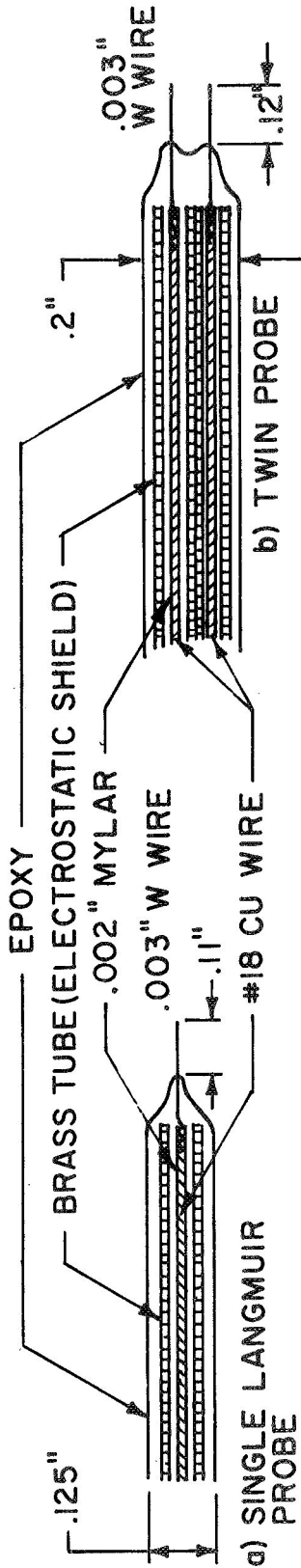
AP25 R 4646 70

CONSTANT FLOATING POTENTIAL CONTOURS, † 100 μ sec.

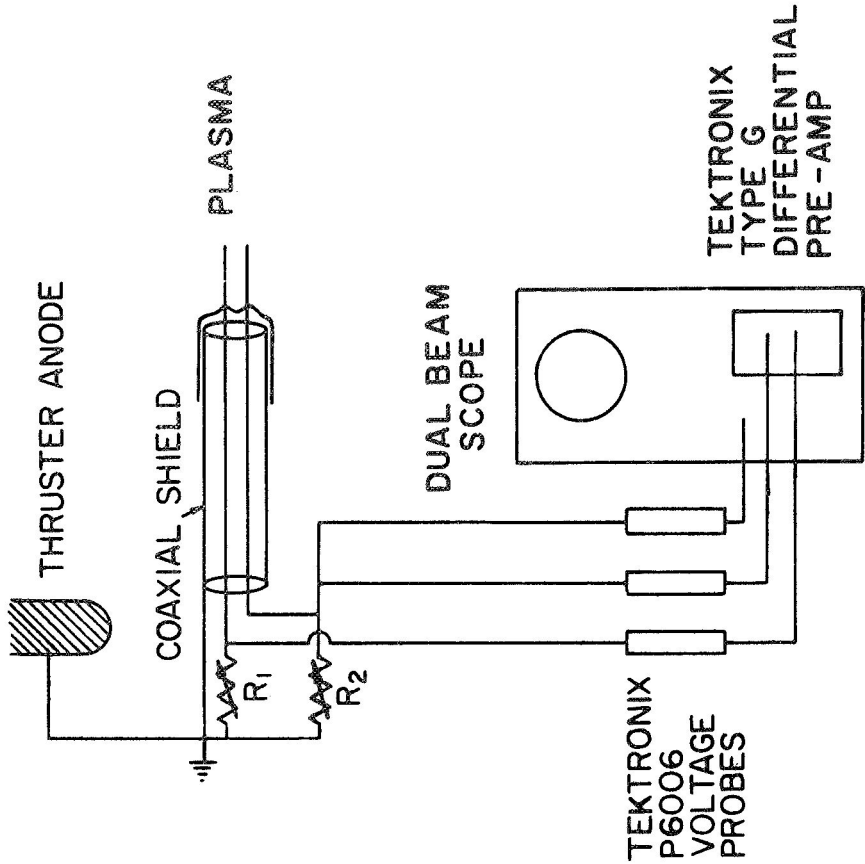
FIGURE 2-9

geometry. A current is drawn through the wire and the surface is established at some voltage. The approach is to relate this current and voltage to the charge transport processes of the plasma and thereby to obtain the particle temperatures and densities. Unfortunately, this procedure is extremely complicated except in a few well-defined situations.¹² To utilize this technique, we are therefore required to design our probe so that such a simple situation obtains. We need a probe with a radius much larger than a Debye length, so that the collection area is well known, yet much smaller than various mean free paths, so that a collisionless formulation may be used. Additionally, we require the probe to survive many exposures to a dense, energetic plasma without variation in its operating character.

Our initial efforts were concerned with the measurement of electron temperature in the MPD exhaust on the arcjet centerline 12 in. downstream of the anode face. We employed a single Langmuir probe, constructed as shown in Fig. 2-10, and aligned parallel to the plasma flow. The voltage drop across a resistor connecting the probe to ground was monitored with a Tektronix P6013A voltage probe, so that the current drawn by the probe and the probe voltage during quasi-steady operation were obtained with a single measurement (see Fig. 2-11a). The procedure was repeated for a range of resistor values, from 9.6Ω to $10^8 \Omega$, to achieve the graph of probe current versus probe voltage shown in Fig. 2-12. The ion current branch of the probe characteristic was obtained by the addition of a 45 V battery in series with the resistor. The probe tip was cleaned initially by submersion in warm clorox until a shiny, light gray surface was obtained. Examination of the probe tip after many exposures to the discharge showed that this condition was maintained, presumably by probe heating in the arc environment. The error bars in Fig. 2-12 are primarily due to the shot-to-shot fluctuations of the total discharge voltage and thus, local plasma potential. Note that both electron and ion current saturations were achieved. Thus,



SINGLE PROBE CIRCUI

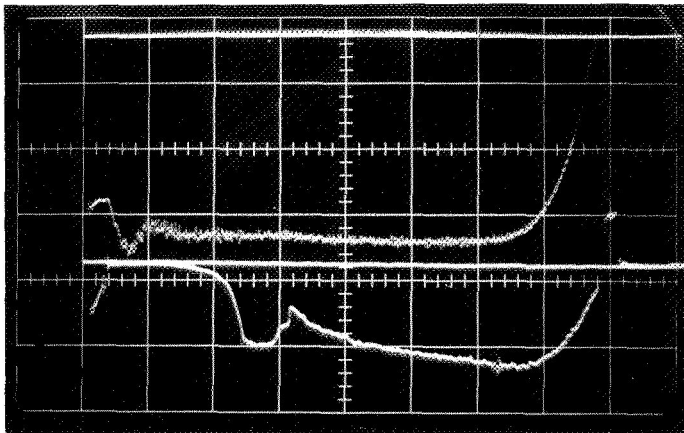


TWIN PROBE CIRCUI

FIGURE 2-10

$t = 20 \mu\text{sec} / \text{DIV}$

I 2680



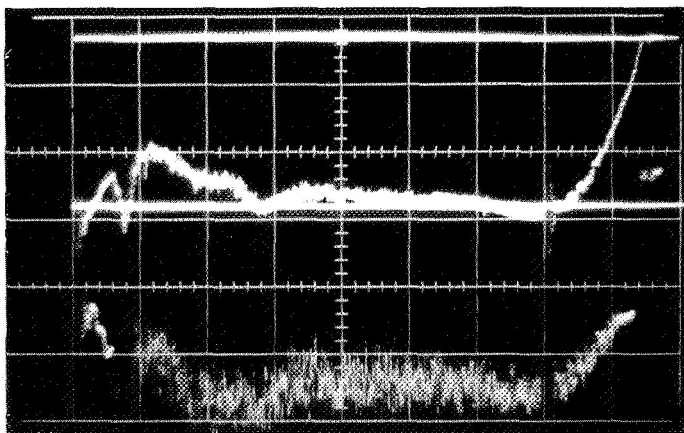
TOTAL ARC VOLTAGE
50 v / DIV

PROBE VOLTAGE WITH
94 Ω RESISTOR TO
GROUND
20 v / DIV

a) SINGLE PROBE IN DOWNSTREAM
EXHAUST PLUME

 $t = 20 \mu\text{sec} / \text{DIV}$

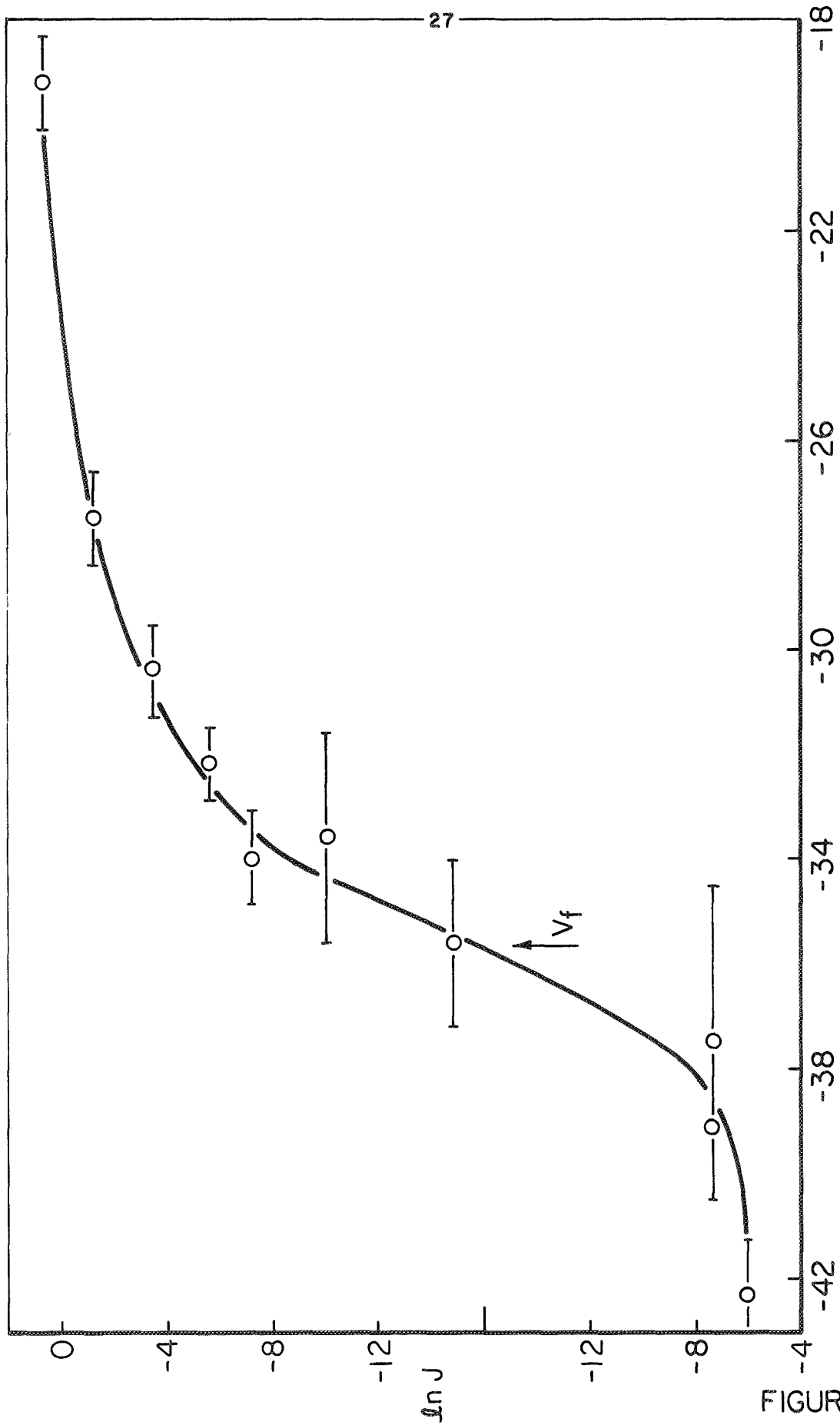
I 3839

 V_1 20 v / DIV $R_1 = 47 \Omega$ $V_1 - V_2$ 2v / DIV $R_2 = 4.7 \Omega$

b) TWIN PROBE IN CATHODE
REGION

LANGMUIR PROBE DATA RECORDS

FIGURE 2-11



LANGMUIR PROBE CHARACTERISTIC AT
 $Z = 30 \text{ cm}, r = 0; J = 17.5 \text{ kA}, \dot{m} = 5.5 \text{ g/sec}$

FIGURE 2-12

we may adjust the total current by the ion current (assumed constant) to obtain a plot of electron current versus probe voltage, Fig. 2-13. We see that a straight line transition portion and a "knee" are present. The electron temperature is obtained from the slope of the straight portion, while the "knee" indicates when the probe has attained plasma potential. Our analysis follows simple Langmuir probe theory and gives:

$$\begin{aligned} kT_e &= (1.4 \pm 0.2) \text{ eV} \\ n_e &= (5.2 \pm 4) \times 10^{19} \text{ m}^{-3} \\ kT_i &= (8.8 \pm 0.6) \text{ eV} \end{aligned}$$

The rather large error bar on n_e reflects the lack of precision involved in determining the location of plasma potential within the knee. This could be improved if more data were obtained, but in view of the uncertainty of the probe collection area at this low density, we are satisfied merely with an estimate of electron density. The ion temperature is determined from the ion saturation current, assuming singly charged argon ions and neglecting far-field sheath effects in view of the high ion energy. (Calculations based on ion current are sensitive to the chemical nature of the flow as well as the exact flow direction and we shall avoid them for these reasons.) We note our probe data is consistent with simple theory in that the measured difference between plasma potential and floating potential agrees with the value computed from the electron temperature and the saturation current ratio.

Although the single Langmuir probe proved useful for measurements of electron temperature and estimates of electron density and ion temperature in the downstream exhaust of the arcjet, this was not the case within the arc chamber. The fluctuations of local plasma potential from shot-to-shot became more significant compared to the difference between floating and plasma potentials, so that we could no longer obtain a probe characteristic. Pulsed operation of the probe (sweeping

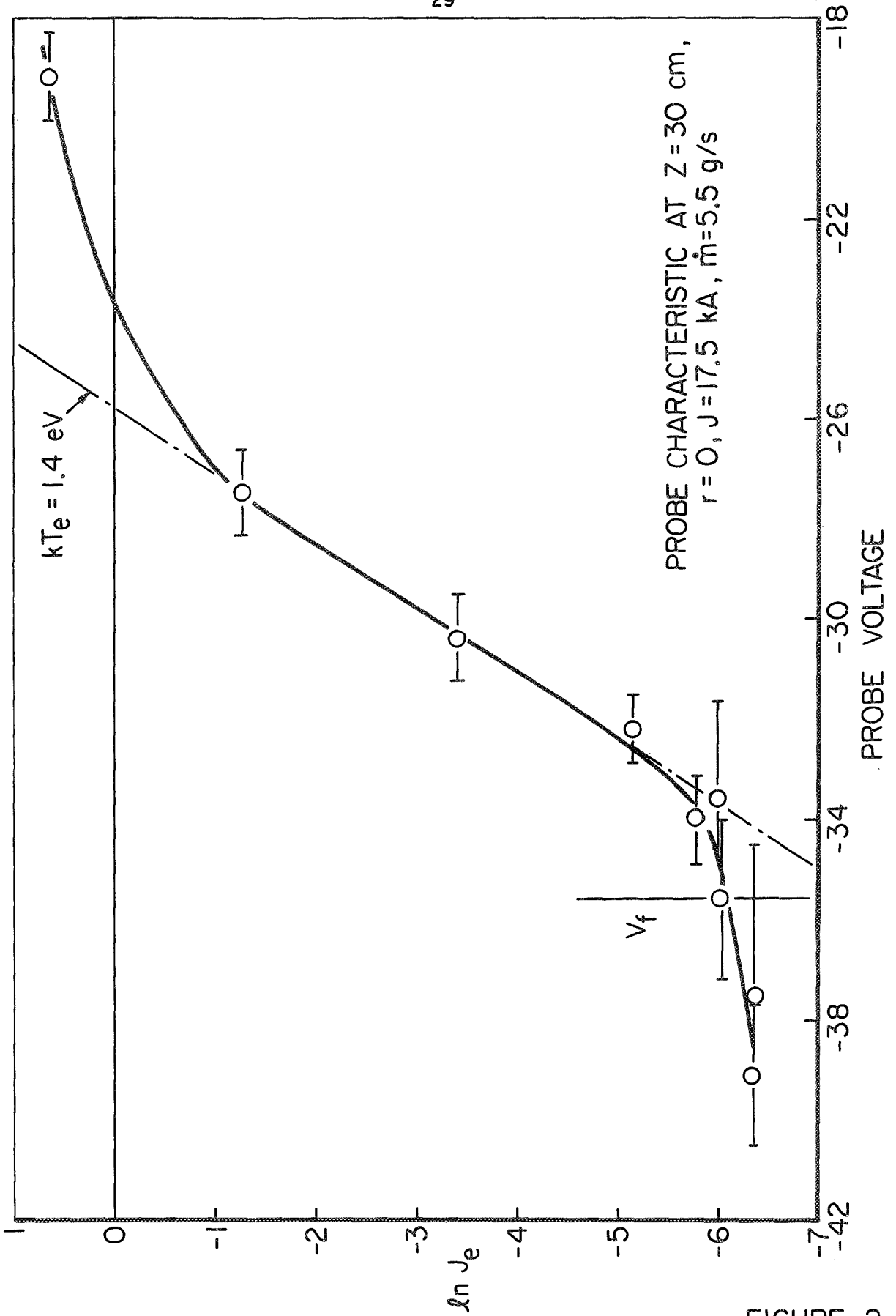


FIGURE 2-13

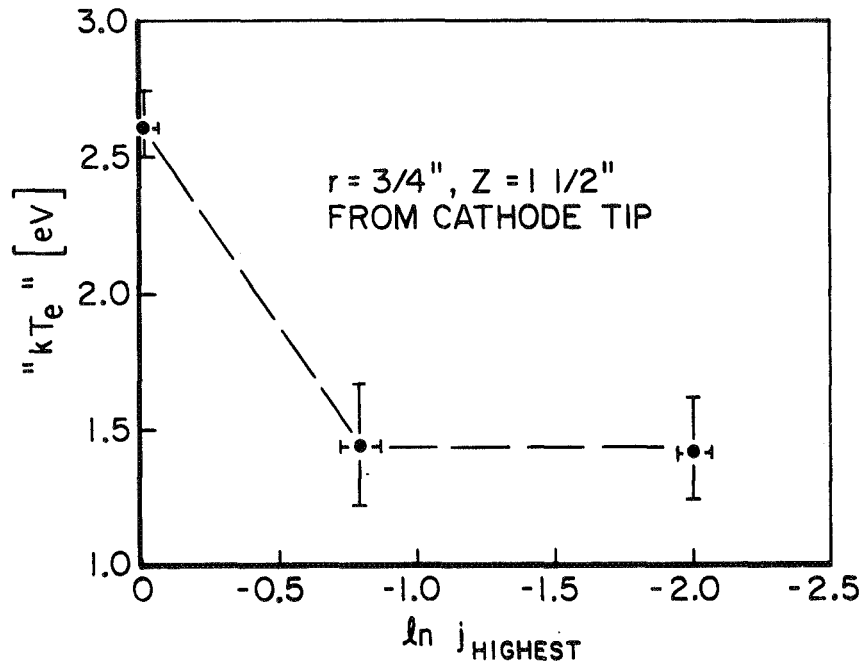
LANGMUIR PROBE ELECTRON CURRENT VARIATION WITH PROBE VOLTAGE

the probe characteristic during the discharge) was considered but discounted because of the inductive voltage drops associated with driving pulses up to electron current saturation on a time short compared to local fluctuation times in the plasma. We therefore developed a technique that is insensitive to fluctuations in plasma potential.

The approach is simply to measure the currents and voltages of two identical probes sampling the same plasma. If we operate on the transition portion of the characteristic and draw currents well above ion saturation current, then the ratio of currents to the probes will be given by the Boltzmann factor based on the difference in probe voltages and the electron temperature:

$$\frac{I_2}{I_1} \approx \frac{I_{2e}}{I_{1e}} = e^{-\frac{e(V_2 - V_1)}{kT_e}} \quad (2-1)$$

Such a twin probe will thus provide the electron temperature if we measure the necessary currents and voltages. The procedure is similar to that used for the single probe, in that each probe is connected to ground through a different resistor, and the voltage drops are monitored using Tektronix P6006 voltage probes. Both currents are determined in this way, while the difference in voltages is obtained using a Tektronix Type G differential pre-amp (see Fig. 2-11b). To insure that we are operating on the proper portion of the probe characteristic, several pairs of resistors are used. Our computed value of kT_e is just the reciprocal of the slope of a line between two points on the probe characteristic. A plot of inverse slope versus the highest current to the probe pair is shown in Fig. 2-14. When both probe tips are on the transition branch, the computed value of kT_e remains nearly constant for different currents (decreasing somewhat as we approach ion saturation current). If one or both of the probe tips are drawing current on the electron saturation branch, however, we suddenly compute high values of kT_e . Thus, the constant portion of Fig. 2-14 provides the electron temperature, while the "kink"



COMPUTED kT_e vs HIGHEST CURRENT TO PROBE

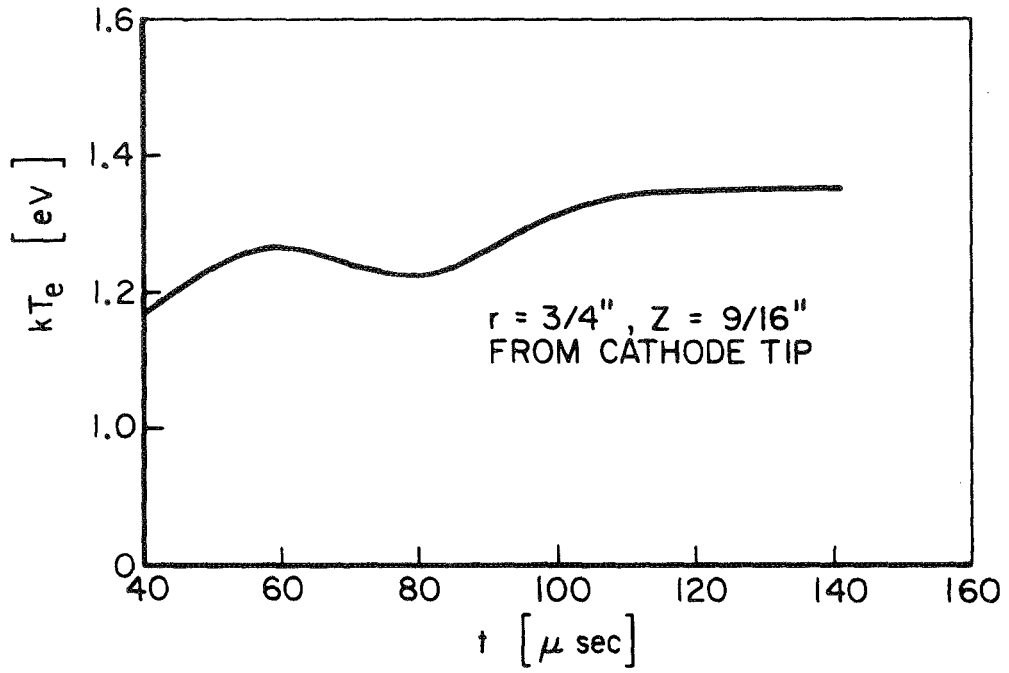
AP 25 R 9607 70

FIGURE 2-14

indicates electron current saturation, from which we may estimate electron density. The results of twin probe and single Langmuir probe techniques are compared at a position on the arcjet centerline, 12 in. from the anode face and found to agree almost exactly ($kT_e = 1.5$ eV, $n_e = 6 \times 10^{19}/\text{m}^3$ versus previous values). A basic limitation on the accuracy of these measurements is the turbulence of the plasma flow. In Fig. 2-15, we see the time variation of kT_e determined by the twin probe during quasi-steady operation.

Values of kT_e and estimates of n_e are shown at various positions within the arc chamber in Fig. 2-16. The values in the cathode jet ($r = 0$, $z = 3/16$ in.) were obtained by sacrificing probe tips that remained from previous operations elsewhere. It was found that a tungsten wire tip would not be lost to the fury of the cathode jet until sometime after the first few pulses of the discharge ringdown. In this way, values of electron saturation current in the cathode jet were accumulated. One experiment with a twin probe at this location (with resistor values estimated to place the probe on the transition branch) yielded the electron temperature shown in Fig. 2-16 at the cathode tip.

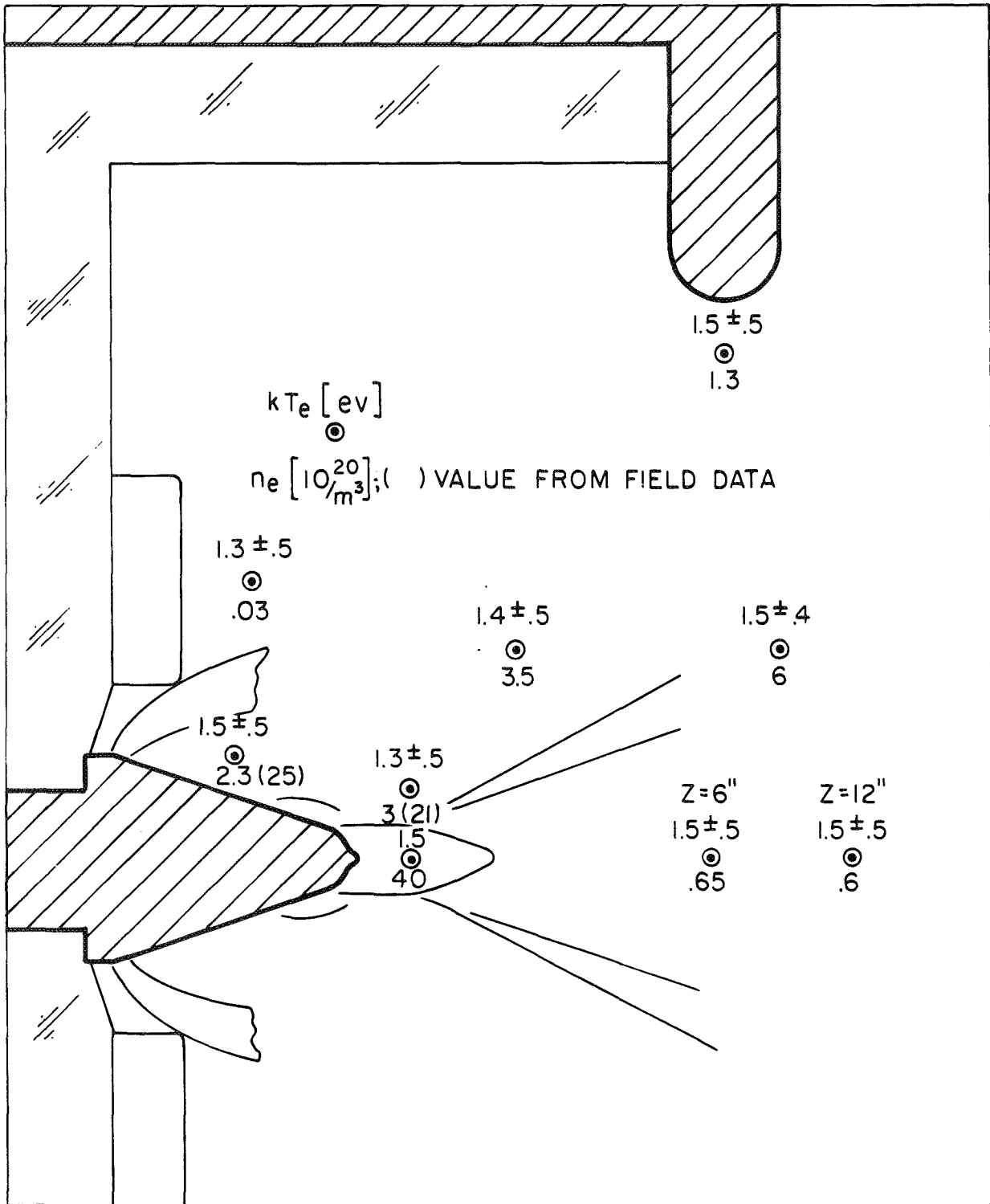
We note that the strong magnetic field in the cathode region will cause the probe characteristic (current-voltage diagram) to plateau before reaching the true saturation electron current, so electrostatic probe data provide only minimum values of the electron density near the cathode. Indeed, later analysis based on the electromagnetic structure of the discharge indicates electron densities almost an order of magnitude higher than values obtained by these probes. The electron temperature measurement should not be affected by the presence of the magnetic field since it is based on the transition portion of the characteristic. Collisional effects near the probe surface also tend to distort the results obtained from probe data. Computations based on the higher densities obtained from analysis of the discharge structure indicate that $\lambda_{ei}/r_p \approx 1$ and $\lambda_D/r_p \approx 10^{-3}$, where λ_{ei} is the electron-ion MFP,



kT_e DURING QUASI-STEADY OPERATION

AP 25 E 4608 70

FIGURE 2-15



AP 25 12 4609 70

ELECTRON TEMPERATURE AND DENSITIES FROM TWIN PROBE DATA

FIGURE 2-16

λ_D is the Debye length, and r_p is the probe radius. The work of Kirchhoff et al.¹³ suggests that transition flow effects are therefore unimportant in our probe situation.

The minimum levels of electron density provided by the twin probe data will be used in Chap. 3 to establish the quasi-neutral, continuum nature of our plasma and thereby to justify a priori the magnetogasdynamic formulation from which the higher density values are obtained.

In the following chapters we shall formulate a cogent, phenomenological picture of the physical processes involved in the cathode region of our MPD arcjet based on the preceding experimental evidence.

CHAPTER 3

THE CATHODE PLASMA

The nature of a plasma is primarily determined by particle collisions. These collisions relate the momentum and energy of a particle to its fellows and to the other types of particles that comprise the plasma. Collisions also prescribe the response of a plasma to its electromagnetic and mechanical environment. We shall examine and compare collisional events in terms of characteristic lengths or mean free paths. In this way, the relative importance of a particular collisional process may be judged on the scale of interest of the experiment.

Ionization Level

An important parameter when comparing collisional processes in a plasma is its ionization level. This provides a measure of the relative concentrations of charged and neutral particles, and thus partially describes the relative collision frequencies of a charged particle with other charges and with neutrals. The long range influence of the Coulomb fields of charged particles will dominate the situation whenever more than a few percent of the gas is ionized (for temperatures of interest here). If this is the case, then our plasma will resemble a fully ionized gas for phenomena involving the transport of one type of charge relative to another, such as electron current conduction. For these processes, the exact level of ionization is no longer very important. Such knowledge will, however, still be required to describe interactions between groups of charged and neutral particles. For example, ion

momentum exchange with neutrals and electron energy loss in inelastic events, such as ionization, clearly depend on the local concentration of neutral particles. In the following discussions, we shall establish minimum levels of plasma ionization based on estimates of electron number density and temperature obtained from electrostatic probe measurements. Maximum limits on plasma ionization are difficult to impose without a priori knowledge of arc processes. For example, an overall power balance may be used to compute the amount of energy available for ionization after the kinetic and thermal energy of the flow and heat losses to electrodes have been subtracted from the total arc power. Unfortunately, uncertainties in our knowledge of plasma flow speed and temperature together with fairly reasonable assumptions as to effective ionization potential and heat losses, allow ionization levels from zero to over 200%. In any event, such overall estimates cannot be usefully applied to local plasma conditions, particularly near the cathode.

To obtain local estimates of the minimum ionization level within the arc chamber, we need to know the total particle density distribution. For our purposes, we shall assume a reasonable velocity profile in the chamber and compute heavy-particle densities using the known mass flow rate. Since the propellant gas is injected into the chamber through choked orifices from a high pressure reservoir, we expect initial heavy-particle speeds on the order of 10^3 m/s. Downstream, at the anode exhaust port, time-of-flight velocity probes indicate speeds¹⁴ of about 2×10^4 m/s. Averaging the mass flow over the entire backwall of the chamber (assuming that the injected flow rapidly expands into the lower pressure expected in the arc chamber), we have a density near the back portion of the cathode region of:

$$n_H \approx 10^{22}/m^3 \quad (3-1)$$

Downstream of the cathode tip, a factor of 10 increase in speed (to $\sim 10^4$ m/s) results in a factor of 10 lower density. From

these estimates of heavy-particle density, we see that in the back portion of the chamber, where $n_e \approx 3 \times 10^{20}/\text{m}^3$, $\alpha \approx 3\%$; while just downstream of the cathode tip, α may exceed 100% (we note that our density estimates fail to consider compression of the flow near the cathode, where n_e was measured).

It is instructive to attempt other approaches to the ionization level. For instance, if we assume that an equilibrium exists between the electrons in the plasma and the various excited states of the heavy particles, we may obtain a two-temperature "equilibrium constant" (generalized Saha equation). The chief approximation is that we may write the heavy-particle partition function as the product of a translational partition function based on the heavy-particle temperature and an internal partition function determined by the electron temperature:

$$z_H = z_{\text{trans}}(T_H) z_{\text{int}}(T_e) \quad (3-2)$$

This should hold as long as the heavy-particle temperature is less than an order of magnitude greater than the electron temperature, since electron heavy-particle collisions are more efficient for inelastic energy exchange. Assuming that neutrals and ions have the same temperature and mass, we have

$$\frac{n_e n_i}{n_A} = \frac{2 (2\pi m_e k T_e)^{3/2}}{h^3} \left\{ \frac{\sum_k g_{i,k} e^{-\epsilon_{i,k}/kT_e}}{\sum_j g_{A,j} e^{-\epsilon_{A,j}/kT_e}} \right\} e^{-\epsilon_i/kT_e} \quad (3-3)$$

where the quantity in braces is the ratio of internal partition functions of the ion and atom, and ϵ_i is the ionization potential.

Since we have both n_e and T_e from probe measurements (say $n_e = 3 \times 10^{20}/\text{m}^3$ and $kT_e = 1.5 \text{ eV}$), we may compute n_i/n_A .

For first ionization of argon, we find $n_i/n_A \approx 5000$. We would thus conclude that our plasma is fully ionized. However, we may continue this approach to discover that the concentration ratios of higher ionization levels are similarly large ($n_{i2}/n_{i1} \approx 20,000$, $n_{i3}/n_{i2} \approx 3700$, etc., where subscripts refer to doubly and triply ionized particles). Even with an order of magnitude increase in electron density this situation persists and computations with other atomic species (C, O, H) yield similar results. This indicates that the basic assumption of our approach is not valid: We do not have a balance of forward and reverse reactions on the scale of interest. That is, the ionization of the plasma has not progressed sufficiently for recombination to occur until some time after the plasma has left the arc chamber. In effect, the breakdown of an initially neutral gas in an electrical discharge is spread over the entire arc chamber by the high speed flow. In that much the same electron temperature and lower electron densities are found in the downstream exhaust, it appears that we do not achieve even a two-temperature equilibrium plasma within our apparatus. This situation has already been suggested by the rather constant level of the electron temperature throughout our system, indicating that while electrons receive energy from the electric field and later from elastic collisions with heavy particles, they continually transfer heat to excited states. The ionization level of the plasma thus derives from the kinetics of electron-atom inelastic encounters.

We may compute the mean distance travelled by an atom before ionization from our knowledge of electron density and temperature, if we assume that the ionization reaction kinetics are dominated by a simple one-step electron-atom excitation process. In argon, the first excitation potential (11.5 eV) is quite close to first ionization potential (15.7), so that excited atoms may be readily ionized. (We note that the actual reaction kinetics may be considerably more complex, so that we only obtain a rough estimate of ionization rate from this

approach.) The collision frequency for excitation may be calculated by considering the cross section for reaction as a constant ramp increase from a threshold energy, and integrating the tail of a Maxwellian electron energy distribution above this level. For $kT_e = 1.5$ eV, we have:¹⁵

$$\nu_{eA}^{EX} = (3.9 \times 10^{-18} \text{ n}^3/\text{sec})n_e \approx \nu_{eA}^{ion} \quad (3-4)$$

with $n_e = 3 \times 10^{20}/\text{m}^3$, the mean free time is:

$$\tau_{ion} \cong 8.5 \times 10^{-4} \text{ sec} \quad (3-5)$$

In the back portion of the arc chamber, we again let $u \approx 10^3$ m/sec to obtain the distance travelled by an atom before it is ionized:

$$\lambda_{ion} \cong 8.5 \times 10^{-1} \text{ m} \quad (3-6)$$

Further downstream, the flow velocity increases by about a factor of 10, but the electron density has a similar increase, so this distance remains about the same. We note that it is much greater than the chamber height (5 cm), so that we cannot expect complete ionization within the arc chamber by a simple two-step process. This correlates quite well with the failure of the quasi-equilibrium formulation.

We may estimate the distance from the injectors at which the argon flow is ionized one percent by means of a simple depletion formula:

$$n(x) = n_0 e^{-x/\lambda_{ion}} \quad (3-7)$$

For $n/n_0 = 0.99$, we have:

$$\begin{aligned} x &= \lambda_{ion} \ln(1.01) \approx 0.01 \lambda_{ion} \\ &\approx 0.85 \text{ cm} \end{aligned} \quad (3-8)$$

This is small in comparison to the extent of the cathode region, so we again find that the ionization level in this region is better than a few percent. After 5 cm of travel downstream, we would have an ionization level of about 10^{-1} . This is also consistent with previous estimates.

Spectroscopic evidence¹¹ tends to confirm these results. The appearance and intensity of various lines are, to some extent, indicators of the ionization level or, in our case, ionization progress of the plasma. For example, the H_{β} line is quite prominent throughout the discharge, requiring the existence of at least some atomic hydrogen everywhere in the chamber. Molecular carbon lines appear throughout the cathode region but become weak in the cathode jet. On the other hand, doubly ionized atomic carbon appears only in the cathode jet. This indicates that the ionization level is higher there than elsewhere in the arc chamber.

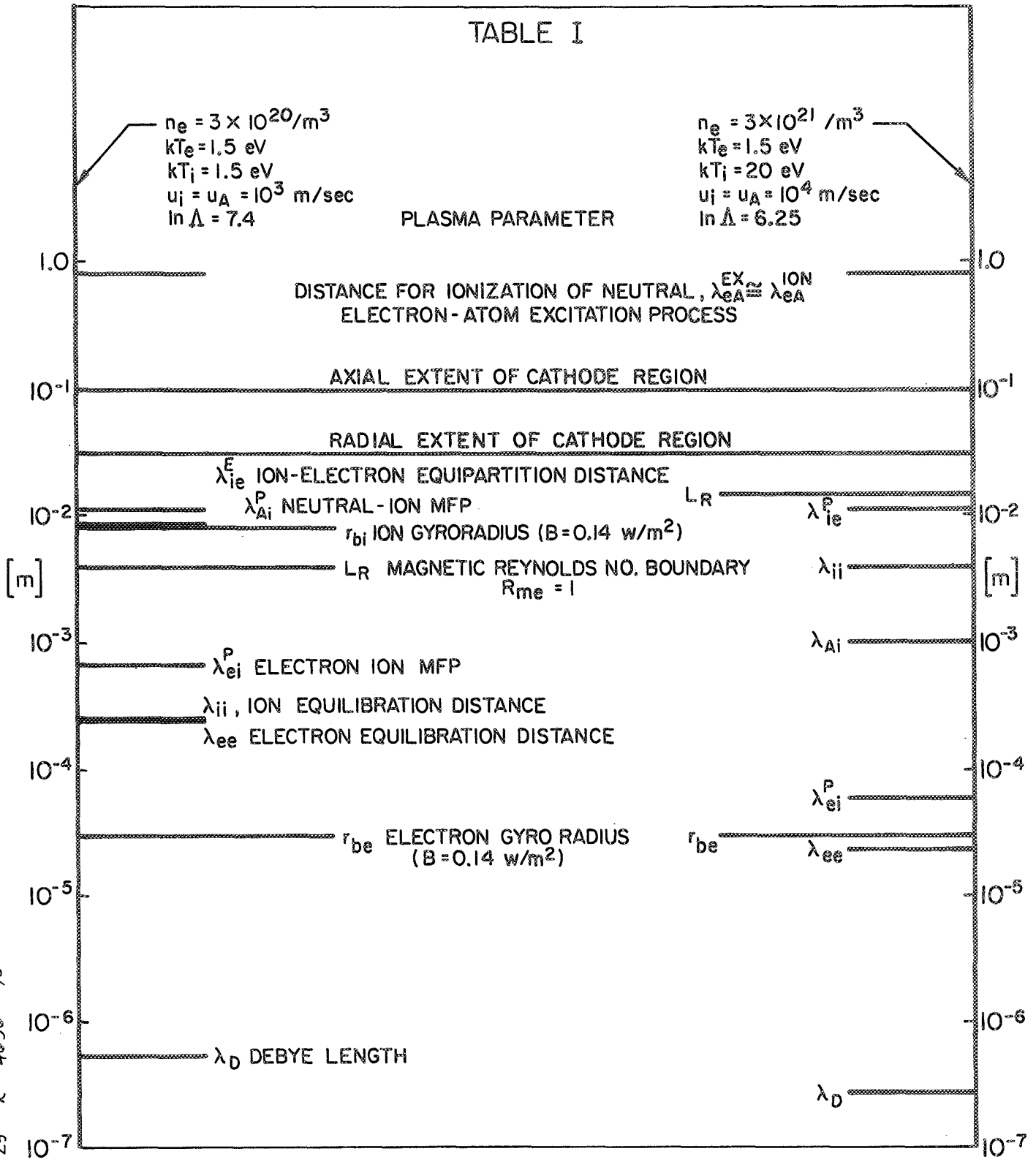
We may conclude from our discussion that the minimum level of ionization of the plasma in the cathode region progresses from a few percent at the back of the chamber to some tens of percent downstream of the cathode tip. With a better knowledge of the composition of our plasma, we may proceed to consider its electromagnetic and mechanical properties.

Debye Length

The Debye length is a measure of the collective nature of a plasma. On a scale smaller than this length, individual charges interact by means of their Coulomb fields. Over larger distances, particle motions are determined by the fields that result from the overall distribution and motion of charges. Thus, the Debye length provides a delineation between microscopic and macroscopic interactions of charged particles in a plasma. It is also the characteristic distance over which a plasma may deviate from quasi-neutrality and thereby support electrostatic fields.

In Table 3-1, the value of the Debye length, λ_D , is

TABLE I



CHARACTERISTICS OF THE CATHODE PLASMA

AP 25 R 4656 70

computed for two typical electron densities, at an electron temperature of 1.5 eV. We see that, in both cases, it is much smaller than any dimension of interest so our working fluid is always a quasi-neutral plasma.

An interesting quantity involving the Debye length is Λ , the so-called plasma parameter. This is the ratio of λ_D to the impact parameter for a 90° deflection of an electron by an ion. Computation of the Coulomb cross section assumes a binary interaction between a charged particle and each charge within one Debye length. If Λ is large, then weak deflection-binary collisions will predominate and a statistical approach may be used to compute the collision frequency.¹⁶ When Λ is not large, strong deflection-many body collisions prevail and the computational approach loses validity. The criterion separating these cases is, $\ln \Lambda \gg 1$. From Table 3-1 we see that this is not exceedingly true in our case. Thus, we are only approximately correct in employing the results of such calculations in our work.

Electrical Conductivity

An important plasma property that results from the calculations indicated above is the scalar electrical conductivity. For a fully ionized gas, this is essentially a function only of the electron temperature. We have:¹⁶

$$\begin{aligned} \sigma_0 &= \frac{C T_e^{3/2}}{\ln \Lambda} \equiv \sigma_F \\ &= (1.53 \times 10^{-2}) \frac{T_e^{3/2}}{\ln \Lambda}, \quad z = 1 \end{aligned} \quad (3-9)$$

where C is a constant for a particular ionic charge number, and $\ln \Lambda$ expresses the rather weak dependence of σ_0 on the charged-particle density.

In a partially ionized gas, electrons can collide with neutral particles, so we would expect σ_0 to depend on the ionization level. However, as mentioned earlier, Coulomb collisions predominate above an ionization level of a few percent. Thus, we should be able to use the above expression in our situation. This is confirmed by Nighan¹⁷ who has computed the electrical conductivity of partially ionized noble gases as a function of temperature, over a wide range of ionization levels.

For an electron temperature of 1.5 (\pm 0.5) eV and an ionization level between 3% and 100%, we find that the conductivity is fairly constant throughout the cathode region at $8.1 (\pm 5) \times 10^3$ mho/m. The error bars reflect the higher values of σ_0 associated with upper estimates of kT_e and the lower values for lower levels of ionization. Considering a change in ionization level from 3% at the back of the chamber to say 100% beyond the cathode tip, the conductivity would increase from 3.2 to 5.85 kmho/m, for $kT_e = 1.5$ eV. This is a rather moderate variation and reflects the diffuse nature of the arc conduction pattern at high-current levels.

It will later be shown that, when the ion velocity perpendicular to the current flow is zero, the electric field parallel to the current is just $E_{||} = j/\sigma_0$. We expect this condition to occur near the back wall of the chamber. At $r = 1/2$ in., where $j \approx 1.4 \times 10^7$ A/m² and $E_{||}$ is about 7×10^3 V/m, we obtain $\sigma_0 \approx 2 \times 10^3$ mho/m, in fair agreement with the theoretical results.

Electron-Ion Collision Frequency

From the electrical conductivity, we obtain an estimate of the frequency with which electrons lose their directed motion in collisions with ions. The Lorentz conductivity of a fully ionized gas is:

$$\sigma_L = \frac{ne e^2}{me \nu_{ei}} \quad (3-10)$$

So the collision frequency of electrons with ions is

$$\nu_{ei} = \frac{m_e e^2}{m_e \sigma_L} = \frac{m_e e^2 \gamma_E}{m_e \sigma_F} \quad (3-11)$$

where we reverse the correction due to electron-electron scattering so that we may use the computed value of conductivity for a fully ionized plasma (from Spitzer, ¹⁶ $\sigma_F/\sigma_L = \gamma_E = 0.582$ for an ionic charge of unity). With $kT_e = 1.5$ eV, we have:

$$\begin{aligned} \nu_{ei} &= (4.1 \times 10)^{-12} \text{ m}^3/\text{sec} n_e \\ &= 1.23 \times 10^9/\text{sec} \quad \text{For } n_e = 3 \times 10^{20}/\text{m}^3 \end{aligned} \quad (3-12)$$

The mean free path of an average electron, estimated using the electron thermal speed, is shown for two values of n_e in Table 3-1. We see that it is small compared to dimensions of interest.

Equilibration Times

In the same manner as the electrical conductivity, the time for a collection of charged particles to establish itself with a Maxwellian energy distribution may be computed. From Spitzer we have (with units modified):

$$t_c = \frac{(1.43 \times 10^{13}) A^{1/2} (kT)^{3/2}}{n_e Z \ln \Lambda} \quad (3-13)$$

where n_e [m^{-3}]
 kT [eV]

A = mass of particle in AMU = 1/1836 for electrons.

Thus, for electrons with $kT_e = 1.5$ eV,

$$\begin{aligned} t_c &= \frac{6.15 \times 10^{11}}{n_e} \\ &= 3 \times 10^{-10} \text{ sec} \quad , \quad \text{for } n_e = 3 \times 10^{20}/\text{m}^3 \end{aligned} \quad (3-14)$$

To check that the electrons have a Maxwellian energy distribution, we compare the rate at which energy is distributed among the electrons to the rate at which energy is transferred to and from them. This latter process includes both elastic energy exchange with ions and inelastic encounters, such as ionization. It is characterized by the electrical power dissipated in electron current conduction, j^2/σ_0 .

The highest current density present in the cathode region is at the cathode tip where $j = 5 \times 10^7$ A/m². So

$$\frac{j^2}{\sigma_0} \approx 6 \times 10^{11} \text{ W/m}^3 \quad (3-15)$$

The energy transferred among electrons may be represented as:

$$\frac{n_e kT_e}{t_c} \approx 2.4 \times 10^{13} \text{ W/m}^3 \gg \frac{j^2}{\sigma_0} \quad (3-16)$$

where n_e and t_c have been adjusted for the higher density at the cathode tip. Even in this extreme case we see that the electrons should maintain a Maxwellian energy distribution. We note that the inequality is not astronomical, which is consistent with the view that the electron temperature is determined by current conduction in the presence of inelastic phenomena, such as ionization.

To apportion the resistive heating in the plasma to elastic and inelastic processes, we must consider the heat transfer between electrons and ions due to elastic collisions. Spitzer¹⁶ provides a formula for the time required to establish two swarms of charged particles at a common temperature.

We have:

$$\begin{aligned}
 t_{eq} &= \frac{(7.34 \times 10^{12}) A_i A_e}{n_e Z^2 \ln \Lambda} \left(\frac{k T_i}{A_i} + \frac{k T_e}{A_e} \right)^{3/2} \\
 &\cong \frac{(7.34 \times 10^{12}) A_i A_e}{n_e Z^2 \ln \Lambda} \left(\frac{k T_e}{A_e} \right)^{3/2} \\
 &= \frac{3.37 \times 10^{15}}{n_e} = 1.13 \times 10^{-5} \text{ sec}, \\
 &\qquad n_e = 3 \times 10^{20} / \text{m}^3 \\
 &\qquad k T_e = 1.5 \text{ eV}
 \end{aligned}
 \tag{3-17}$$

With a plasma speed of 10^3 m/sec back in the chamber, we have a characteristic length for ion-electron equilibration of about 1 cm. (In the cathode jet, the density increases along with the velocity so the distance there is about the same.) We note that the length for energy equilibration should be about the same as the distance over which the motion of an ion will be affected by electron collisions. This indicates a reasonable degree of coupling of ions to electrons by means of elastic collisions.

Distribution of Resistive Heating

We may now compare the heat transfer rates due to resistive heating, elastic collisions, and ionization. With the equilibration time just computed, we may write the heat transfer rate from electrons to ions as:

$$\frac{n_e k T_e}{t_{eq}} = 6.4 \times 10^6 \text{ w/m}^3 \tag{3-18}$$

The energy transfer rate for ionization is the product of the frequency of ionization reactions and the effective ionization

energy (cost/ion):

$$\frac{n_A \epsilon_{iEFF}}{\tau_{ion}} = \frac{n_e \epsilon_{iEFF}}{\left(\frac{\alpha}{1-\alpha}\right) \tau_{ion}} \quad (3-19)$$

where τ_{ion} is the time for a single atom to be ionized.

As a representative current density within the arc chamber, we take $j \cong 10^6$ A/m²; so that $j^2/\sigma_0 \cong 2.5 \times 10^8$ W/m³. Then, requiring that:

$$\frac{j^2}{\sigma_0} = \frac{n_e k T_e}{t_{eq}} + \frac{n_e \epsilon_{iEFF}}{\left(\frac{\alpha}{1-\alpha}\right) \tau_{ion}} \quad (3-20)$$

we may examine the ionization of the plasma. Rearranging, we obtain:

$$\left(\frac{\alpha}{1-\alpha}\right) \tau_{ion} = \frac{n_e \epsilon_{iEFF}}{j^2/\sigma_0 - \frac{n_e k T_e}{t_{eq}}} \quad (3-21)$$

$$\approx 1.2 \times 10^{-5} \text{ sec,}$$

$$n_e = 3 \times 10^{20} / \text{m}^3$$

where we have assumed that $\epsilon_{iEFF} = 4 \epsilon_i$.

The product $(\alpha / 1 - \alpha) \tau_{ion}$ reflects the ionization progress of the plasma. When α is small, the characteristic time for ionization is long. As the gas breaks down, the possibility of further ionization increases, so τ_{ion} decreases. With $\alpha = 3 \times 10^{-2}$, we have

$$\tau_{ion} = 4 \times 10^{-4} \text{ sec} \quad (3-22)$$

in good agreement with our previous calculations, in which the ionization time was computed directly from the electron

temperature. Thus, our experimental data and theoretical analysis are consistent in terms of an electronic heat balance. The minor influence of elastic collisions in this balance indicates that the electron temperature is indeed limited by inelastic processes. We note that $(\alpha / 1 - \alpha) \zeta_{\text{ion}}$ decreases rapidly as we enter regions of higher current density. We therefore expect the ionization level of the plasma to increase well above a few percent near the cathode surface, even at the back of the arc chamber.

Heavy Particle Interactions

In principle, calculations similar to those above may be performed to illuminate heavy-particle interactions. Unfortunately, our merely qualitative knowledge of ion temperature and plasma composition limits us to rather crude estimates; these may, however, prove sufficient for our purposes.

Ion-Ion Mean Free Path

For example, the ion-ion MFP for energy equilibration or momentum exchange depends on the ion temperature and flow speed. In Table 3-1, we compute λ_{ii} for two extreme values of ion temperature, $kT_i = 1.5$ eV and 20 eV. We find that, in both cases, this distance is smaller than the extent of the cathode region. While we may not be able to follow the ion energy and momentum distribution in detail, we can reasonably speak of an ion fluid velocity and therefore use a magnetogasdynamic analysis. (The criterion is that the ion velocity is well-defined on the scale of field variation; so that $\vec{u}_{\text{aver}} \times \vec{B} = (\vec{u} \times \vec{B})_{\text{aver}}$, averaging over the volume of interest).

Ion-Neutral Collision Distance

As indicated earlier, the interaction of ions and neutrals depends on the exact level of ionization of the local plasma. We may write the distance travelled by an ion before

colliding with an atom as:

$$\lambda_{iA}^P \approx \frac{1}{n_A Q_{iA}} \quad (3-23)$$

where Q_{iA} is the total cross section for ion-neutral momentum transfer, including charge-exchange reactions (which are particularly important for argon). For relative energies less than a few hundred volts, the total cross section is greater than about $4 \times 10^{-19} \text{ m}^2$. In terms of the degree of ionization,

$$\lambda_{iA}^P \approx \left(\frac{\alpha}{1-\alpha} \right) \frac{1}{n_e Q_{iA}} \quad (3-24)$$

So, for $\alpha = 3 \times 10^{-2}$ and $n_e = 3 \times 10^{20} / \text{m}^3$, we have:

$$\lambda_{iA} \approx 2.5 \times 10^{-4} \text{ m} \quad (3-25)$$

This is quite small compared to the dimensions of the cathode region. For a mean free path greater than 1 cm, we need an ionization level above 50%, at the above density.

Reversing our point of view, the distance travelled by a neutral particle before collision with an ion is:

$$\lambda_{Ni}^P \approx \frac{1}{n_e Q_{iA}} = 8.3 \times 10^{-3} \text{ n} \quad (3-26)$$

$$\text{For } n_e = 3 \times 10^{20} / \text{m}^3$$

Thus, we may expect several ion-neutral interactions before particles leave the arc chamber. It appears, therefore, that the ions and neutrals are rather well coupled in the cathode region. In view of the small ion-neutral MFP, at low degrees of ionization, compared to the scale of field variation, we may represent this coupling as an increase in the effective mass of the ion:

$$m_{i, \text{eff}} = [1 + f(\alpha, \lambda_{iA}/L)] m_i \quad (3-27)$$

where $f(\alpha, \lambda_{iA}/L)$ expresses the degree of coupling, and its importance over a distance L . Essentially, we may treat the ions and neutrals together as a single fluid, taking care to correct terms involving charge transport or electromagnetic body forces. (For high levels of ionization, this approximation is no longer valid, but neither is it very important since few neutrals are present.)

Magnetic Interactions

The connection of the plasma to the magnetic field of the discharge occurs at two levels. The charged particles that give the plasma its electrical character experience directly a force due to their motion in the magnetic field. The extent to which this force is important in the trajectory of a particle depends on the size of the magnetic gyro radius compared to collisional mean free paths and the dimensions of the region of interest. On a macroscopic level, the plasma flow and the magnetic field are coupled through Faraday's law for a moving conductor. The degree of coupling is determined by the conductivity of the plasma and its velocity across the magnetic field.

Gyro Radii

The radius of gyration of a charged particle in a uniform magnetic field is:

$$r_b = \frac{m v_{\perp}}{Z e B} \quad (3-28)$$

where v_{\perp} is the particle speed in the plane perpendicular to the magnetic field and $Z e$ is the particle charge. For an electron, we have:

$$\begin{aligned} r_b &= \frac{m_e (2kT_e/m_e)^{1/2}}{eB} = \frac{(2m_e kT_e)^{1/2}}{eB} \\ &= 2.95 \times 10^{-5} \text{ m.} \end{aligned} \quad (3-29)$$

for a representative value of $B = 0.14 \text{ w/m}^2$ and $kT_e = 1.5 \text{ eV}$. This is quite small on our scale of interest. For argon ions, at the same temperature, we have:

$$r_{bi} = 271 r_{be} = 8 \times 10^{-3} \text{ m.} \quad (3-30)$$

Again, this is less than the dimensions of the cathode region. Thus, we are assured that the magnetic field can be of importance in our operation.

Hall Parameters

The actual influence of the magnetic field depends on the relative frequency of deflections of the particle path due to the magnetic field compared to collisions with other types of particles. This is expressed by the Hall parameter, the ratio of gyration frequency to collision frequency. For electrons in a moderately ionized gas, we have:

$$\Omega_e = \frac{\omega_{ce}}{\nu_{ei}} = \frac{eB/me}{\nu_{ei}} \quad (3-31)$$

$$= 20 \quad \text{for conditions as above}$$

This is a rather high value and indicates that the electron density in the cathode region is higher than estimated from the electrostatic probe data.

For argon ions, again at 1.5 eV, we have a total collision frequency of:

$$\nu_c \cong \frac{1}{t_{eq}} + \left(\frac{8kT_i}{\pi m_i} \right)^{1/2} / \lambda_{iA}^p \quad (3-32)$$

where the first term accounts approximately for electron-ion collisions, and the second assumes that the ion and neutral fluid speeds are the same. For $\alpha = 3\%$ and $n_e = 3 \times 10^{20} / \text{m}^3$,

we have:

$$\Omega_i = 2.8 \times 10^{-2} \quad (3-33)$$

As the ionization level increases, however, Ω_i also increases, so that near the cathode, it may exceed 0.5. Thus, as we approach the cathode surface, the importance of the magnetic field increases. This is because of the higher ionization levels associated with higher current densities; in addition to the increase in magnetic field strength.

We see that, as expected, the magnetic field exerts a considerable influence on the motions of charged particles in the cathode region. On the other hand, the magnetic field is itself determined in part by the collective motions of charged particles.

Magnetic Reynolds Number

It will later be shown that the degree of coupling between the plasma flow and the magnetic field is characterized by the magnetic Reynolds number based on the electron flow speed, written here as:

$$R_{me} = \sigma \mu_0 u_e L \quad (3-34)$$

For $R_{me} \gg 1$, coupling to the flow is strong and the field lines distend downstream. If $R_{me} \ll 1$, on the other hand, the magnetic field distribution is determined by the electrode geometry and the conductivity distribution. The latter case is the usual thermal arc, while the former is an aspect of high-current MPD accelerators. In our situation, we have $\sigma = 8(\pm 5) \text{ kmho/m}$ and $u_e \approx j/n_e e \approx 2 \times 10^4 \text{ m/sec}$ for $j = 10^6 \text{ A/m}^2$. So

$$\begin{aligned} R_{me} &= 8\pi\sigma L, \quad \sigma [\text{kmho/m}] \\ &= 2(\pm 1.25)L, \quad L [\text{cm.}] \end{aligned} \quad (3-35)$$

For $R_{me}=1$,

$$L_R = 3 \text{ mm. to } 1.3 \text{ cm.} \quad (3-36)$$

This distance delineates between the two extremes. Thus, on the scale of the cathode region convective effects are significant. (As we approach the cathode surface, the current density increases inversely with L ; so coupling improves in this direction only because of the higher σ at higher ionization levels.)

From both microscopic and macroscopic points of view, therefore, we are justified in differentiating our device from the usual (thermal) arcjet by the term magnetoplasmdynamic.

Summary

In Table 3-1, we collect the quantitative results of our discussions in terms of characteristic distances for interaction. We see that all such distances are smaller than the dimensions of the cathode region, with the exception of the ionization mean free path. The relative size of this last quantity indicates the chemical nonequilibrium of our flow and suggests the progress of ionization from a few percent to some tens of percent through the cathode region.

For all other processes, the scales of events are sufficient to place us in a transition flow regime (as opposed to free particle on continuum flow) with respect to coupling between different types of particles within the cathode region. We find, however, that the electrons can maintain themselves with a Maxwellian energy distribution at a temperature of about 1.5 eV; determined by a balance primarily between resistive heating and cooling due to ionization. Although we cannot treat the plasma exactly, we may utilize both gasdynamic and particle kinetic approaches to reveal various aspects of the problem. (This was anticipated by the free particle vs. continuum models for the MPD arcjet.) We note that

slightly higher charged-particle densities (than indicated by our measurements) do not radically change this situation, since we remain in the transition flow regime. The exception is again ionization which would progress faster to higher levels. It is important to keep in mind that the dimensions of the cathode region are not fixed. Rather, they are determined in the same manner by which the cathode fall extent of a glow discharge depends on collisional MFP's or viscous boundary layer thickness depends on Reynolds number.

The magnetic field complicates matters further. We find that its effect on charged-particle motions is quite significant. In particular, the electron Hall parameter is much greater than unity upstream of the cathode tip, suggesting tensor and/or ion current conduction there. The scalar electrical conductivity of the plasma is rather uniform throughout the cathode region at $\sigma = 8 (\pm 5)$ kmho/m. This reflects the diffuse conduction pattern in the cathode region at high-current levels, similar to the diffuse mode current attachment at the cathode in static, high-current arcs. The high conductivity and estimated electron flow speed together indicate substantial coupling of the magnetic field distribution (and thus the conduction pattern) to the plasma flow. At higher charged-particle densities, this coupling diminishes somewhat. On a microscopic level, collisional MFP's become more important compared to gyro radii. While in continuum terms, the electron flow speed for a given current level decreases so the electron magnetic Reynolds number is smaller. Magnetic interaction still occurs but at locations closer to the cathode surface. Thus, as with collisional phenomena, our physical picture remains the same.

In a few long words, then, the cathode is enveloped by a magnetoplasma dynamic transition flow of ionizing gas. We now proceed to examine the electromagnetic structure of this flow.

CHAPTER 4

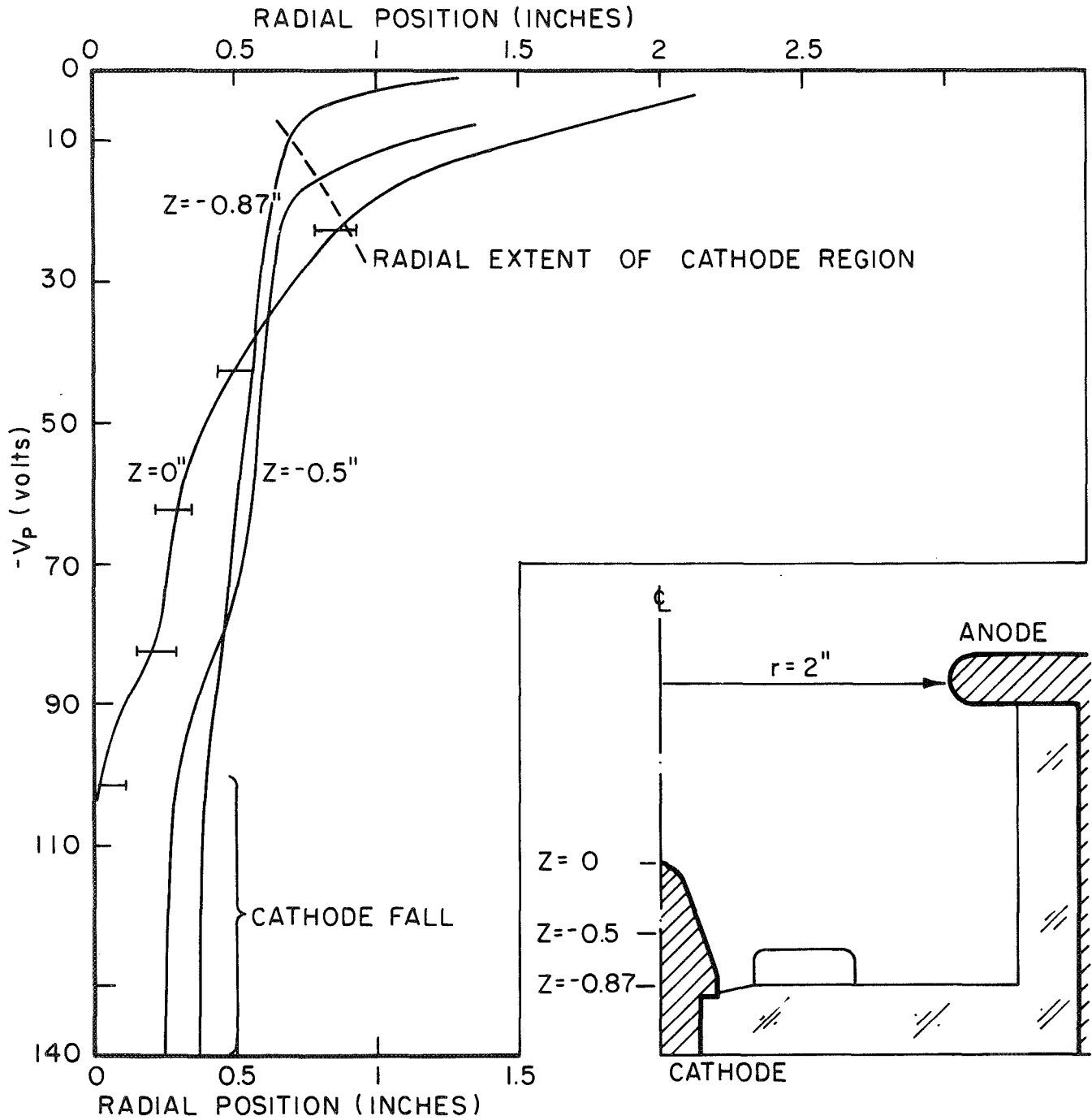
DISCHARGE STRUCTURE

The electromagnetic structure of an MPD discharge results from the conduction of high current through low density gas. The high-current level creates a substantial magnetic body force in the plasma, leading to high flow speeds. The plasma flow in turn affects the current conduction pattern and, thus, the magnetic body force distribution. At these strong magnetic fields and low particle densities, electron Hall parameters often exceed unity, so tensor and/or ion current conduction may prevail. We shall now analyze the experimentally determined electric and magnetic field distributions within the cathode region to reveal current conduction and plasma acceleration processes.

Voltage Distribution

The voltage distribution through a discharge may be used to delineate regions of interest. Typically, we have high field layers (rapid voltage changes with position) associated with both electrodes, separated by a moderate field region or column. In Fig. 4-1 the plasma potential is plotted versus radial position within the arc chamber for three representative stations along the cathode. Plasma potential was obtained from floating probe data by the subtraction of $\Delta v = (kT_e/e) \ln (m_{\text{argon}}/m_e)^{1/2}$ from the values shown in Fig. 2-11. (As mentioned there, this is only approximately correct since we do not know the exact ratio of ion-to-electron saturation currents.)

We see that the field zone of the cathode extends one or two (base) radii from the cathode surface and involves over



PLASMA POTENTIAL vs RADIAL POSITION

FIGURE 4-1

AP 25 R 4052 70

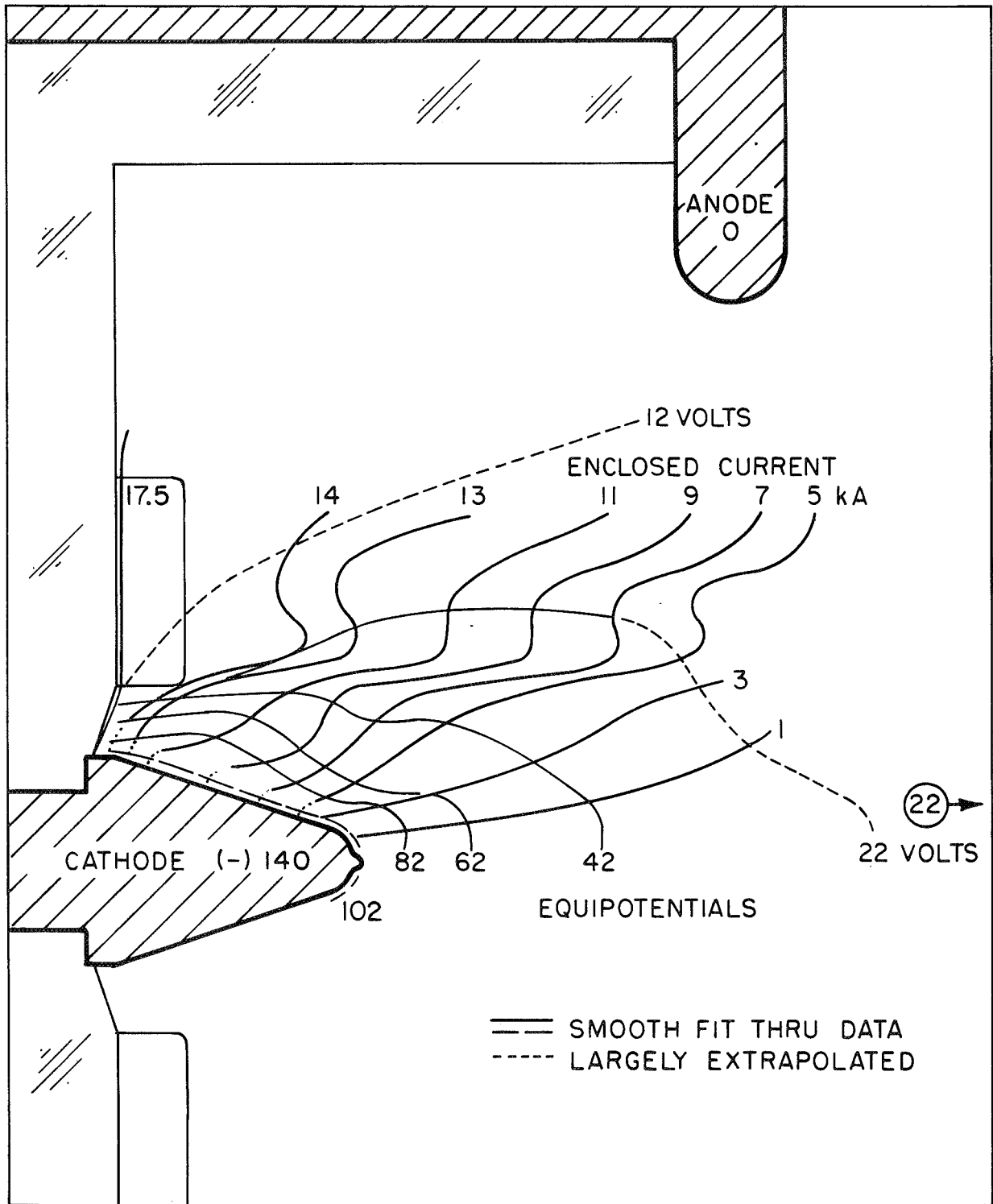
80% of the total arc voltage. Within the cathode field zone, a sharp voltage change occurs adjacent to the cathode surface. We shall refer to this increment (of 38 V) as the cathode fall. A voltage drop of 80 V to 90 V occurs across the rest of the cathode region, where, as we have seen, a transition flow of ionizing gas exists.

The cathode region may thus be separated into a cathode surface layer or sheath, and a more moderate field, quasi-neutral envelope. The first region is similar to that in more common arcs, while the second resembles the cathode region in a glow discharge, in that it is many MFP's in extent and supports a rather large voltage difference. In this latter region, ions (and potential ions) are brought to the vicinity of the cathode surface, where bombardment and electron emission occurs. We have previously referred to this region as the convective zone. Our primary concern in this chapter will be with the operation of this portion of the cathode region.

We note, in passing, that the remainder of the arc voltage (about 20 V) may be associated with conduction across the injected flow of argon atoms, since their ionization potential is numerically similar (15.7 V). The resistive field across this flow increases until sufficient ionization reactions occur to provide additional charge carriers. (Hence, we expect the voltage drop to resemble the ionization potential). In our case, the anode is rather removed from regions of high particle density so we associate the voltage drop beyond the cathode region with the injected gas, rather than with a neutral gas layer at the anode surface. The anode then behaves merely as a probe, whose sheath voltage is determined from electrostatic probe theory.

Overall Discharge Structure

In Fig. 4-2 we present a combined plot of enclosed current contours and equipotential lines. The current lines have been smoothed within the error bars of the data, while the values of the potential contours have been adjusted to



CURRENT STREAMLINES AND EQUIPOTENTIALS

FIGURE 4-2

represent plasma potential more accurately. Several things are immediately revealed by this plot.

First of all, we see that the current flow is not everywhere parallel to the electric field. At first glance, this suggests tensor current conduction in much of the cathode region. The exact mechanism of conduction, however, depends in part on the plasma flow (back emf) and will be considered in detail later.

We also see the distribution of electrical power within the arc. At each area, this is just the product of the current enclosed between adjacent contours and the voltage difference between equipotentials. The total electrical power input to the arc (2.45 MW) may be apportioned approximately to various regions of the discharge as follows: (Note that at the junction of the cathode base and insulator backwall, the enclosed current is 14 kA; thus 3.5 kA travel very close to the insulator there. Since this insulator is seriously eroded, we label this area the ablation jet.)

	ΔV	J_{en}	% Total Power	
Cathode fall.....	38 V	17.5 kA	27.0	} 85.7%
Ablation jet.....	90 V	3.5 kA	13.0	
Cathode plasma.....	80 V	14.0 kA	45.7	
Elsewhere in arc chamber.....			14.3	

A direct result is that 85% of the total arc power is deposited in the cathode region. We also see that more than a quarter of the total power is involved in the cathode fall. This indicates that the cathode surface layer may have an important role in plasma acceleration. Since we expect pressure gradients to be significant near the cathode surface, a continuum or electrothermal aspect of MPD arcjet operation is suggested there.

The distribution of electrical power correlates with the luminosity pattern shown in Fig. 2-3e. Regions of more intense power deposition are most prominent. For example, the bright green regions, labelled as ablation jets, involve over 12% of the total arc power. Downstream of the cathode tip, a smaller amount of power is deposited in a somewhat smaller volume, but in the presence of higher particle densities, so that this region is quite bright. Beyond the cathode region, however, the small fraction of arc power remaining is distributed over a large volume and little luminosity is evident. The overall picture obtained from the field patterns confirms the impression provided by the light intensity distribution: The cathode region is of primary importance in MPD arcjet performance.

Current Conduction

Electric current is the relative motion of opposite charges. In an MPD discharge, the current conduction pattern and the electric and magnetic field distributions form a dynamical system, coupled through the equations of motion of the oppositely charged species. As we have seen, the electron energy equation establishes the nature of the plasma, in terms of a balance between resistive heating and ionization. We shall now show that the electron momentum equation provides a link between the field structure and the conduction pattern.

Previously, we obtained that the collisional MFP's for an electron are much smaller than the dimensions of the cathode region. The velocity of the electron fluid should, therefore, be well-defined and we may write its momentum equation as:

$$m_e m_e \frac{D\vec{u}_e}{Dt} = -m_e e [\vec{E} + \vec{u}_e \times \vec{B}] - \nabla P_e - m_e m_e (\vec{u}_e - \vec{u}_i) \nu_c^p \quad (4-1)$$

The last term approximates the drag force of the ions on the electrons by means of the collision frequency for.

momentum transfer (we choose this form for its simplicity and because it leads to a result that is consistent with Ohm's law for less involved situations). We have ignored collisions between electrons and neutrals since the ionization level is above a few percent. Included in this neglect is the force associated with accelerating new electrons created by ionization. This term is much smaller than the ion-electron drag force since the electron collision frequency for ionization is much lower than that for elastic momentum transfer with ions. As indicated above, electron-neutral collisions influence the situation through the electron energy equation. We note that, if our approach is valid, the ion fluid velocity should also be well-defined. Again, our previous calculations show that ion collisional MFP's are smaller than field dimensions, so that the ions can establish a meaningful average velocity.

Both the collisional mean free path and gyro radius of the electron are much smaller than the dimensions of our region, so the scale of the electron acceleration process is much smaller than that of interest. For this reason, we neglect the inertial term on the left in our equation. In this approximation, electrons respond immediately to the force structure created by the fields and plasma flow. We now rearrange our terms to obtain the relationship between the electromagnetic fields and the current flow.

The collisional term may be written as:

$$-m_e m_e (\bar{u}_e - \bar{u}_i) \nu_c^p = \frac{m_e \nu_c^p}{e} \vec{j}, \quad \sum_{z=1} \quad (4-2)$$

so

$$\frac{m_e \nu_c^p}{e} \vec{j} = m_e e [\vec{E} + \bar{u}_e \times \vec{B}] + \nabla P_e \quad (4-3)$$

Then

$$\begin{aligned} \vec{j} &= \frac{m_e e^2}{m_e \nu_c^p} \left[\vec{E} + \bar{u}_e \times \vec{B} + \frac{\nabla P_e}{m_e e} \right] \\ &= \sigma_0 \left[\vec{E} + \bar{u}_e \times \vec{B} + \frac{\nabla P_e}{m_e e} \right] \end{aligned} \quad (4-4)$$

where we write the proportionality constant as the scalar conductivity, discussed earlier. (Our purpose here is to display the influence of the magnetic field and pressure gradients on current conduction, not to repeat the sophisticated analyses of electron collision phenomena.) We have used ν_c^p in a symbolic way to relate the current density and the collisional drag force, both of which involve the relative motion of opposite charges. For a moderately ionized gas in which the ionic charge number is unity, our equation may be deduced from other forms of Ohm's law for a plasma flow.

The Electric Field

It is common to express the current density as a function of the electric field, as we have done. It is also misleading. The independent variable in our operation is the current level. The voltage distribution is determined by the conductivity, magnetic field and plasma flow that result at this current level, for a given particle (and mass) density. In analogy with fluid flow in a nozzle, we prescribe a certain mass flow and the pressure distribution is then determined. If the pressure at some station is inconsistent with other requirements, then either a pressure jump occurs or the input mass flow must change. Similarly, if the voltage required for current conduction is inconsistent with other physical processes, either sheaths will form or the total current will adjust.

Thus, the electric field in a plasma arises from the need to conduct current in the presence of collisions, magnetic fields, and pressure gradients. So, we should actually write:

$$\vec{E} = \eta \vec{j} - \vec{u}_e \times \vec{B} - \frac{\nabla p_e}{n_e e} \quad , \quad (4-5)$$

$$\eta = \frac{1}{\sigma_c}$$

Electron Motion

From our generalized Ohm's law, we may derive formulas for the electron motion parallel and perpendicular to the current flow. We have:

$$\vec{u}_e \times \vec{B} = \vec{j} / \sigma_0 - \left(\vec{E} + \frac{\nabla P_e}{m_e e} \right) = \vec{j} / \sigma_0 - \vec{E}', \quad (4-6)$$

$$\vec{E}' = \vec{E} + \frac{\nabla P_e}{m_e e}$$

Then the electron velocity parallel to the current flow is obtained from the vector product of the above equation with \vec{j} :

$$\begin{aligned} \vec{j} \times (\vec{u}_e \times \vec{B}) &= -\vec{j} \times \vec{E}' \\ &= \vec{u}_e (\vec{j} \cdot \vec{B}) - \vec{B} (\vec{j} \cdot \vec{u}_e) \\ &= -\vec{B} j u_{e||} \end{aligned} \quad (4-7)$$

so

$$u_{e||} = \frac{\vec{B} \cdot (\vec{j} \times \vec{E}')}{j B^2} = \frac{-\vec{E}' \cdot (\vec{j} \times \vec{B})}{B j B} \quad (4-8)$$

where $u_{e||}$ is the component of \vec{u}_e parallel to \vec{j} . Defining E'_\perp by the scalar product above, we have:

$$u_{e||} = -\frac{E'_\perp}{B} \quad (4-9)$$

For the component of \vec{u}_e perpendicular to \vec{j} , we use the scalar product of \vec{j} with Ohm's law:

$$\begin{aligned} \vec{j} \cdot (\vec{u}_e \times \vec{B}) &= j^2 / \sigma_0 - \vec{j} \cdot \vec{E}' \\ &= -\vec{u}_e \cdot (\vec{j} \times \vec{B}) = -u_{e\perp} j B \end{aligned} \quad (4-10)$$

So

$$u_{e\perp} = \frac{E_{\parallel}' - j/\sigma_0}{B} \quad (4-11)$$

We note that $u_{e\perp} = u_{i\perp}$ since $j_{\perp} \equiv 0$. The other component of ion velocity is related to \vec{u}_e through the current density:

$$u_{i\parallel} = \frac{j}{m_e e} + u_{e\parallel} = \frac{j}{m_e e} - \frac{E_{\perp}'}{B} \quad (4-12)$$

Expressions of such simple form are normally found only in certain special situations. (For instance, $u_{e\parallel} = -E_{\perp}/B$ is usually related to the cross field drift of a collisionless, gyrating electron.) Our results obtain, however, because of the special way we have chosen components. The current density, magnetic field, and $\vec{j} \times \vec{B}$ force in this sense provide a natural coordinate system for a magnetoplasma dynamic discharge.

The usefulness of these formulas derives from our knowledge of the electromagnetic structure of the discharge. We are in reality solving the problem in reverse. The current density, ion velocity, and particle density define the electron motion. The magnetic field and pressure distributions are also coupled to the geometry of current conduction and the mechanics of the ion flow. The electric field distribution is a result of this dynamical system.

Ion Motion

This viewpoint is particularly important in understanding ion acceleration and current conduction. We may write the ion momentum equation as:

$$n_i m_i \frac{D\vec{u}_i}{Dt} = n_i e [\vec{E} + \vec{u}_i \times \vec{B}] - \nabla P_i + m_e m_e (\vec{u}_e - \vec{u}_i) \mathcal{V}_i^p + \vec{P}_{in} \quad (4-13)$$

where the last two terms represent the force due to collisions

with electrons and atoms, respectively. Substituting for the electric field, we have:

$$n_i m_i \frac{D\vec{u}_i}{Dt} = m_e e (\vec{u}_i - \vec{u}_e) \times \vec{B} - \nabla(P_i + P_e) + \vec{F}_{iA} \quad (4-14)$$

$$= \vec{j} \times \vec{B} - \nabla(P_i + P_e) + \vec{F}_{iA}$$

It is important to note that in this equation the net electrical force acting on an ion in a plasma is the $\vec{j} \times \vec{B}$ force. Ion acceleration occurs only in this direction, which is not necessarily parallel to the electric field measured in the laboratory. The measured electric field includes a resistive component which arises to balance exactly the collision drag force between ions and electrons.

Neglecting pressure gradients, ions will participate in current conduction only insofar as the $\vec{j} \times \vec{B}$ force in one part of the discharge accelerates them parallel to the current density further downstream. Examining our current pattern, we see that the $\vec{j} \times \vec{B}$ vector does not change direction much in the cathode region. This indicates that ion motion may always be normal to the current flow and, therefore, electron current will predominate. We may investigate this further by considering the ion kinetic energy.

Returning to the ion momentum equation, we include the effects of ion-atom collisions by the addition of the atom momentum equation:

$$n_A m_A \frac{D\vec{u}_A}{Dt} = -\vec{F}_{iA} - \nabla P_A \quad (4-15)$$

Assuming good coupling between ions and atoms, based on our previous computations, so that $\vec{u}_A \cong \vec{u}_i$, we have:

$$n m_i \frac{D\vec{u}}{Dt} = \vec{j} \times \vec{B} - \nabla P_p \quad (4-16)$$

where P_p is the total plasma pressure ($P_i + P_e + P_A$), and $n = n_i + n_A$. In terms of the ionization level, then:

$$\frac{m_e}{\alpha} m_i \frac{D\vec{u}}{Dt} = \vec{j} \times \vec{B} - \nabla P_p \quad (4-17)$$

The kinetic energy of a heavy particle due to acceleration by the $\vec{j} \times \vec{B}$ force is then (in volts):

$$\mathcal{E} = \int \frac{jB}{m_e} dx_{\perp} = \int \alpha \frac{jB}{m_e e} dx_{\perp} \quad (4-18)$$

The maximum energy acquired by an ion occurs when $\alpha = 1$.

If the electrons carry all the current, we have:

$$jB = m_e e E_{\perp} \quad (4-19)$$

so the maximum kinetic energy of an ion is:

$$\mathcal{E} = \int E_{\perp} dx_{\perp} = \int \vec{E} \cdot \vec{dl} = (V - V_0)_{\text{ALONG } X_{\perp}} \quad (4-20)$$

where we note that the ion motion is parallel to \hat{X}_{\perp} under these conditions. Thus, the maximum ion kinetic energy is just the voltage difference along its path. For this maximum condition, we assumed $\alpha = 1$, with all ions created at the beginning of the acceleration path. Therefore, since V_0 is about the same for all trajectories in the cathode region, the maximum ion kinetic energy at any location just depends on the local voltage.

On the other hand, we have the case of strictly ion current. The maximum kinetic energy of an ion is obtained when its motion is collisionless, since energy is otherwise lost to electrons and atoms. This maximum energy is given by the

voltage difference along the ion's path from its origin. If we again assume that ions are all created at the same potential, V_0 , in the low field region near the injectors (since this provides the maximum voltage difference), then the ion kinetic energy is again determined at any point by the local voltage.

From the measured distributions of electric and magnetic field and current density, we may compute the electron speed normal to the current flow. Since this is also the ion speed in that direction, we may therefore calculate the kinetic energy associated with ion motion normal to the current flow. We also know the voltage at the same location, so we may compare this kinetic energy with the maximum possible ion kinetic energy. In this way, we may assess the distribution of ion energy to motion parallel and perpendicular to the current flow.

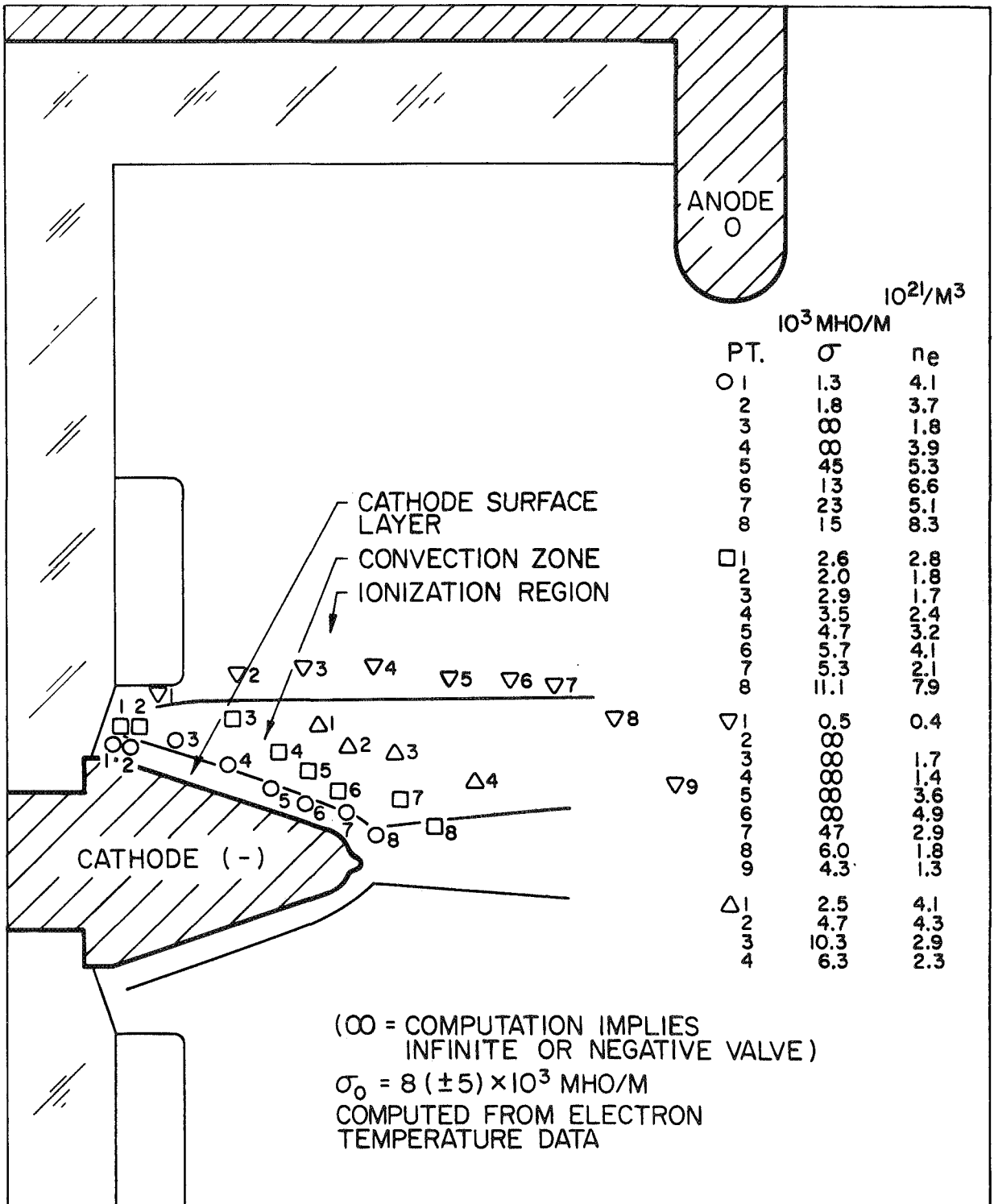
We perform this comparison by calculating the conductivity of the plasma from the field data, based on the maximum possible ion speed normal to the current flow. We have:

$$u_{e\perp} = u_{i\perp} \leq \left(\frac{ze}{m_i} (V - V_0) \right)^{1/2} \quad (4-21)$$

so, the scalar conductivity is:

$$\sigma_c = \frac{j}{E_{\parallel}' - u_{e\perp} B} \leq \frac{j}{E_{\parallel}' - \left(\frac{ze}{m_i} (V - V_0) \right)^{1/2} B} \quad (4-22)$$

If we ignore the electron pressure gradient effects, we find that σ_c is less than or equal to the value previously computed from the electron temperature, everywhere in the cathode region, except near the cathode surface and near the gas injection region, where it is much higher (see Fig. 4-3).



CONDUCTIVITIES AND ELECTRON DENSITIES COMPUTED FROM FIELD DATA

FIGURE 4-3

AP 42 K 7077 70

These latter cases indicate that strong electron density gradients (associated with the cathode surface plasma and gas ionization, respectively), supplement the electric field measured in the direction of current flow. (That is, $E_{\parallel}' > E_{\parallel}$, in these regions.) Thus, ion motion normal to the current flow accounts for essentially all the ion kinetic energy, and we may conclude that little energy is associated with ion motion parallel to the current flow.

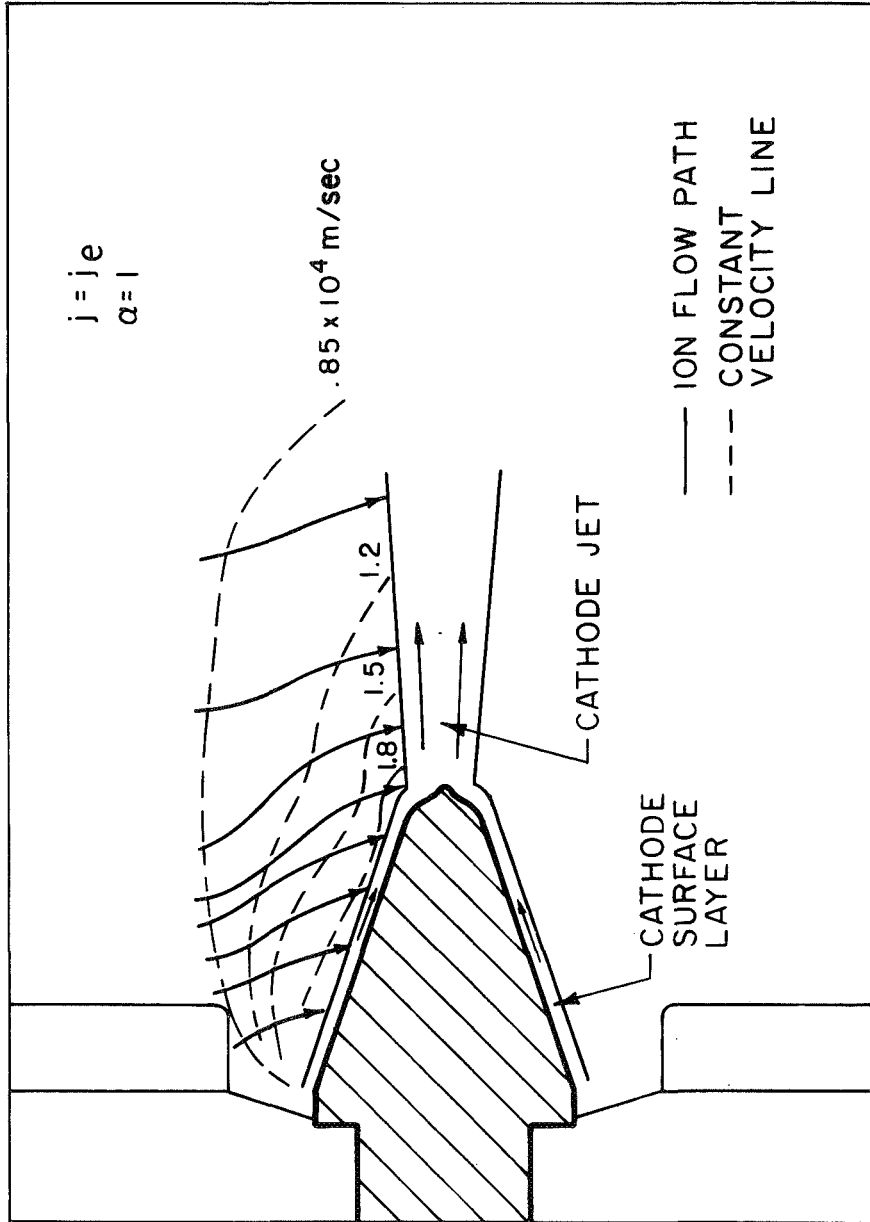
Our present results are based on the nature of the plasma and the voltage distribution within the cathode region, while our previous estimates of ion motion derive from the geometry of the current pattern. The consistency obtained assures us that the convective zone is characterized by electron, rather than ion, current conduction. Ion flow paths are shown in Fig. 4-4, along with the ion speed at various stations. It was assumed here that the ionization level was unity, so that with $j = j_e$ the ion kinetic energy is just:

$$\mathcal{E}_i = \int \frac{jB}{m_e e} dx_{\perp} = (V - V_c)_{\text{ALONG } x_{\perp}} \quad (4-23)$$

It is important to note that our integration terminates near the centerline (or cathode surface) of our device, since pressure gradients must be included there. Above all, observe that the relation between ion kinetic energy and voltage obtains only along an ion trajectory parallel to the $\vec{j} \times \vec{B}$ force. Again: The net electrical force on an ion in a plasma discharge is the $\vec{j} \times \vec{B}$ force, not the gradient in electric potential. The ion does not lose its kinetic energy in leaving the vicinity of the cathode as would be implied by a collisionless, electrostatic acceleration model. The force exerted on the ion by the electric field in the cathode jet is exactly balanced by the collision force of electrons.

The Cathode Plasma Revisited

Given that all the current in the convective zone is



ION FLOW IN CATHODE REGION

FIGURE 4-4

AP25 2 4612 70

carried by electrons, we may compute the electron density from the field data. We have: $j = j_e = n_e e E / B$. So

$$n_e = \frac{j B}{e E_{\perp}} \quad (4-24)$$

We observe that this equation expresses the balance of electric and magnetic forces on the electrons in the direction normal to the current flow. If this balance did not occur, electrons would accelerate away from the ions in this direction, violating the condition that $j_{\perp} = 0$.

Using this formula, we compute electron densities that are about an order of magnitude higher than our estimates based on the electrostatic probe data. As indicated earlier, electric probe results will tend to underestimate particle densities because of collisional and magnetic field effects. Such measurements are important as lower bounds on the particle densities since we needed to justify the use of a magnetogasdynamic formulation before we could proceed. We note that the electron velocities parallel to the current are everywhere greater than the maximum ion velocities, so that ion contribution to the current conduction will not greatly affect the plasma densities computed by the above formula. Such densities are displayed in Fig. 4-3 at various positions in the cathode region.

As already indicated in the previous chapter, higher charged-particle densities imply higher ionization levels and more nearly continuum flow. These changes improve the applicability of the MGD formulation. The dominance of the electron current conduction process is further assured by the higher values of σ computed from the electron temperature at higher ionization levels.

Electron Pressure Gradients

Our computations indicate that the charged-particle density does not vary greatly through the cathode region,

except near the boundaries. Since the electron temperature is also rather uniform, the electron pressure gradient does not contribute significantly to current conduction in the convective zone.

At the edges of this region, however, we do expect sharp changes in electron pressure. For example, the electron density should decrease rapidly as we approach the injector orifices. This leads to pressure gradients both parallel and perpendicular to the current flow. The addition of the latter to E_{\perp} in this region would reduce the computed electron density and thus remove the apparent but questionable increase in density there. Further into the injector flow, the downstream progress of ionization introduces an axial pressure gradient that may explain the inflection of the current lines there, since no strong field effect is evident.

The increase in electron density at the cathode surface reflects the plasma pressure gradient that must exist there to turn the radially directed ion flow into an axial exhaust. We shall discuss the region further in the next chapter.

Summary

We have been concerned with the flow of current and plasma in the convective zone of the cathode region. The overall discharge structure indicates that almost 60% of the total arc power is involved in this zone, while more than a quarter of the arc power is associated with the cathode surface layer.

The motions of ions and electrons are considered using a magnetogasdynamic formulation. It is seen that the electric field in the plasma results from the need to conduct current in the presence of collisions, magnetic fields, and pressure gradients. The gradient of electric potential thus reflects the conduction process; it does not determine the ion motion. The net electrical force acting on the ion fluid is the $\vec{j} \times \vec{B}$ force.

Examination of the current pattern then indicates that

the ion flow should generally be normal to the current flow. While a minor amount of ion current may occur in some portions of the discharge, considerations of the energy available to the ion indicate that current conduction is primarily accomplished by electrons in a tensor manner.

The ion flow is directed inward by the $\vec{j} \times \vec{B}$ force toward the cathode and the arcjet centerline. Radial flow speeds of about 1.8×10^4 m/sec are attained near the cathode surface, comparable to exhaust velocities measured in the arcjet plume ($\sim 2 \times 10^4$ m/sec). Pressure gradients at the cathode surface are required to turn the radial ion flow axially downstream. Computations of plasma conductivity and electron number density indicate that such gradients indeed occur. This recalls the "pumping mode" of MPD arcjet operation.⁴ In our case, this process is not confined to the cathode jet but extends upstream over the lateral surface of the cathode.

CHAPTER 5

THE CATHODE SURFACE LAYER

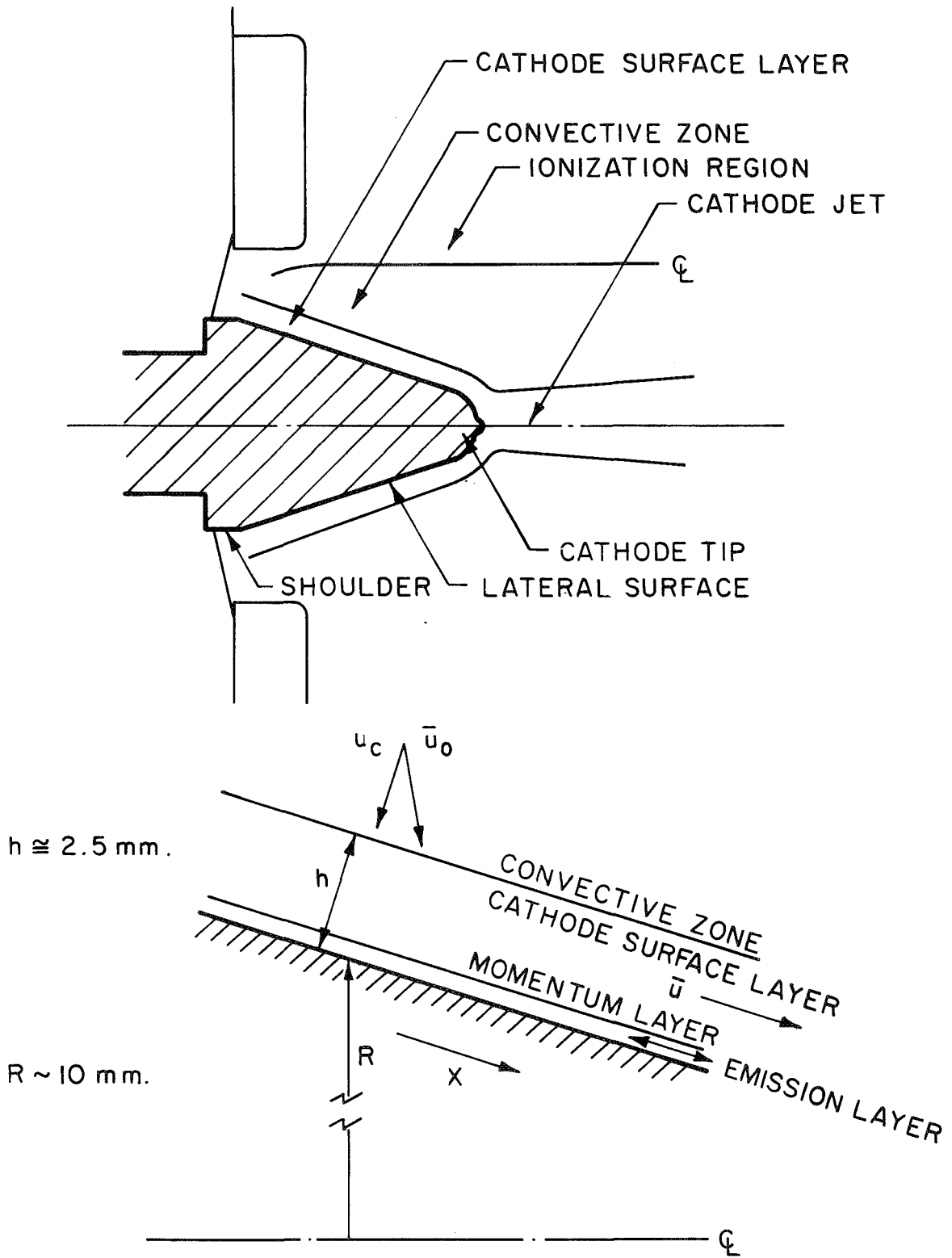
In the preceding chapter, we analyzed the discharge structure in the convective zone and found that a high speed plasma flow is delivered to the immediate vicinity of the cathode surface. We also indicated that pressure gradients should be significant near the surface. We now continue the analysis of our experimental situation into this portion of the cathode region, which we label the cathode surface layer (see Fig. 5-1).

Three processes of critical importance to MPD arcjet performance are involved here: Deflection of the radial plasma flow into an axial, thrust-producing direction; protection of the cathode surface from erosion by this high-energy flow; and conduction of current across the cathode-plasma interface. All this occurs within a few millimeters of the cathode surface. Since this is beyond the resolution of our experiment, we must concern ourselves with the overall characteristics of the plasma flow, and conduction and emission processes. Our primary interest will be with the layer adjacent to the lateral surface of the cathode. The cathode tip involves some special phenomena that depend to a large extent on the flow along the slope, and will therefore be considered later.

Nature of the Flow Problem

We may understand the nature of the flow near the cathode surface by supposing that no deflection occurs, so that the current density at the cathode surface is just the unobstructed ion flow. Assuming recombination of these ions at the cathode,

DELINEATION OF THE CATHODE REGION



AP 25 R 4653 70

DETAILS OF CATHODE SURFACE LAYER

FIGURE 5-1

the distance travelled by the resulting neutral atoms is:

$$\lambda_{Ai} \cong \frac{V_{thA}}{m_i v_i Q_{Ai}} = \frac{V_{thA}}{\frac{j_i Q_{Ai}}{e}} \quad (5-1)$$

$$\approx 3.5 \times 10^{-5} \text{ m}$$

where $j_i = j \cong 1.5 \times 10^7 \text{ A/m}^2$, $Q_{Ai} \approx 4 \times 10^{-19} \text{ m}^2$, and V_{thA} is the mean thermal speed of the returning atoms, based on a surface temperature $T_W = 3000^\circ \text{ K}$, (an upper estimate used to obtain the maximum value of λ_{Ai}). This distance is much smaller than the dimensions of the cathode surface layer ($\approx 2.5 \text{ mm}$), so the incoming ions will experience many collisions in this region. Thus, it appears that a continuum flow situation exists near the cathode surface. Since the directed speed of the heavy particles from the convective zone greatly exceeds their random (thermal) speed, our problem resembles the interaction of a hypersonic flow with a blunt body. Such a flow is too complex to treat in detail here, along with the additional complications of electromagnetic body forces and current conduction. We shall therefore return to our magnetogasdynamic formulation to determine the plasma flow from the electromagnetic structure of the surface layer.

MGD Analysis Including Pressure Gradients

In the previous chapter, we saw that the effect of an electron pressure gradient must be included in our generalized Ohm's law calculations near the cathode surface. That is, the electric field there is:

$$\vec{E} = \gamma \vec{j} - \vec{u}_e \times \vec{B} - \frac{1}{m_{ee}} \nabla P_e \quad (5-2)$$

or

$$\vec{E} = \gamma \vec{j} - \vec{u} \times \vec{B} + \frac{\vec{j} \times \vec{B}}{m_{ee}} - \frac{1}{m_{ee}} \nabla P_e \quad (5-3)$$

where \vec{u} is the velocity of our highly ionized plasma flow.

We shall show in the next chapter that current flow becomes normal to the cathode surface in a region adjacent to the cathode. The criterion is that the magnetic Reynolds number based on the electron flow speed is small in this region. In our case, we have:

$$R_{me} = \sigma \mu u_e L \approx .28 \quad (5-4)$$

with $\sigma \cong 5 \times 10^3$ mho/m, $u_e \cong 1.8 \times 10^4$ m/s, and $L (= h) \cong 2.5 \times 10^{-3}$ m. Thus, at the edge of the cathode surface layer, our current flow lines should turn to enter the cathode normally. Within the cathode surface layer, we shall therefore simplify our problem by assuming that \vec{j} and \vec{E} are both perpendicular to the surface (and are thereby parallel). We have then that:

$$E = \eta j + uB - \frac{1}{m_e e} \frac{\partial P_e}{\partial x_{||}} \quad (5-5)$$

where u is the plasma flow speed along the cathode surface.

Approximate Equations for the Surface Layer Flow

Rearranging the last equation above, we have:

$$uB = E - \eta j + \frac{1}{m_e e} \frac{\partial P_e}{\partial x_{||}} \quad (5-6)$$

Now,

$$E = \frac{\partial V}{\partial x_{||}} \quad (5-7)$$

(Since all our voltages are negative, there is no minus sign involved.) Then, assuming that the electron temperature remains about constant at its value in the convective zone,

we have:

$$\begin{aligned}
 \int u B dx_{11} &= \int \left(E + \frac{1}{n_e e} \frac{\partial P}{\partial x_{11}} \right) dx_{11} - \int \gamma j dx_{11} \\
 &= \int \left(\frac{\partial V}{\partial x_{11}} + \frac{k T_e}{e} \frac{\partial}{\partial x_{11}} \ln n_e \right) dx_{11} - \int \gamma j dx_{11} \\
 &= \Delta V + \frac{k T_e}{e} \ln \frac{n_e}{n_c} - \int \gamma j dx_{11}
 \end{aligned} \tag{5-8}$$

where n_e and n_c are the values of electron density in the surface layer and convective zone, respectively.

Noting that the surface layer is thin compared to the radius of the cathode, we have that B is about constant with respect to x_{11} and may be removed from the integral on the left. Also, $\gamma = \gamma(T_e)$ and j are constant through the surface layer. Thus, if we write h as the thickness of the surface layer, we may obtain the average speed along the surface \bar{u} :

$$\begin{aligned}
 \bar{u} &= \frac{1}{h} \int u dx_{11} \\
 &= \frac{\left[\Delta V + \frac{k T_e}{e} \ln \frac{n_e}{n_c} - \gamma j h \right]}{B h}
 \end{aligned} \tag{5-9}$$

In this way, we are using our measurements of electric and magnetic fields and current density near the cathode surface as a type of MHD channel flow meter. We measure the voltage across the flow, correct for the resistive voltage drop and pressure gradients, to obtain the back emf and then compute \bar{u} from the known (measured) magnetic field strength.

The density within the surface layer reflects the influx

of plasma from the convective zone. Neglecting mass addition at the shoulder of the cathode, we have:

$$\int \rho u (2\pi R) dx_{||} \cong \int \rho_c u_c (2\pi R) dx \quad (5-10)$$

where x is measured from the cathode shoulder along the slope, and $\rho_c u_c$ is the mass influx from the convective zone. We are interested merely in the characteristic densities in the surface layer, so we shall neglect the variation of $\rho_c u_c$ and R with x . We then write:

$$\bar{\rho} \cong \frac{\rho_c u_c x}{\bar{u} h} \quad (5-11)$$

The particle density in the cathode surface layer is typically then,

$$n = \frac{\bar{\rho}}{m_i} = \frac{\left(\frac{\rho_c}{m_i}\right) u_c B x}{\Delta V + \frac{k T_e}{e} \ln \frac{m_e}{m_c} - \tau j h} \quad (5-12)$$

with $n \cong n_e$, we thus have an implicit equation for n_e , which may be quickly solved by successive substitution, since the logarithmic dependence involved is rather gentle.

The characteristic temperature of the heavy particles in the cathode surface layer may be derived in a similarly approximate manner. Again neglecting variations along the cathode slope of particle and energy fluxes, and ignoring the complications of conical geometry, we have:

$$\rho u h \left[\mathbb{h}(T) + \frac{1}{2} \bar{u}^2 \right] = \left[j \Delta V + \tau P + \rho_c u_c \frac{u_c^2}{2} \right] x \quad (5-13)$$

where $\mathbb{h}(T)$ is the enthalpy of the flow; $j \Delta V$ is the electric

power deposited; q_p is the energy transfer from the cathode fall zone or emission layer; and $\rho_c u_c u_o^2/2$ is the energy flux from the convective zone.

The heavy-particle temperature may be found from the enthalpy, if equilibrium conditions are assumed.¹⁸ We have (noting that $\rho u h \approx \rho_c u_c x$):

$$Th(\tau) = \left[\frac{j \Delta V + q_p}{\rho_c u_c} - \frac{(\bar{u}^2 - u_o^2)}{2} \right] \quad (5-14)$$

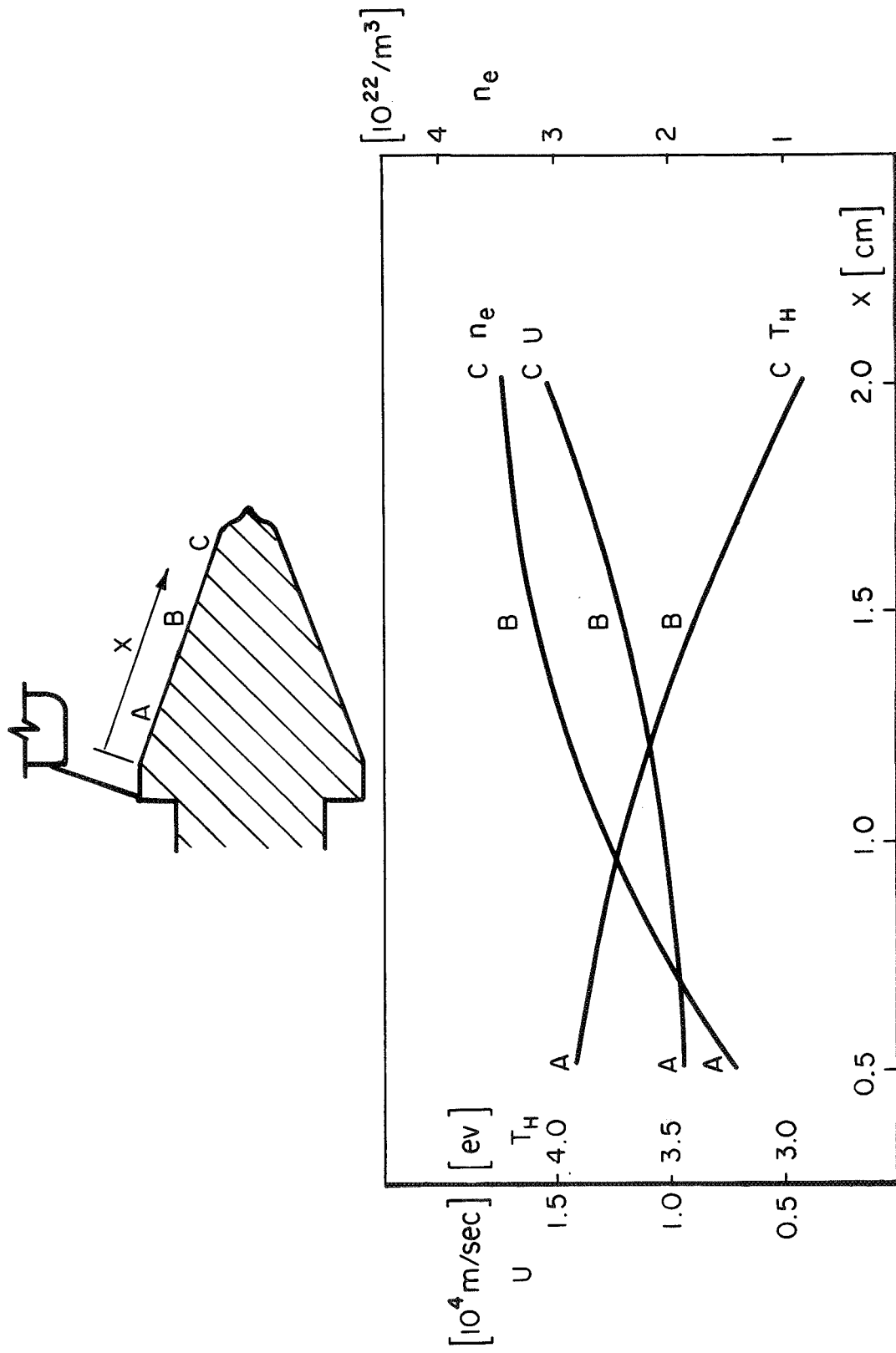
The procedure used to solve these approximate equations for the cathode surface layer is to find n_e , compute the pressure gradient correction to the field structure to obtain \bar{u} , and then substitute this in the above equation for T.

Solution of the Cathode Surface Layer Flow

Solutions of the preceding equations are shown in Fig. 5-2, at three stations along the cathode surface. These curves merely provide us with indications of the flow properties at the cathode. The experimental and theoretical situation does not permit much more. From our simple formulation, we obtain the average densities, velocities and temperatures in the surface layer, appropriate to the overall electrical and fluid mechanical conditions near the cathode. Thus, we see that the density and heavy-particle temperature both increase from their values in the convective zone. Particularly interesting is the observation that the ion flow velocity retains much of its magnitude after deflection near the cathode surface. In addition, the variation of flow properties along the cathode is indicated. We see that the particle density increases as more plasma is collected from the convective zone. This rise is offset somewhat by the increase in plasma velocity due to acceleration by the $\vec{j} \times \vec{B}$ force along the surface.

The heavy-particle temperature was obtained from equilibrium computations of argon enthalpy at high temperatures by

FIGURE 5-2



CATHODE SURFACE LAYER FLOW

Cann and Ducati.¹⁸ While equilibrium may not actually exist in our situation, we note that the equilibration time between ions and electron, t_{eq} , (as in Chap. 3), is about 10^{-7} sec at the high densities found in the surface layer. This indicates good coupling between ions and electrons over a distance $\bar{u}t_{eq} \approx 1$ mm, so that energy may be transferred from high temperature ions to electrons and thence to ionization and excitation of the plasma. The essential point is that the plasma flow effectively has a very large specific heat because of ionization and excitation. The plasma flow is accelerated to high speed by the $\vec{j} \times \vec{B}$ force along the surface, thereby convecting away the heat absorbed in the deflection process. It appears then that the cathode is protected, in part at least, by strong blowing of a high specific heat gas along the surface. (In these calculations, the energy transfer from the cathode fall zone, q_p , is computed from a model of the cathode fall developed later in this chapter. This model indicates that about half the electrical power deposited in the cathode fall is available to heat the plasma flow in the surface layer.)

Preliminary results from spectroscopic observations of the discharge in the cathode region (with a longer duration, nonreversing current pulse) indicate¹⁰ that the particle density indeed increases from a value of about $3 \times 10^{21}/m^3$ in the convective zone to about $2 \times 10^{22}/m^3$ in a thin layer (~ 2 mm thick) adjacent to the cathode surface. Early estimates of heavy-particle temperature near the cathode tip (with a higher input mass flow, however) indicate¹⁰ values of 2 to 4 eV. Extrapolating our velocity calculations to the vicinity of the cathode tip, we find that the flow along the surface has been accelerated to a speed about equal to that measured by time-of-flight velocity probes¹⁴ at the anode exhaust port ($u \approx 1.8 \times 10^4$ m/sec). Thus, our approximate analysis yields results that are consistent with the available evidence from other experimental techniques.

Boundary Layer Considerations

Having obtained in this approximate fashion the average flow conditions along the cathode, we now consider the viscous interaction of this flow with the surface. First, we must compute the kinematic viscosity of a quiescent plasma at the same temperature as our flow. From kinetic theory,¹⁹ we have that this is:

$$\nu_{\mu} \approx \frac{1}{2} V_{th} \lambda_{ii} \quad (5-15)$$

where V_{th} is the mean thermal speed of the ions ($\approx 4.6 \times 10^3$ m/s at station B) and λ_{ii} is the ion-ion mean free path derived from the ion thermal speed and the self-equilibration time discussed in Chap. 3. At station B, $\lambda_{ii} = V_{th} t_c = 1.47 \times 10^{-5}$ m. With this, we have

$$\nu_{\mu} = 3.4 \times 10^{-2} \text{ m}^2/\text{sec} \quad (5-16)$$

The Reynolds number of our flow is then:

$$\text{Rey} = \frac{\bar{u} L}{\nu_{\mu}} = 4.3 \times 10^3 \quad , \quad (5-17)$$

Again evaluated at station B where $L = x = 1.3$ cm. The boundary layer thickness of an incompressible flow under these conditions is approximately given by:

$$\bar{\delta} = \frac{x}{\sqrt{\text{Rey}(x)}} = 2 \times 10^{-4} \text{ m} \quad (5-18)$$

in the present case. For a compressible boundary layer, however, we must multiply this by the square of the Mach number. The speed of sound based on the ion temperature is:

$$a = \sqrt{\frac{\gamma R T'}{m_i}} = 3.3 \times 10^3 \text{ m/s} \quad (5-19)$$

for $\gamma = 1.3$ (obtained from equilibrium computations similar

to those used to evaluate T).¹⁸ So the Mach number of our flow is:

$$M = \frac{u}{a} = 3.4 \quad (5-20)$$

The compressible boundary layer thickness is then approximately $\delta = M^2 \bar{\delta} = 2.3 \times 10^{-3}$ m.

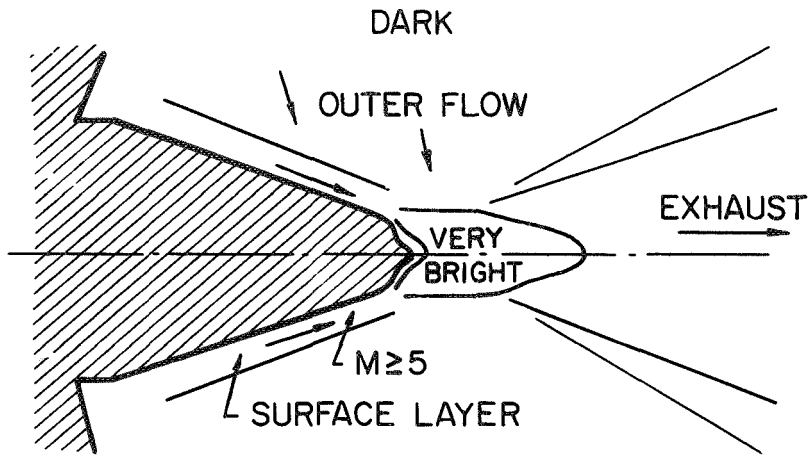
We see that $\delta \approx h$. Thus, the velocities and temperatures obtained by our analysis are averaged over the viscous boundary layer (in addition to the early stages of flow deflection), so that the values used in computing Re and M should be amended for higher velocities and lower temperatures. However, since the change in speed and temperature from the convective zone ($u \approx 18$ km/sec, $T_i \approx 1.5$ eV) to the surface layer ($\bar{u} \approx 11$ km/sec, $\bar{T}_i \approx 3.5$ eV) is rather moderate, the overall character of the situation should be maintained.

Discussion of the Cathode Tip and Jet

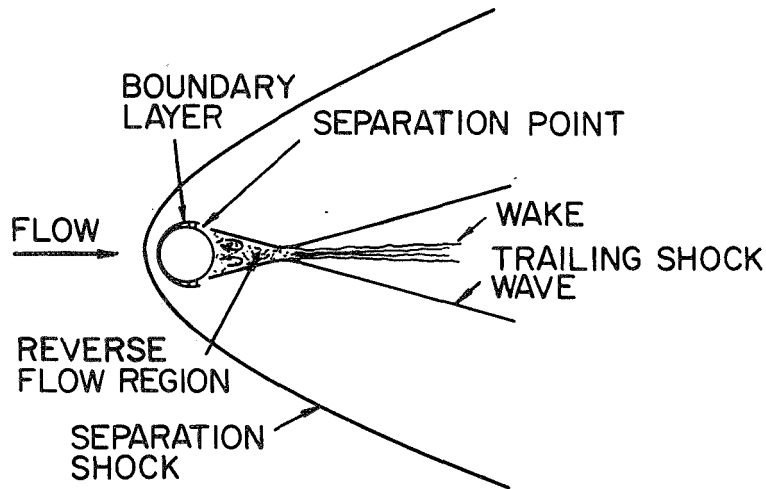
If we extend our calculations toward the cathode tip, we find that the flow Mach number exceeds five. We may, therefore, consider the cathode in this region to be enveloped by a hypersonic flow. The situation at the cathode tip thus resembles the base and wake flow behind a hypersonic blunt body.

This impression is readily obtained by comparing our color photographs (Fig. 3-3e of Chap. 2) to schlieren photos or shadowgraphs of hypersonic flow interaction with circular cylinders.^{20, 21} In Fig. 5-3a,b we depict these situations schematically. Note that the cathode tip flow (Fig. 5-3a) is characterized by a straight section extending parallel to the centerline for a few tip diameters, followed by a bright conical region. Within the section at the cathode tip, the luminosity is particularly bright.

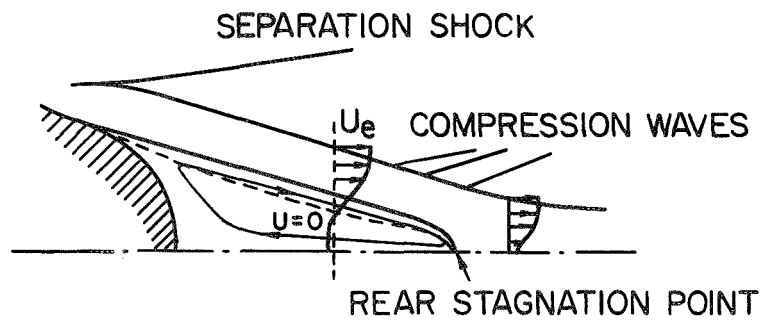
The hypersonic flow pattern shown (Fig. 5-3b) is from the experimental work of McCarthy and Kubota²⁰ for a cylinder in $M = 5.7$ wind tunnel flow. It is typical of hypersonic flow around a smoothly curved, convex blunt body. The boundary layer



a) LUMINOSITY PATTERN OF CATHODE FLOW



b) HYPERSONIC FLOW AROUND CYLINDER (REF. 10)



c) DETAILS OF HYPERSONIC BASE FLOW AND NEAR WAKE (REF. 11)

AP 25 12 4611 70

FIGURE 5-3

separates along the trailing surface so the lateral flow tends to overshoot the end of the body and stagnate a few diameters downstream instead. The high pressure region thus created induces a reverse flow toward the base of the body which stagnates there and recirculates between the separated boundary layer, the flow centerline, and the body surface. This is seen in Fig. 5-3c which also indicates the compression of the outer flow as it is turned at the centerline. Note that these compression waves will coalesce into the trailing shock wave shown in Fig. 5-3b. We associate the sharply defined cone of luminosity with this shock, while the base flow and stagnation region occur in the straight section downstream of the cathode tip.

Our situation is complicated by the addition of mass, momentum, and energy from the convective zone, and by conduction and emission processes at the cathode tip. We may expect that the influx of plasma from the convective zone is not important compared to the flow from the cathode surface layer since the collection area is much smaller than the lateral surface of the cathode. On the other hand, heat addition at the cathode surface should be significant since the current density is about a factor of three higher at the cathode tip than along the slope. Such heating should have the effect of expanding the base flow volume, offsetting any compression of this region by the momentum flux from the convective zone.

Within the confines of our model for the emission layer presented in the next section, the higher total current density at the tip increases the level of both q_c and q_p (q_c is the heat transferred to the cathode). Thus, a factor of three or four increase in current density, coupled with the more constricted geometry of the cathode tip, can account for the fact that melting is evident only in this area. We note that the flow of the molten surface appears to be opposite to the motion of the freestream plasma, indicating that a reverse flow indeed exists in the base region at the cathode tip (see Fig. 2-5, Chap. 2).

While we again cannot treat the problem in detail, some

qualitative understanding may be obtained by recognition of the overall flow situation. In particular, we note that the high pressure and temperature presumed to exist at an MPD arc-jet cathode may be displaced downstream by the hypersonic flow off the lateral surface of the cathode. Base flow measurements with hypersonic blunt bodies²⁰ suggest that a relatively low pressure should exist at the cathode tip. This is associated with another interesting feature of such flows. We see in Fig. 5-3c that the inviscid flow is turned parallel to the centerline with little loss in magnitude (note that close to the centerline the compression waves have not yet formed a shock). Only a portion of the surface layer flow will be stagnated and contribute to the recirculation at the cathode tip. In this way the conversion of the radial ion flow from the convective zone into a useful, axial exhaust is completed without stagnating and re-expanding the entire plasma flow. As mentioned earlier, if we extrapolate our calculation of flow velocity in the cathode surface layer to the vicinity of the cathode tip, we find an average speed of the outer flow approximately equal to the flow speed in the convective zone, $u = 1.8 \times 10^4$ m/sec. This value agrees quite well with the plasma speed measured in the arcjet exhaust at the anode orifice using time-of-flight velocity probes.¹⁴ (It should be mentioned that these probes measure large scale, high-frequency perturbations in plasma density and temperature, a feature consistent with the turbulent wake behind a hypersonic blunt body.)

Model for the Emission Layer

In the preceding work, we saw that the rate of energy transfer to the surface flow from the cathode fall or emission layer is required to calculate the heavy-particle temperature in the flow. We, therefore, depart now from the analysis of the cathode surface flow in our experiment to formulate a simple model for the current conduction and energy transfer processes in the immediate vicinity of the cathode surface. We are particularly interested in the division of cathode fall power

(27% of the total arc power) between electronic heating of the plasma, and ionic heating of the cathode. The former is an electrothermal component of arcjet operation, while the latter reflects both the cost of freeing electrons from the cathode and the loss of energy from the system by heat conduction to the cathode interior.

The extent of the cathode fall in an arc is typically a few MFP's.²² We, therefore, expect that the emission layer should have a thickness on the order of an ion-neutral mean free path. Since we also expect ion current conduction to be significant in this portion of the discharge, we may compute as before to find that:

$$\lambda_{Ai} \sim 4 \times 10^{-5} \text{ m} \ll 2.5 \times 10^{-3} \text{ m} \sim h \approx \delta \quad (5-21)$$

Thus, the emission layer should be very much thinner than the viscous boundary layer. Our concept of the situation then is that a thin layer of high density, low heavy-particle temperature ($\ll 1$ eV), low velocity plasma exists immediately adjacent to the cathode surface. Current conduction is accomplished by ion bombardment of the cathode, in addition to electron emission. The amount of emission depends on the difference between the heat transferred to the cathode surface by ion bombardment and the heat conducted away in the metal. Electron emission relieves the net heat load at the surface. (In all this, we neglect the effects of radiation. From the color photographic work, we have indicated that the lateral surface is not incandescent. We neglect transfer of energy to the cathode by radiation, compared with the electrical power deposited in the cathode fall, since otherwise the radiative loss of energy from the arc chamber would greatly exceed the total electrical power supplied.)

The electrons emitted at the cathode surface are then accelerated by the cathode fall voltage to an energy sufficient

to ionize the neutral atoms that result from ion recombination at the cathode. This process may be repeated with a single ion (heavy particle) returning to the cathode surface many times. Each time it causes some electrons to be emitted. It also collects another electron from the surface by recombination and then deposits it in the local plasma upon reionization. We may refer to this repetitive operation as the ion truck process. In Fig. 5-4 we show schematically the operation of the emission layer by our model.

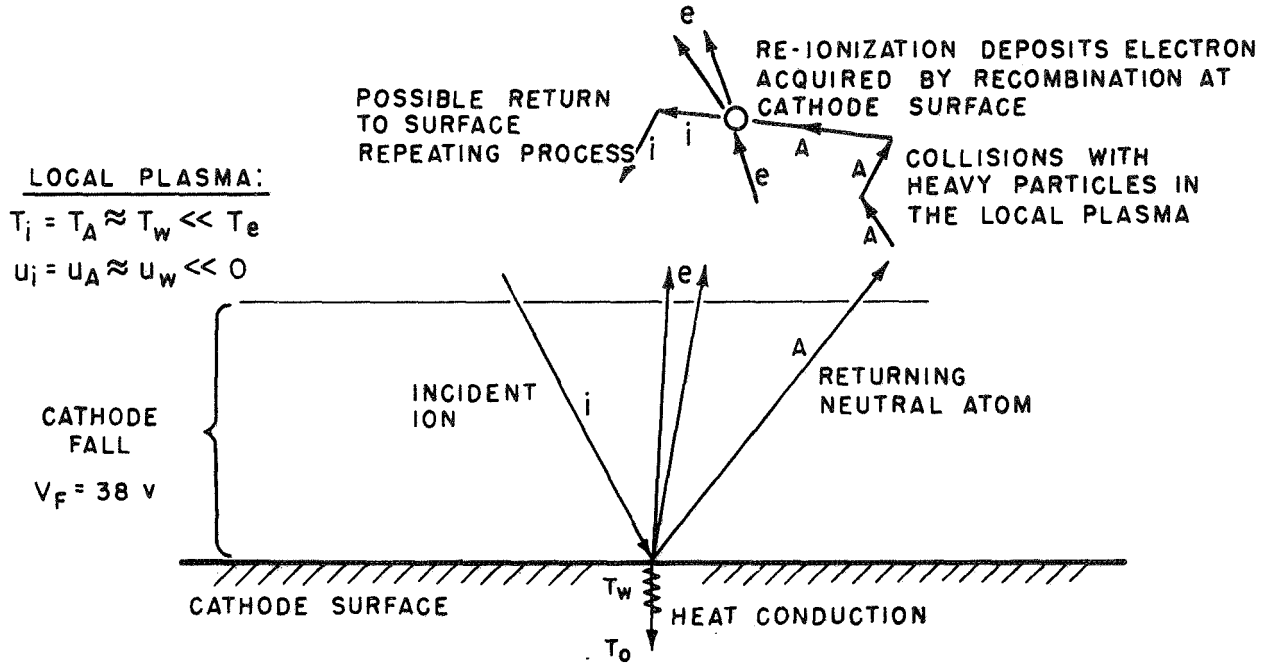
In the following treatment, we shall avoid any dependence on a particular emission mechanism since the properties of the cathode surface and the microscopic details of current attachment and energy transfer are poorly known. We shall instead formulate and solve the overall energy balances required at the cathode surface and in the local plasma.

Energy Balance at the Cathode Surface

The cathode surface is heated by particle bombardment and cooled by heat conduction in the metal and electron emission. Ions accelerate through the cathode fall and deposit an amount of energy $(V_F + z k T_i + m_i u_i^2 / 2e)$ at the surface. If an ion recombines there, it also provides an additional energy $(\epsilon_i - \phi_w)$, where we have subtracted the cost of collecting an electron from the surface. We expect the resulting flow of neutral atoms to return to the local plasma with the surface temperature, T_w , and net velocity parallel to the surface, $u_w = 0$. In the local plasma these atoms will collide with other heavy particles establishing some (kinetic) temperature not greatly different from T_w , and slowing the local plasma flow along the surface so that $u \ll \bar{u}$. With these approximations, we shall neglect simple kinetic energy transfer in comparison to the electrical and chemical energy fluxes to the surface $(\frac{1}{2} \frac{m_i u_i^2}{e} \ll V_F + \epsilon_i - \phi_w)$. Thus, our energy balance at the cathode surface is:

$$j_i (V_F + \epsilon_i - \phi_w) = j_c + j_e \phi_w \quad (5-22)$$

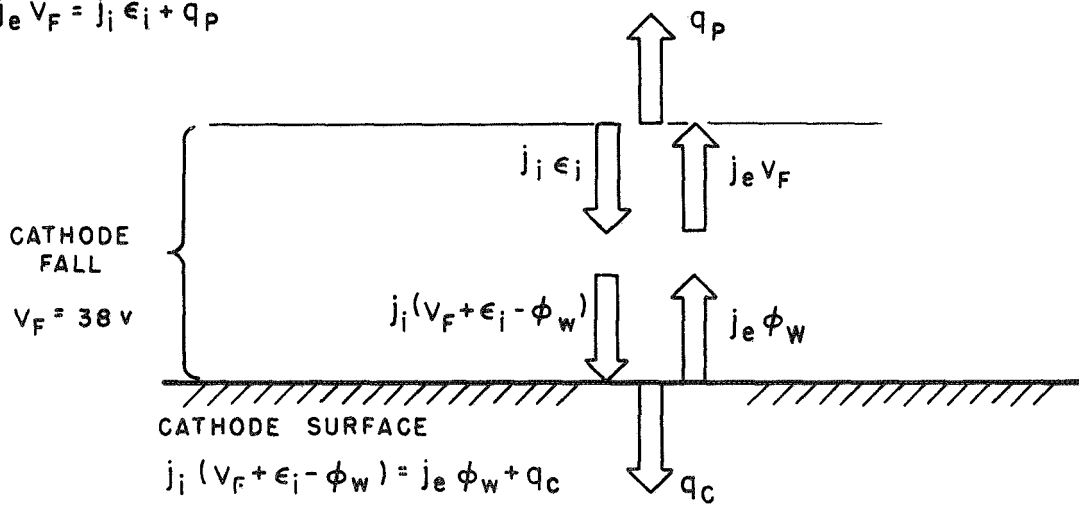
SURFACE LAYER FLOW



KINETICS OF THE EMISSION LAYER

LOCAL PLASMA:

$$j_e V_F = j_i \epsilon_i + q_p$$



ENERGY BALANCES IN THE EMISSION LAYER

AP 25 R 4651 70

FIGURE 5-4

where q_c is the heat conducted away in the metal. (We have assumed here that all the ions striking the surface recombine there. This is appropriate for a situation of nearly complete thermal accommodation between the heavy particles and the surface.)

In our experiment heat conduction to the cathode interior is an unsteady process. The time for the temperature, a distance x within the cathode, to attain half the surface temperature value is given by:²³

$$\frac{x}{2\sqrt{\chi t}} = .477 \quad (5-23)$$

For tungsten, $\chi \approx 0.5 \text{ cm}^2/\text{sec}$; so with $x = 0.6 \text{ cm}$ (cathode radius at the middle of the lateral surface), $t = 0.735 \text{ sec}$. This is much longer than the time scale of the experiment. We shall, therefore, use the heat conduction formula for unsteady flow in a semi-infinite slab. For constant heat flux at the surface, this is:²³

$$q_c = \frac{K(T_w - T_0)}{2} \sqrt{\frac{\pi}{\chi t}} \quad (5-24)$$

where K is the heat conductivity and T_0 is the initial temperature. Note that at any particular time higher surface temperatures are associated with greater heat fluxes at the surface.

Now, the heat flux to the surface is related to the ion current which depends on the surface temperature, since this determines the heavy-particle temperature in the local plasma. That is:

$$j_i (V_F + (\epsilon_i - \phi_w)) = n_i e \left(\frac{kT_w}{2\pi m_i} \right)^{1/2} (V_F + (\epsilon_i - \phi_w)) \quad (5-25)$$

Our energy balance at the cathode surface thus becomes:

$$j_e \phi_w + \frac{k(T_w - T_0)}{2} \sqrt{\frac{\pi}{\alpha t}} = m_i e \left(\frac{k T_w}{2\pi m_i} \right)^{1/2} (V_F + (\epsilon_i - \phi_w)) \quad (5-26)$$

To proceed, we must formulate the other requirements of our model.

Energy Balance in the Local Plasma

The voltage drop at the cathode exists, on one hand, to provide electrical heating of the cathode by ion bombardment, and on the other, to maintain the necessary operating environment by electronic heating of the local plasma. By the latter requirement, we have that the product of cathode fall voltage and emitted electron current must at least equal the power needed to re-ionize the heavy particles returning from the cathode. In general then:

$$j_e V_F = j_i \epsilon_i + q_p \quad (5-27)$$

where q_p represents the additional power transferred to the plasma by electronic heating. Since this is beyond the needs of the emission process, we may classify q_p as an electrothermal contribution to arcjet performance.

The total current is $j = j_i + j_e$, so we have:

$$\begin{aligned} q_p &= j_e V_F - j_i \epsilon_i \\ &= j V_F - j_i (V_F + \epsilon_i) \end{aligned} \quad (5-28)$$

In terms of the local heavy-particle temperature then:

$$q_p = j V_F - m_i e \left(\frac{k T_w}{2\pi m_i} \right)^{1/2} (V_F + \epsilon_i) \quad (5-29)$$

We note that T_w is proportional to the heat conduction at the cathode surface. Thus, for given particle and current densities, the power deposited in the plasma is related to the heat lost by conduction at the cathode.

Plasma Density in the Emission Layer

The pressure in the local plasma just beyond the cathode fall is equal to the component of momentum flux normal to the surface from the convective zone. This is because, with the $\vec{j} \times \vec{B}$ force parallel to the cathode surface, only the normal pressure gradient exists to balance the dynamic pressure of the plasma flow to the cathode surface layer. Thus, the plasma density just beyond the strong field of the cathode fall is related to the heavy-particle and electron temperatures by:

$$\begin{aligned} P_w &= (n_i + n_A) k T_w + n_e k T_e = n (k T_w + \alpha k T_e) \\ &= n_c m_i u_c^2 \end{aligned} \quad (5-30)$$

where $n_c m_i u_c^2$ is the normal momentum flux from the convective zone. The ion number density is then:

$$n_i = n_e = \alpha n = \frac{\alpha n_c m_i u_c^2}{(k T_w + \alpha k T_e)} \quad (5-31)$$

We expect that $\alpha k T_e \gg k T_w$, so that a simpler result obtains:

$$n_i = \frac{n_c m_i u_c^2}{k T_e} \approx 2.7 \times 10^{23} / \text{m}^3, \quad k T_e = 1.5 \text{ eV} \quad (5-32)$$

The physical picture here is that near the cathode surface, the plasma pressure is just the electron pressure since the heavy particles are cooled by interaction with the cathode, while

electrons receive energy from the emitted electrons accelerated through the cathode fall (and have a temperature limited again by inelastic processes). The normal momentum flux to the cathode surface layer is thus balanced by the electron pressure. The electrons are, in turn, repelled from the surface by the intense field of the cathode fall. The force involved in turning the flow in the surface layer is transmitted to the cathode largely through this field. We note that the predominance of the electron pressure allows lower heavy-particle densities near the relatively cold cathode and lower bombardment rates than would otherwise obtain.

Equations of the Emission Layer

Before substituting and rearranging terms, we collect our equations for ready reference.

Conduction:

$$j = j_i + j_e \quad (5-33)$$

Energy Balance at the Surface:

$$j_e \phi_w + q_c = j_i (V_F + (E_i - \phi_w)) \quad (5-34)$$

Energy Balance in the Local Plasma:

$$j_e V_F = j_i E_i + q_p \quad (5-35)$$

Heat Conduction:

$$q_c = \frac{k(T_w - T_0)}{2} \sqrt{\frac{\pi}{\lambda t}} \quad (5-36)$$

Ion Current Flow:

$$j_i = m_i e \left(\frac{k T_w}{2\pi m_i} \right)^{1/2} \quad (5-37)$$

Momentum Balance:

$$m_i = \frac{m_e m_i u_c^2}{kT_e} \quad (5-38)$$

This set of six equations involves six unknowns (j_i , j_e , q_c , q_p , T_w , and n_i) and one parameter (kT_e). We shall now solve this system for various values of kT_e , discuss the limitations on this parameter, and consider the implications of the results.

Surface Temperature

Substituting in the equation for the energy balance at the surface, we have:

$$\begin{aligned} \frac{k}{2} (T_w - T_0) \sqrt{\frac{\pi}{\chi t}} &= j_i (V_F + \epsilon_i) - j \phi_w \\ &= \frac{m_e m_i u_c^2}{(kT_e/e)} (V_F + \epsilon_i) \left(\frac{kT_w}{2\pi m_i} \right)^{1/2} - j \phi_w \end{aligned} \quad (5-39)$$

This is a quadratic equation for $T_w^{1/2}$:

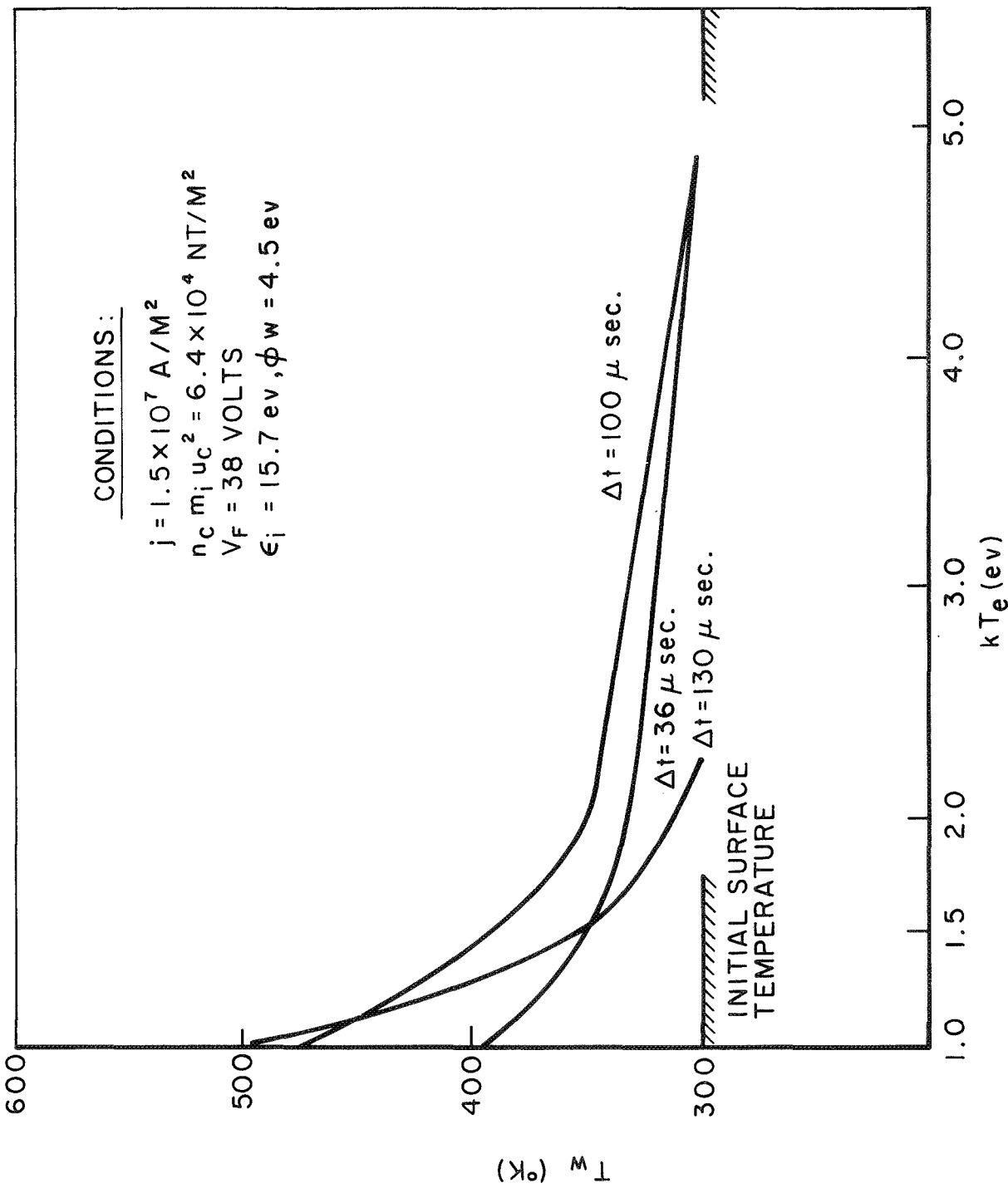
$$\begin{aligned} \frac{k}{2} \sqrt{\frac{\pi}{\chi t}} (T_w^{1/2})^2 - \frac{m_e m_i u_c^2}{(kT_e/e)} (V_F + \epsilon_i) \left(\frac{k}{2\pi m_i} \right)^{1/2} T_w^{1/2} \\ - \left(\frac{k}{2} \sqrt{\frac{\pi}{\chi t}} T_0 - j \phi_w \right) = 0 \end{aligned} \quad (5-40)$$

Solutions of this equation for several values of kT_e and t are shown in Fig. 5-5. Conditions are: $j = 1.5 \times 10^7$ A/m²,

$m_e m_i u_c^2 = 6.4 \times 10^4$ eV/m² and $V_F = 38$ V. Other properties are: $\epsilon_i = 15.7$ V (argon) and $\phi_w = 4.5$ V (tungsten).

We note that the surface temperature decreases with increasing electron temperature so that the maximum value of kT_e

AP 25 L 4647 70



CATHODE SURFACE TEMPERATURE vs. ELECTRON TEMPERATURE

FIGURE 5-5

at any time is defined by $T_W = 300^\circ \text{K}$. We also observe that the operating temperature of our system decreases at later times if the electron temperature is higher than about 1.5 eV. Since we expect that T_W should increase or at least remain constant, this implies that kT_e is less than the indicated maximum values. For constant electron and heavy-particle temperatures during quasi-steady operation, we have $kT_e \leq 1.5 \text{ eV}$.

A minimum electron temperature of 1 eV was assumed because lower values would indicate heat transfer from the electrons in the plasma to those in the emission layer. This is unlikely in view of the large fraction (27%) of the total arc power deposited there.

For this range of electron temperatures, then, the surface temperature is about 400°K . This indicates that the lateral surface of the cathode should not be incandescent, consistent with the negative result of the photographic work. It also underscores the inadequacy of thermionic emission processes (as usually formulated) to provide the high-current densities observed. (Even at temperatures approaching the melting point of tungsten, however, thermionic emission computed from either the Richardson or Dushman equations is insufficient.)

Current Conduction in the Emission Layer

The ion current to the surface is determined by T_W and T_e . In Fig. 5-6a we plot j_i and j_e versus electron temperature for $t = 100 \mu\text{sec}$. The ion contribution to current conduction diminishes at higher electron temperatures because the densities needed to obtain the required electron pressure are lower. Enhancing this is the lower heavy-particle and surface temperature that results from the decrease in ion bombardment heating of the cathode. This latter process implies a lower rate of cathode erosion at higher electron temperatures. Essentially, the momentum flux to the surface from the convective zone is balanced to a greater extent by the repulsion of the electron fluid from the cathode. Thus, we have "electrostatic" rather than "magnetic" protection of the cathode in a high-current discharge.

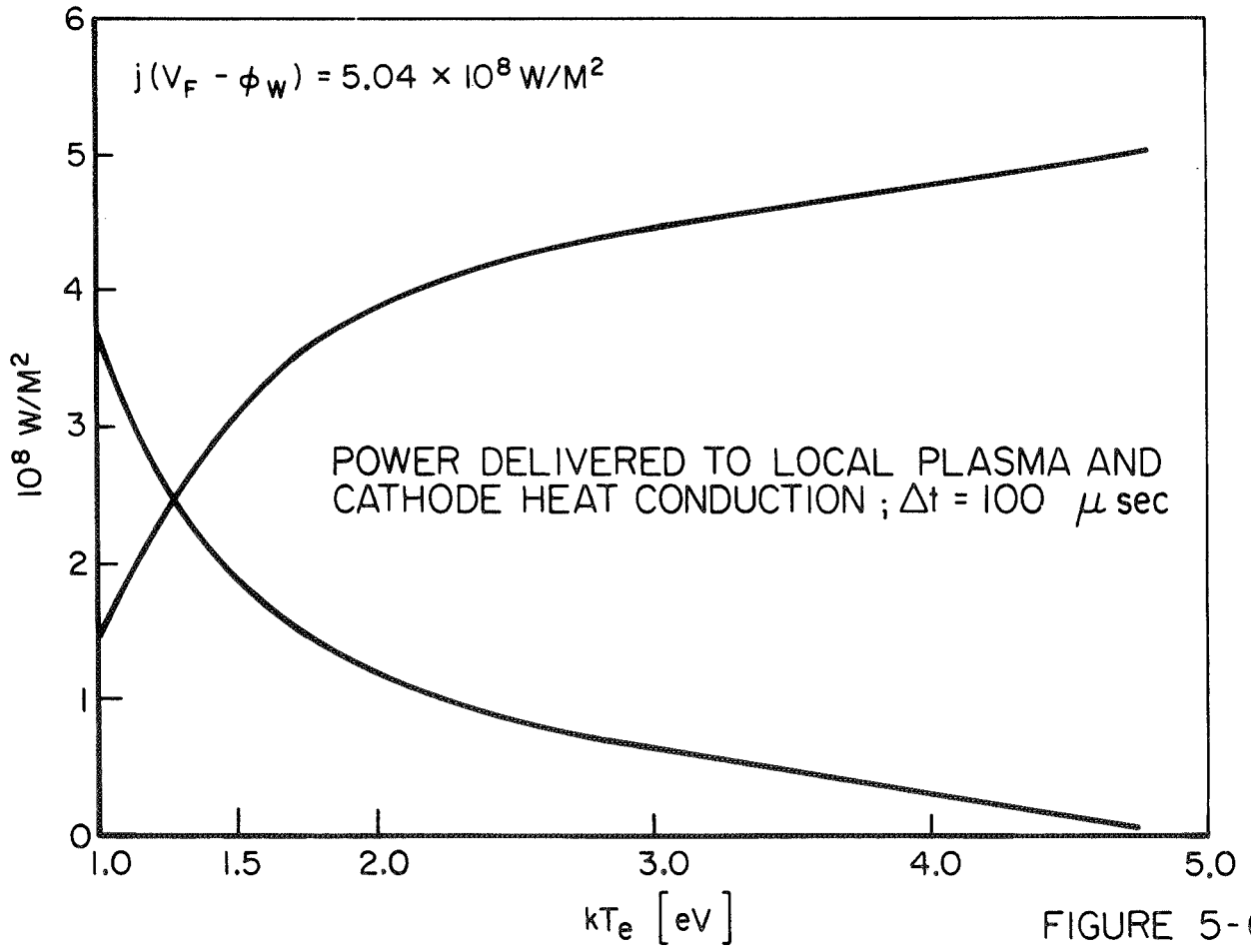
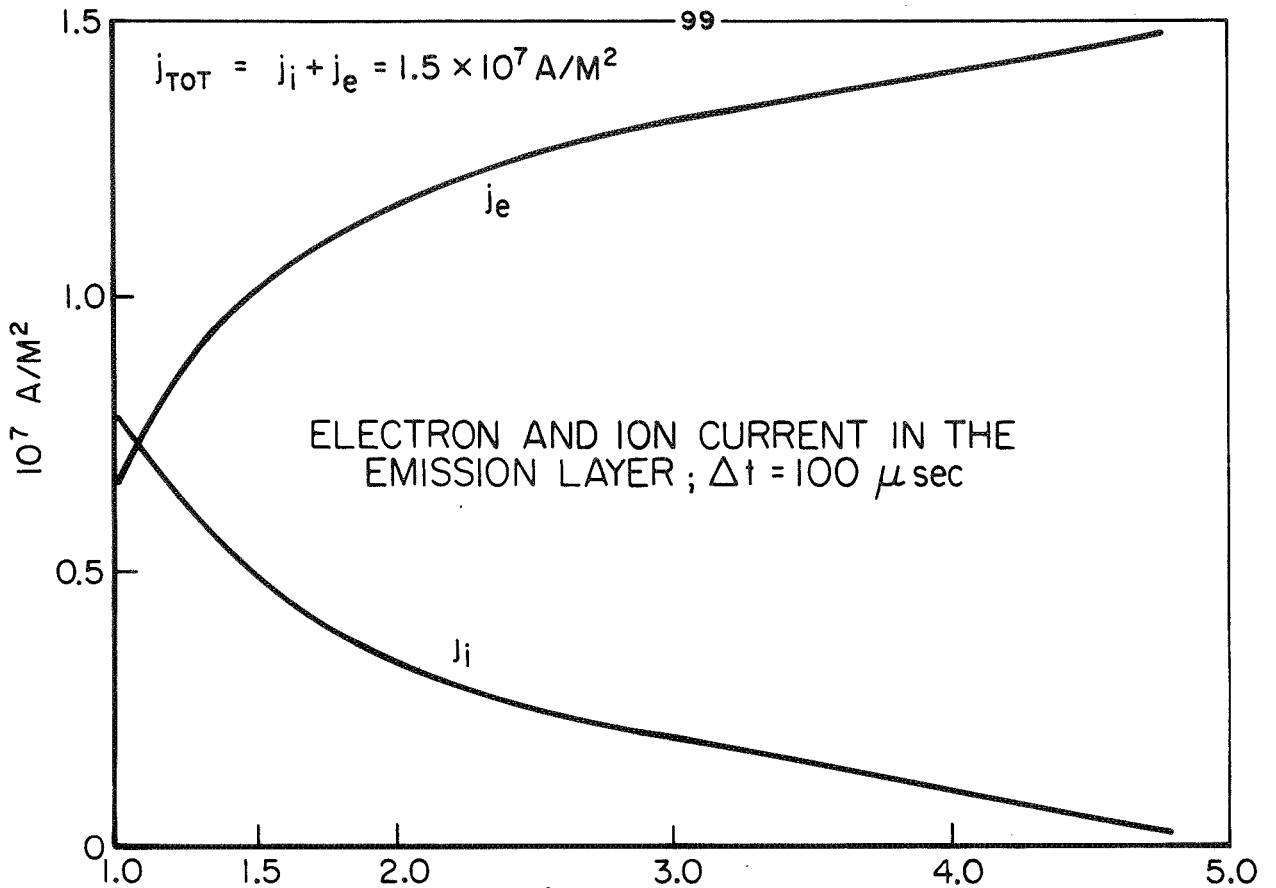


FIGURE 5-6

AP 25 R 1649 70

(The latter effect will be involved in the momentum layer.)

With $kT_e \leq 1.5 \text{ eV}$, we see that the ion and electron contributions to current conduction are comparable. For example, at $kT_e = 1.5 \text{ eV}$, $j_e = 2j_i$, indicating that two electrons are emitted for each ion incident at the cathode surface.

Origin of the Cathode Fall

As in the convective zone, we have actually been solving the problem in reverse. Experimentally, we know V_F and therefore we have used it as an independent variable. Physically, however, the cathode fall arises from the operating conditions at the cathode. These are determined by the current and particle densities in the vicinity of the cathode, the heat conduction and convection processes there, and the mechanical balance required by the static pressure in the arc column, or in our case, the dynamic pressure of the plasma flow. This may be seen most readily in terms of the overall energy balance at the cathode:

$$jV_F = j\phi_w + q_c + q_p \quad (5-41)$$

so

$$V_F = \phi_w + \frac{q_c + q_p}{j} \quad (5-42)$$

The cathode fall must at least account for the cost of removing electrons from the metal. In addition, it must provide enough energy to balance the heat losses to the cathode and the plasma. The cathode fall thus arises from a balance of energy transfer processes.

The cathode fall performs work by giving charged particles ordered motions. The heat losses reflect a randomization of these motions, associated with inefficiencies in electron emission and plasma ionization processes. Conduction of current in the presence of collisions thus leads to entropy production.

If we assert that the cathode fall operates so that the entropy production rate is minimized, we may obtain the required fall voltage.

The entropy production rate is:

$$\begin{aligned}\dot{S} &= \frac{\dot{q}_P}{T_e} + \frac{\dot{q}_C}{T_w} = \frac{j(V_F - \phi_w)}{T_e} + \frac{\dot{q}_C}{T_w} \left(1 - \frac{T_w}{T_e}\right) \\ &= \frac{j(V_F - \phi_w)}{T_e} + \frac{k}{2} \sqrt{\frac{\pi}{\chi t}} \left(1 - \frac{T_0}{T_w}\right) \left(1 - \frac{T_w}{T_e}\right) \quad (5-43)\end{aligned}$$

(where we have divided the heat and entropy production rates by the lateral surface area of the cathode).

Assuming that T_e is largely determined by processes just beyond the emission layer, we have:

$$\frac{d\dot{S}}{dV_F} = \frac{j}{T_e} + \frac{k}{2} \sqrt{\frac{\pi}{\chi t}} \left(\frac{T_0}{T_w^2} - \frac{1}{T_e} \right) \frac{dT_w}{dV_F} \quad (5-44)$$

Now, in our case, we expect that $T_e \gg T_w \gtrsim T_0$, so that the expression in parentheses above is positive. From our quadratic equation for $T_w^{1/2}$, we see that (dT_w/dV_F) is also positive. Then,

$$\frac{d\dot{S}}{dV_F} > 0 \quad (5-45)$$

Thus, the rate of entropy production increases with fall voltage. The minimum rate is therefore associated with the minimum voltage allowed by other requirements of the system.

Previously, we determined the maximum electron temperature possible for a given fall voltage. Assuming that temperatures in our system do not decrease with time, the electron temperature is limited to $kT_e \leq 1.5$ eV. Reversing our point of view, we

may specify the electron temperature and compute the minimum possible fall voltage. Using the value of electron temperature measured near the cathode surface, $kT_e = 1.5 (\pm 0.5)$ eV, we immediately see that the minimum voltage is just the previously used experimental value, $V_f = 38$ V. That is, the cathode fall appears to be operating in our case so as to produce entropy at the minimum rate.

From Fig. 5-7a,b we see that under these conditions the cathode fall involves comparable levels of ion and electron current ($j_e \approx 2j_i$) and delivers comparable amounts of power to the cathode surface and the local plasma. Thus, some 60% of the cathode fall power is available to arcjet processes beyond the surface.

EXPERIMENTAL CONCLUSIONS

In the preceding chapters, we have sought to develop a cogent, phenomenological picture of the cathode region in our MPD arcjet. The approach has been qualitative in that we have been interested in establishing the physical nature of the situation, in lieu of detailed excursions into a problem fraught with analytical and experimental difficulties. Thus, our computations have employed quantities that are characteristic of the regimes of interest to yield results that, though approximate, allow some physical insight into the various processes involved.

We have seen that a transition flow of ionizing gas exists in the cathode region. The ionization level progresses from a few percent near the gas injectors, to some tens of percent closer to the cathode, and further downstream. Electrically, then, the plasma behaves like a fully ionized gas, having a conductivity of $8 (\pm 5)$ kmho/m. Since the electron Hall parameter and the (electron) magnetic Reynolds number both exceed unity in most of the cathode region, we expect significant interaction between the plasma flow and the current conduction pattern.

Such interaction is confirmed by analysis of the electromagnetic structure of the discharge. Noting that, in the absence of pressure gradients, ion acceleration reflects the $\vec{j} \times \vec{B}$ force distribution in the plasma, we see from the geometry of the current and plasma flow patterns that current conduction is achieved primarily by electrons in a tensor manner. This geometric impression is substantiated by considerations of the work performed on the ions by electromagnetic forces. We find that in our high conductivity situation, essentially all of the ion energy is associated with motion normal to the current flow direction.

Ion velocities and plasma flux rates are then computed from the electric and magnetic field distributions. It is found that approximately half the input mass flow is convected to the vicinity of the cathode surface, arriving there with a velocity of 1.8×10^4 m/sec, largely in the radial direction. A portion of the remaining input mass apparently is not ionized until it has drifted further downstream from the injectors. It is then also accelerated toward the arcjet centerline, but does not attain the same high speed as the mass flow to the cathode.

Near the cathode surface we find that the effects of pressure gradients should be included in our analysis of the discharge structure. Estimates of heavy-particle mean free paths also suggest that a continuum flow exists in a thin layer adjacent to the cathode. The situation at the cathode thus resembles a hypersonic-blunt body interaction in that the high speed, low-temperature ion flow to the cathode undergoes a large deflection in the vicinity of the surface. As in a blunt body problem, the normal momentum flux to the surface layer is reflected by a pressure gradient in this region. In our case, the plasma also experiences acceleration by the $\vec{j} \times \vec{B}$ force along the cathode surface. In addition, heat is deposited by current conduction through the surface layer and by heat conduction from the cathode fall.

To account for this last process, we formulated a simple model for an emission layer at the cathode surface, based on a balance of particle and energy fluxes to the cathode and to the local plasma. This model indicates that ion and electron currents are comparable near the cathode surface, and that comparable heat energies are deposited in the cathode and in the local plasma. It is also suggested by our model that the emission layer operates to produce entropy at the minimum rate, preferring to deliver heat to the high temperature plasma, rather than the relatively cold cathode. The surface temperature along the cathode slope is seen to remain at a level well below the melting point of tungsten, reflecting the protection of the cathode by a thin layer of high pressure plasma consisting of cold ions and hot electrons.

In addition to unsteady heat transfer to the interior, the cathode surface is cooled by electron emission. Again by our model about two electrons are emitted for each ion incident at the cathode. This result indicates that some form of individual field (I/F) ion bombardment emission process^{24, 25} is operating at the cathode surface. Simple thermionic emission is completely inadequate at the current densities with which we are involved.²⁶ At the cathode tip where melting is evident, T/F emission²⁶ can make a significant contribution to the electron current. But even at this limiting temperature, T/F processes cannot account for all the emission, since the current densities at the tip are also higher than on the lateral surface. It should be noted that our analysis averages phenomena over the cathode surface to obtain an average electron yield associated with an average surface temperature. Since emission processes are very sensitive to surface conditions, such averaging may obscure the actual emission mechanism. This approach, however, is quite serviceable in providing an overall power balance at the cathode surface. In particular, we find that some 50% of the electrical power deposited in the emission layer is delivered to the plasma flow along the surface. (The remaining power goes to cathode and anode heating.)

Using conservation principles and simplifying the geometry somewhat, we computed the properties of the plasma flow in the cathode surface layer. As expected, both the particle density and heavy-particle temperature increase above their values in the convective zone, confirming the existence of a pressure gradient near the surface. More importantly, the velocity of the plasma flow along the surface is comparable to the ion speed prior to deflection. We thus find that a highly supersonic to hypersonic flow exists parallel to the lateral surface of the cathode. (Estimates of viscous effects indicate that the cathode surface layer coincides with the compressible viscous boundary layer. We have, therefore, averaged over the lower speeds and higher densities and temperatures of this boundary layer in obtaining our flow properties.)

Near the cathode tip, this flow separates from the surface, collapsing onto the arcjet centerline a few diameters further downstream. A portion of the flow stagnates there and a reverse flow is created that circulates back to the cathode. The rest of the flow from the cathode surface layer is turned parallel to the centerline, maintaining a speed of about 1.8×10^4 m/sec, comparable to velocities measured at the anode exhaust port. (Other features of this hypersonic base flow and near wake are the formation of a trailing shock by the compression waves associated with flow turning at the centerline, and the existence of a turbulent wake.) In conclusion, we note that the high pressure "pumped" plasma core previously thought to exist at the cathode tip⁴ is replaced by a high pressure, high velocity layer along the lateral surface of the cathode. Boundary layer separation and flow recirculation near the cathode tip then allows most of the flow from the surface to exit the cathode region as a thin, conical annulus, escaping both stagnation point and shock wave interactions. In this way, the deflection of the high velocity plasma flow to the cathode is completed without additional losses to stagnation and re-expansion of a hypersonic flow.

CHAPTER 6

FUNDAMENTALS OF MPD DISCHARGE STRUCTURE

We shall now consider the fundamental physical basis for the structure of a magnetoplasdynamic discharge. In particular, we are concerned with the current distribution and its relation to the plasma flow.

Origin of the Conduction Pattern

As we have emphasized, the current distribution through a plasma prescribes the electric field there. We thus compute the electric field in a plasma from a generalized form of Ohm's law, with current density as the independent variable. We cannot arbitrarily specify the electric field pattern and then compute the current density distribution in an actual MPD arc. As in the experimental situation, we can only prescribe the total current level and the electrode geometry (and in some cases, the particle density or mass flow). To obtain the current distribution, we must combine our constitutive equation (Ohm's law) with the basic principles of electromagnetism (Maxwell's equations).

Faraday's Law for an MPD Discharge

The basic process governing current conduction in an MPD discharge that differentiates it from simple current conduction is the generation of a back emf by plasma flow in the magnetic field. That is, as a parcel of conducting fluid travels through the current distribution, the magnetic flux it intercepts changes. Such variation results in a circulation of current within the fluid element, which distorts the local current conduction pattern so as to diminish the change in magnetic flux through the fluid.

This is simply Lenz's or Faraday's law. In differential form, we state this law as:

$$\nabla \times \vec{E} = - \frac{\partial \vec{B}}{\partial t} \quad (6-1)$$

where in the preceding discussion, \vec{E} and $\partial \vec{B} / \partial t$ are both measured in a frame of reference travelling with the fluid parcel. In this case, the time rate of change of \vec{B} reflects the changing magnetic field strength seen by the fluid element as it passes through the region of nonuniform magnetic field associated with the current conduction pattern.

To proceed formally, we shall base our coordinate system in the laboratory, so $\partial \vec{B} / \partial t = 0$ is a steady situation. (For generality, we shall allow $\partial \vec{B} / \partial t \neq 0$ in the following derivation.)

Now, our constitutive equation is:

$$\vec{E} = \eta \vec{j} - \vec{u}_e \times \vec{B} - \frac{1}{m_e e} \nabla P_e \quad (6-2)$$

so,

$$- \frac{\partial \vec{B}}{\partial t} = \nabla \times \eta \vec{j} - \nabla \times (\vec{u}_e \times \vec{B}) \quad (6-3)$$

where we have assumed that the electron temperature is constant so: $\nabla \times (\frac{1}{m_e e} \nabla P_e) = \nabla \times (\nabla \cdot \frac{k_B T_e}{e} \vec{u}_e / m_e) = 0$. By vector identity then (with $\nabla \cdot \vec{B} = 0$), we have:

$$\begin{aligned} \nabla \times (\vec{u}_e \times \vec{B}) &= \vec{u}_e (\nabla \cdot \vec{B}) - \vec{B} (\nabla \cdot \vec{u}_e) + (\vec{B} \cdot \nabla) \vec{u}_e - (\vec{u}_e \cdot \nabla) \vec{B} \\ &= -\vec{B} (\nabla \cdot \vec{u}_e) - (\vec{u}_e \cdot \nabla) \vec{B} + (\vec{B} \cdot \nabla) \vec{u}_e \end{aligned} \quad (6-4)$$

Typically, in self-field accelerators, flow conditions do not change in the direction of \vec{B} , so we may drop the last term

on the right, in the previous equation. Thus,

$$\nabla \times \vec{j} = \left(\frac{\nabla \sigma}{\sigma} \right) \times \vec{j} + \sigma \left[-\vec{B} (\nabla \cdot \vec{u}_e) - (\vec{u}_e \cdot \nabla) \vec{B} - \frac{\partial \vec{B}}{\partial t} \right] \quad (6-5)$$

We may use particle continuity to account for the variation in electron flow speed through the discharge:

$$\nabla \cdot \vec{u}_e = \frac{\dot{M}_e}{m_e} - \frac{1}{m_e} \frac{D_e m_e}{D t} \quad (6-6)$$

where \dot{M}_e is the local change in electron density due to ionization and $D_e/D t = \partial/\partial t + \vec{u}_e \cdot \nabla$ is the convective derivative based on the electron fluid velocity. We then combine terms in our equation as follows:

$$-\vec{B} (\nabla \cdot \vec{u}_e) - (\vec{u}_e \cdot \nabla) \vec{B} - \frac{\partial \vec{B}}{\partial t} = -\frac{\dot{M}_e}{m_e} \vec{B} + \frac{\vec{B}}{m_e} \frac{D_e m_e}{D t} - \frac{D_e \vec{B}}{D t} \quad (6-7)$$

But,

$$\frac{D_e}{D t} \left(\frac{\vec{B}}{m_e} \right) = \frac{1}{m_e} \frac{D_e \vec{B}}{D t} - \frac{\vec{B}}{m_e^2} \frac{D_e m_e}{D t} \quad (6-8)$$

so our equation becomes:

$$\nabla \times \vec{j} = \left(\frac{\nabla \sigma}{\sigma} \right) \times \vec{j} + \sigma \left[-\frac{\dot{M}_e}{m_e} \vec{B} - m_e \frac{D_e}{D t} \left(\frac{\vec{B}}{m_e} \right) \right] \quad (6-9)$$

Now, neglecting the displacement term,

$$\vec{j} = \frac{1}{\mu_0} \nabla \times \vec{B} \quad (6-10)$$

so

$$\nabla \times \vec{j} = \frac{1}{\mu_0} \nabla \times (\nabla \times \vec{B}) = \frac{\nabla(\nabla \cdot \vec{B}) - \nabla^2 \vec{B}}{\mu_0} \quad (6-11)$$

In addition, we may simplify the term involving variable conductivity. We have:

$$\begin{aligned} \left(\frac{\nabla \sigma}{\sigma}\right) \times \frac{(\nabla \times \vec{B})}{\mu_0} &= \frac{1}{\sigma \mu_0} \left[\nabla(\nabla \sigma \cdot \vec{B}) - (\nabla \sigma \cdot \nabla) \vec{B} - (\vec{B} \cdot \nabla) \nabla \sigma - \vec{B} \times (\nabla \times \nabla \sigma) \right] \\ &= -\frac{1}{\mu_0} \left[\left(\frac{\nabla \sigma}{\sigma}\right) \cdot \nabla \right] \vec{B} \end{aligned} \quad (6-12)$$

Our equation becomes upon substitution of these results:

$$\nabla^2 \vec{B} = \sigma \mu_0 \left[m_e \frac{D_e}{Dt} \left(\frac{\vec{B}}{m_e} \right) + \frac{\dot{m}_e}{m_e} \vec{B} \right] + \left(\frac{\nabla \sigma}{\sigma} \cdot \nabla \right) \vec{B} \quad (6-13)$$

This equation, along with appropriate boundary and initial conditions, determines the magnetic field distribution in the arc chamber, and thus the current flow pattern.

In a steady state, we have:

$$\nabla^2 \vec{B} = \sigma \mu_0 \left[m_e \vec{u}_e \cdot \nabla \left(\frac{\vec{B}}{m_e} \right) + \frac{\dot{m}_e}{m_e} \vec{B} \right] + \left(\frac{\nabla \sigma}{\sigma} \cdot \nabla \right) \vec{B} \quad (6-14)$$

If the electron density is constant (and ionization is neglected), this becomes:

$$\nabla^2 \vec{B} = \sigma \mu_0 (\vec{u}_e \cdot \nabla) \vec{B} + \left(\frac{\nabla \sigma}{\sigma} \cdot \nabla \right) \vec{B} \quad (6-15)$$

Taking just the first two terms, we see that the magnetic field distribution is determined by a balance between convection (in the direction of \vec{u}_e) and diffusion, in much the same manner as the temperature distribution in a flowing, heat conducting gas. In the absence of significant electron flow (low current or high density situation), we see that the first and third terms above merely provide the distribution of current in a nonuniform conductor. These two cases account for the two basic types of arcjet discharge. In a low current and/or high particle density arc, we have the scalar situation in which the current pattern follows the distribution of electrical conductivity in the gas. We note that the conductivity gradient resembles the electron flow velocity, so that we may define an effective velocity due to conductivity variation as:

$$\sigma \mu \vec{u}_\sigma \equiv \frac{\nabla \sigma}{\sigma} \quad (6-16)$$

Much in the same way that the electron flow will tend to convect the current pattern in the direction of \vec{u}_e , the sharp conductivity variation at the edge of an arc discharge will cause the current to collect in the arc column. (This merely says that most of the current will flow where the conductivity is highest, so the current pattern in the arc chamber depends on the thermal transport processes that determine the conductivity distribution. In a thermal arcjet in which heat from the arc is carried away by convection, strong thermal gradients can be maintained, and there will be a tendency to spoke.)

For a high-current and/or low-density arc, conductivity variations are less important (σ tends to be uniformly high). The high electron flow speed associated with the need to conduct high current with few charge carriers convects the current distribution so that it tends to represent the electron flow trajectory. This trajectory is determined by the magnetic field of the current distribution and the electrostatic coupling of the electrons to the ions in a quasi-neutral plasma. Thus, the ion momentum equation must be combined with Faraday's law and Ohm's

law (the electron momentum equation) to compute the current flow pattern. Since the ion motion depends primarily on the $\vec{j} \times \vec{B}$ force distribution in a high-current discharge, we see the fundamental nonlinearity of the problem. We shall return to this discussion later. We first wish to delineate more formally between thermal and magnetoplasmadynamic arcjets.

Magnetic Reynolds Number Based on u_e

To explore the relative importance of the terms in our equation, we nondimensionalize the simplified expression above as follows:

Let

$$\begin{aligned}\vec{B} &= \vec{B}^* B_0 \\ \vec{u}_e &= \vec{u}_e^* u_0 \\ \sigma &= \sigma^* \sigma_0\end{aligned}\tag{6-17}$$

and $L = L^* L_0$; where L and L^* represent any spatial dimension, and B_0 , u_{e0} , σ_0 , and L_0 are constant quantities characteristic of the discharge and flow situation. We have then:

$$\nabla^{*2} \vec{B}^* = (\sigma_0 \mu_0 u_{e0} L_0) \sigma^* (u_e^* \cdot \nabla^* \vec{B}^*) + \left(\frac{\nabla^* \sigma^*}{\sigma^*} \cdot \nabla^* \right) \vec{B}^*\tag{6-18}$$

$$= R_{me} \sigma^* (\vec{u}_e^* \cdot \nabla^*) \vec{B}^* + \left(\frac{\nabla^* \sigma^*}{\sigma^*} \cdot \nabla^* \right) \vec{B}^*$$

where $R_{me} = \sigma_0 \mu_0 u_{e0} L_0$ is the magnetic Reynolds number based on the electron flow speed. From this expression, we see that scalar conduction (thermal arcjet) will obtain for $R_{me} \ll 1$. While convective effects (MPD arcjet) will prevail for $R_{me} \gg 1$. In the former limit, with constant σ , the current pattern is a solution of Laplace's equation (at least in rectangular situations, where the direction of \vec{B} is constant). The latter case, on the other hand, resembles boundary layer flow in that the current pattern distends downstream following the plasma flow,

and decouples from the flow in a thin region of current conduction (for which R_{me} is locally small). From Chap. 3, we see that, in our experimental situation, $R_{me} \approx 5$, where L_0 is based on the cathode length. Thus, as we indicated previously, we should expect significant but not overwhelming interaction between the current and plasma flow patterns. Near the cathode surface, L_0 is much smaller so that, with constant conductivity, the current flow lines should resemble electrostatic field lines, and enter the surface normally.

Solution of the Current Pattern

Because of the moderate value of R_{me} in our situation, we cannot simplify the differential equation governing the current pattern. Even with such approximations as negligible electron flow speed and uniform conductivity, this equation is still difficult to solve in our coaxial situation because the direction of \vec{B} varies along a magnetic field line. In rectangular geometry, where \vec{B} is unidirectional, the equation for the scalar conduction case is:

$$\nabla^2 \vec{B} = 0 = \nabla^2 B \quad (6-19)$$

which is just the Laplace equation. For a particular electrode geometry (specifying the boundary conditions on B), we may refer to known solutions²³ of the steady heat conduction equation ($\nabla^2 T = 0$) to obtain the appropriate isotherms, or in this case, constant enclosed current contours.

In our coaxial situation, where $\vec{B} = B\hat{e}$ and \vec{j} is in the plane normal to \vec{B} , we have:

$$\nabla^2 \vec{B} = \frac{\partial^2 B}{\partial r^2} + \frac{1}{r} \frac{\partial B}{\partial r} + \frac{\partial^2 B}{\partial z^2} - \frac{B}{r^2} = 0 \quad (6-20)$$

or

$$r^2 \frac{\partial^2 B}{\partial r^2} + r \frac{\partial B}{\partial r} + (r^2 \frac{\partial^2 B}{\partial z^2} - B) = 0 \quad (6-21)$$

Solution of this equation requires an expansion in terms of Bessel and hyperbolic trigonometric functions. We shall not pursue this here, since we are interested in the contours of constant enclosed current, not of constant B. (These are not equivalent in a coaxial situation.)

The current distribution in the coaxial case is obtained by noting that in the scalar situation \vec{j} is parallel to \vec{E} so the current flow lines follow the electrostatic field pattern. Equivalently, we see that if $\vec{j} = \sigma \vec{E}$ and $\sigma = \text{constant}$, then in steady state:

$$\nabla \times \vec{j} = 0 \quad (6-22)$$

so we may write

$$\vec{j} = \nabla \psi \quad (6-23)$$

Then, since $\nabla \cdot \vec{j} = 0$, we have:

$$\nabla^2 \psi = 0 \quad (6-24)$$

Again, we may utilize solutions from heat conduction theory. We now specify the flux at the boundaries, since the current pattern is equivalent to the heat flow distribution. We note that such solutions are not readily available because of the rather specialized geometry of MPD arcjets.

In the limit of high magnetic Reynolds number (R_{me}), our equation has the form of a heat conduction problem in high fluid mechanical Reynolds number (Rey) flow. This is not quite true in our situation because \vec{u}_e depends on \vec{j} and thus on the magnetic field distribution. That is:

$$\begin{aligned} \frac{1}{\sigma \mu_0} \nabla^2 \vec{B} &= (\vec{u}_e \cdot \nabla) \vec{B} = \left(\vec{u}_e - \frac{\vec{j}}{m_{ee}} \right) \cdot \nabla \vec{B} \\ &= \left[\left(\vec{u}_e - \frac{\nabla \times \vec{B}}{\mu_0 m_{ee}} \right) \cdot \nabla \right] \vec{B} \end{aligned} \quad (6-25)$$

where \vec{u}_i and $n_e (= n_i)$ are determined by the ion fluid mechanics and are, therefore, also related to the magnetic field pattern through the $\vec{j} \times \vec{B}$ force distribution.

If the relative motion of ions and electrons is negligible compared to the plasma flow, as would be the case in a low current, high density situation, the magnetic field pattern will be determined by the plasma flow, since

$$\vec{u}_e - \frac{\vec{j}}{me} \approx \vec{u}_i \quad (6-26)$$

Another special situation in which the true boundary layer equation obtains is rectangular geometry. In this case, $(\vec{j} \cdot \nabla) \vec{B}$ is zero. Lam²⁷ has obtained solutions, for R_{me} large, under these conditions, with the additional approximation of point electrodes. By analogy with heat conduction, the current pattern near electrodes of finite extent resembles the heat flow pattern near a body in high speed flow.

As we have indicated, the problem is more complicated in coaxial geometry ($B_e/m_e r$ is now constant along a streamline, rather than B_e/m_e). The main feature of interest is, however, that the current flow will be distended in the direction of the electron flow, but will enter and leave the electrodes as in the scalar situation. The thickness of these electrode boundary layers may be estimated, as before, by analogy with viscous boundary layer flow. If $\vec{u}_e \approx \vec{u}_i$ and the plasma flow is parallel to the electrode, then the conduction boundary layer thickness is:

$$\delta_E(x) \approx \frac{x}{\sqrt{R_{me}(x)}} \sim x^{1/2} \quad (6-27)$$

where x is measured along the electrode. If, however, $|\vec{u}_e| \gg |\vec{u}_i|$ then we must measure x along the current flow lines. In this case $\delta_E(x) \approx x$ so the extent of the conduction boundary

layer is given by $R_{me}(x) = 1$ or

$$\delta_E(x) = L_R = \frac{1}{\sigma_0 \mu_0 u_{e0}} \quad (6-28)$$

This result was used in Chap. 3 to assess the interaction of the current and plasma flows, and in Chap. 5 to show that in the cathode surface layer the current flows normal to the surface.

Meaning of R_{me}

We may manipulate the dimensionless group R_{me} to obtain some insight into its physical implications. We have:

$$\begin{aligned} R_{me} &= \sigma_0 \mu_0 u_{e0} L_0 \\ &= \frac{u_{e0} B_0}{\frac{\eta}{\mu_0} \frac{B_0}{L_0}} \cong \frac{u_{e0} B_0}{\eta j_0} \end{aligned} \quad (6-29)$$

where $\eta = 1/\sigma_0$ and $j_0 \approx \frac{1}{\mu_0} B_0/L_0$. From this we see that the electron magnetic Reynolds number reflects the relative importance of the induced electric field, due to electron motion in the magnetic field, to the resistive electric field component. This is not surprising in that R_{me} is a measure of the tensor versus scalar nature of current conduction. We may illuminate this further with a few more manipulations. If we write $j_0 = M_{ee} u_{e0}$, then

$$R_{me} = \frac{u_{e0} B_0}{\left(\frac{m_e v_c}{m_e e^2}\right) M_{ee} u_{e0}} = \frac{e B_0}{m_e v_c} = \Omega_e \quad (6-30)$$

That is, insofar as the current density is represented by the electron flow, the electron magnetic Reynolds number equals the electron Hall parameter. Thus, the microscopic and macroscopic

approaches to magnetic field interaction with the current flow pattern are directly connected.

The value of R_{me} (and Ω_e), which we have seen is an important parameter in determining the current pattern, may be related to the overall parameters of the discharge. We have from the first expression above:

$$\begin{aligned} R_{me} &= \sigma_0 \mu_0 u_{e0} L_0 = \sigma_0 \mu_0 u_P L_0 \left(\frac{u_{e0}}{u_P} \right) \\ &= R_m \left(\frac{u_{e0}}{u_P} \right) \end{aligned} \quad (6-31)$$

where R_m is the magnetic Reynolds number based on the plasma flow speed. Now, the electron flow speed includes both the electron motion with the plasma flow and motion across the flow in carrying current. That is, we may write approximately:

$$\frac{u_{e0}}{u_P} \cong \frac{(u_{e11}^2 + u_P^2)^{1/2}}{u_P} = \left[\left(\frac{u_{e11}}{u_P} \right)^2 + 1 \right]^{1/2} \quad (6-32)$$

where

$$u_{e11} \cong \frac{j}{m_e e} \cong \frac{J/A}{m_e e} \quad (6-33)$$

But,

$$\begin{aligned} u_P &\cong \frac{n_i/m}{\frac{m_e A}{\alpha}} \\ \frac{u_{e0}}{u_P} &\cong \left[\left(\frac{J/e}{\alpha n_i/m} \right)^2 + 1 \right]^{1/2} \end{aligned} \quad (6-34)$$

Then, the electron magnetic Reynolds number is:

$$R_{me} \cong R_m \left[\left(\frac{J/e}{\alpha n_i/m} \right)^2 + 1 \right]^{1/2} \quad (6-35)$$

From the overall momentum equation, in the high-current limit,

$$u_F \sim J^2 / m \quad (6-36)$$

so

$$R_{me} \sim \frac{J^2}{m} \left[\left(\frac{J/e}{\alpha n a / m} \right)^2 + 1 \right]^{1/2} \quad (6-37)$$

Thus, as we asserted previously, the high R_{me} limit is associated with high-current, low-density operation. Note that we have used the final speed of the plasma flow to obtain R_m .

Distortion of the Current Pattern by Plasma Convection

In a self-magnetic field plasma accelerator, the plasma flow speed is expected to increase greatly through the current distribution. Therefore, the magnetic Reynolds number at any point within the discharge will be less than the value computed from the final maximum plasma speed. The distortion of the current pattern from the scalar situation by plasma convection will thus occur to a lesser extent than would be indicated by the high terminal value of u_F .

We may see this most readily in a discharge flow between parallel-plate electrodes, separated by a distance D . The conduction boundary layer thickness associated with the trailing edge of the current distribution is

$$\delta = \frac{x}{\sqrt{R_m(u_F, x)}} \quad (6-38)$$

where $R_m(u_F, x)$ is the magnetic Reynolds number computed from the flow speed of the plasma after it has been accelerated through the entire discharge. The current pattern will be completed when the conduction boundary layers fill the interelectrode gap; that is, when $2\delta = D$. The streamwise distance at which this occurs is given by

$$\frac{D}{2} = \frac{L}{\sqrt{R_m(u_F, L)}} \quad (6-39)$$

We may use this distance, L , as the length of the current distribution, and thus as the distance over which the plasma flow is accelerated by the $\vec{j} \times \vec{B}$ force in the discharge. If we assume that the plasma accelerates from a negligible inlet speed to its final velocity in a linear fashion:

$$u(x) = u_F \left(\frac{x}{L} \right) \quad (6-40)$$

we may compute a magnetic Reynolds number characteristic of the overall discharge, in terms of the interelectrode separation. We have:

$$\bar{R}_m = \sigma \mu u D = \sigma \mu \frac{u_F D^2}{L} \quad (6-41)$$

but,

$$D^2 = \frac{4 L^2}{R_m(u_F, L)} = \frac{4 L^2}{\sigma \mu u_F L} \quad (6-42)$$

from the definition of L . So:

$$\bar{R}_m = 4 \quad (6-43)$$

By this order of magnitude approach, we see that the magnetic Reynolds number characteristic of self-field plasma accelerators should be rather moderate in value. The essential point here is that an overwhelming distortion of the current pattern by flow convection cannot occur in a self-field plasma accelerator because the flow is created by the current pattern.

Interaction of the Plasma Flow with the Current Pattern

We have previously considered the plasma motion to be one-dimensional. Actually, the two-dimensional current distribution will, in general, provide a two-dimensional plasma flow since ions will be accelerated in the $\vec{j} \times \vec{B}$ direction. As we

indicated in Chap. 4, an ion will contribute to current conduction only insofar as the direction of current flow is parallel to the motion achieved by the ion earlier in its dynamic history. We see from our one-dimensional approach, however, that higher flow speeds deflect the enclosed current contours further downstream. That is, further into the current distribution, the angle between the ion flow and the current flow (initially 90°) will tend to become smaller. Thus, in the cathode region, any component of ion velocity along a current line will be associated with motion away from the cathode, rather than in the direction of current flow. Offsetting this, is the acceleration of the ion normal to its initial path by the $\vec{j} \times \vec{B}$ force of the deflected current flow. Ion motion should therefore tend to be normal to the current flow lines, at least in the early stages of ion acceleration. We note that this situation prevails even in the scalar case since the cathode is convex and current lines will diverge.

Thus, the absence of significant ion current in our experiment does not seem unusual. Rather, these qualitative arguments suggest that it is characteristic of the cathode region of an MPD discharge. Asserting this, we may obtain the ion flow trajectory in the cathode region from the current pattern. We also may directly connect the ion kinetic energy to the voltage difference along its path, as in Chap. 4.

Physical Hierarchy of an MPD Discharge

We shall now unravel the interconnections of an MPD discharge by establishing a hierarchy of physical processes that govern arcjet operation. As in the experiment, we specify the total arc current, the input mass flow, and the accelerator geometry. The distribution of current within the arc chamber will be determined through Faraday's law for an MPD arcjet and will depend, as we have seen, on the conductivity and velocity of the plasma, and the electrode and insulator boundary conditions.

At high-current levels, our experience indicates that the ionization level will be above a few percent, so that the

plasma conductivity will depend largely on the electron temperature. We have also seen that the electron temperature will be limited by the rapid activation of inelastic cooling processes at higher electron temperatures. (In Chap. 3 we noted this in terms of an energy balance between ohmic heating and ionization cooling of the electrons within the discharge.) Thus, we expect the conductivity to be rather uniformly high throughout an MPD discharge, since the electron temperature will everywhere tend to its upper limit.

The current pattern would therefore resemble simple heat conduction were it not for the distortion resulting from plasma convection. The extent of such interaction depends on the magnetic Reynolds number. For a self-field plasma accelerator, we have seen that $R_m \sim 4$. The current pattern displacement by convection will, therefore, be rather moderate. The maximum distension of the enclosed current contours may be computed from the plasma exhaust velocity, estimated using the electromagnetic thrust equation with the specified current, mass flow, and geometry. In this way, the actual current distribution is bracketed by the scalar, low R_m , solution (obtained approximately by erecting normals to equipotential contours sketched around the electrodes) and the convective, high R_m , situation.

The ion motion within this current pattern is obtained from the associated $\vec{j} \times \vec{B}$ force distribution. With the inclusion of density and temperature gradients and collisional processes, the mechanics of the ion flow may be determined (that is, the three equations of the ion fluid, continuity, momentum, and energy may be solved given the body force distribution). The initial estimate of plasma flow velocity can then be corrected and the density distribution can be calculated. Iteration through the preceding steps to obtain the new current pattern and ion flow, and finally a self-consistent solution, occurs automatically in nature. We have merely indicated the physical processes involved.

Once the ion flow and density are determined, comparison

with the current flow pattern provides the electron flow velocity. Ion motion normal to the current prescribes the electron speed in that direction, while the electron contribution to current flow must complement that of the ions. The electric field within the plasma is then obtained from the generalized Ohm's law. That is, the $\vec{u}_e \times \vec{B}$ term may now be evaluated so that the electric field required to conduct current across a magnetic field in the presence of collisions ($\vec{\tau} \vec{j}$) and pressure gradients ($\frac{1}{m_e e} \nabla P_e = \frac{1}{m_i e} \nabla (m_i k T_e)$) is determined. Integration of this electric field, with the addition of the electrode falls, provides the total arc voltage.

We note that the arc voltage and the ion kinetic energy both derive from the current density distribution. Thus, there should be a correlation between them, but this need not be causal. We have seen, however, that in the cathode region of an MPD discharge significant ion current should not be expected and, therefore, the ion kinetic energy is directly related to the voltage difference along its path. This arises from the electromagnetic structure of the discharge which, in turn, derives from the electron momentum equation. The need to conduct current with electrons requires an electric field that exactly balances the $\vec{j} \times \vec{B}$ force attempting to deflect the electrons from the current flow path. This electric field then exerts a force on the ions equal to the $\vec{j} \times \vec{B}$ force in the discharge. This is the net force acting on the ions, neglecting pressure gradients and collisions with neutrals, since there is no current conduction in this direction. (In a scalar situation, the electric field arises to move electrons against the collisional drag of the ions; thus, the net force on the ions is zero). We note that if there is some ion motion along the current path away from the cathode, u_e must increase. The increased electric field normal to the current flow then provides the ions with a greater deflection in that direction, reducing the presumed ion motion.

In terms of the origin of the electric field within the plasma, we may consider that the convective zone of the cathode

region behaves like a Hall field accelerator. In the cathode surface layer the tensor character of current conduction is diminished (since n_e is greatly increased) so the electric field there reflects the back emf in an MGD channel accelerator. While, in the cathode jet and plume, we merely have the resistive field as in an electrothermal device. Thus, our MPD arcjet incorporates three basic types of electric thruster in different portions of the discharge.

CHAPTER 7

GENERAL CONSIDERATIONS

We shall now apply our understanding of discharge and flow processes to the overall operation and performance of an MPD arcjet. In particular, the relationships between various arcjet characteristics and their connection with the electromagnetic and mechanical structure of the discharge will be established.

Voltage-Current Relation in a Self-Field Plasma Thruster

With the addition of the electrode fall voltages, the total arc voltage is obtained from the line integral of the electric field in the plasma, along some contour between the anode and the cathode. The electric field within a plasma is, neglecting pressure gradients,

$$\vec{E} = \eta \vec{j} - \vec{u}_e \times \vec{B} = \eta \vec{j} - \vec{u} \times \vec{B} + \frac{\vec{j} \times \vec{B}}{m_e e} \quad (7-1)$$

$$(\vec{u} = \vec{u}_i = \frac{\vec{j}}{m_e e} + \vec{u}_e)$$

Integrating this along a current flow line between the electrodes, we have:

$$(V_{TOT} - V_F) = \int_{\text{ALONG } \vec{j}} \vec{E} \cdot d\vec{\ell} = \int_{\text{ALONG } \vec{j}} \eta j d\ell - \int_{\text{ALONG } \vec{j}} \vec{u} \times \vec{B} \cdot d\vec{\ell} \quad (7-2)$$

where V_F is the combined voltages of the electrode falls. From the previous chapter, we have that the ion motion will be essen-

tially normal to the current flow in most of the discharge, so $\vec{u} \times \vec{B} \cdot \vec{dl} = -uBdl$. We then have approximately,

$$(V_{TOT} - V_F) \approx \eta j L + u B L \quad (7-3)$$

where L is the characteristic length of the current path and η , j , u , and B are all quantities typical of the situation within the discharge and plasma flow.

Now, from the preceding chapter again, we have:

$$R_m = \sigma \mu u L \approx \frac{u B}{\eta j} \quad (7-4)$$

in the same manner as the electron magnetic Reynolds number. But we also found there that the magnetic Reynolds number characterizing a self-field plasma accelerator is a constant fixed by electrode geometry and plasma conductivity. Thus, we write

$R_m = \bar{R}_m$, so

$$u B \approx \eta j \bar{R}_m \quad (7-5)$$

Then the voltage across the plasma flow is:

$$(V_{TOT} - V_F) = \eta j L (1 + \bar{R}_m) \quad (7-6)$$

Now, we may express j in terms of the total arc current and geometry approximately as:

$$j \approx \frac{J}{A} \approx \frac{J}{2\pi R L} \quad (7-7)$$

where R is a radial distance about midway between the cathode and anode radii. We then have:

$$(V_{TOT} - V_F) = \frac{\eta}{2\pi R} (1 + \bar{R}_m) J \quad (7-8)$$

So we see that, if the electrode fall voltages remain relatively constant and/or small, the arc voltage increases linearly with current. We also note that the above relation defines the characteristic impedance of a self-field MPD arcjet. We have:

$$Z = \frac{(V_{\text{TOT}} - V_F)}{J} = \frac{\mathcal{Z}}{2\pi R} (1 + \bar{R}_m) \quad (7-9)$$

with $\mathcal{Z} = 1/\sigma \cong 2 \times 10^{-4} \text{ } \Omega\text{-m}$, $\bar{R}_m \approx 4$, and $R = 2.5 \times 10^{-2} \text{ m}$, we may compute Z for our experimental situation:

$$Z \approx 6.3 \text{ milliohms} \quad (7-10)$$

This number compares quite well with the value computed from the experimentally known voltage and current ($V_{\text{tot}} = 140 \text{ V}$, $V_{\text{CF}} = 38 \text{ V}$, $V_{\text{AF}} \sim 5 \text{ V}$, so $V_{\text{tot}} - V_F \approx 97 \text{ V}$, and $J = 17.5 \text{ kA}$):

$$Z = \left(\frac{V_{\text{tot}} - V_F}{J} \right)_{\text{experiment}} \approx 5.5 \text{ milliohms} \quad (7-11)$$

Such impedances are typical of MPD discharge operation at high currents.

Heavy-Particle Kinetic Energy

Again, using the condition that ions travel normal to the current flow lines, so that $j \approx j_e$, we compute the total work done on the heavy particles in the plasma by the $\vec{j} \times \vec{B}$ force:

$$\mathcal{E}_f = \int_{\hat{x}_L \parallel \vec{j} \times \vec{B}} \frac{\vec{j} \times \vec{B} \cdot d\vec{x}_L}{me} = \int \frac{\alpha j B dx_L}{m_e e} \approx \frac{\alpha j B}{m_e e} L_{\perp} \quad (7-12)$$

where $n = n_i + n_A$ so $n_e = \alpha n$, and L_{\perp} is the characteristic length of the acceleration path.

From the previous expression for the arc voltage, we have that the back emf is:

$$-\int_{\text{ALONG } \vec{j}} \vec{u} \times \vec{B} \cdot d\vec{l} = \int \frac{\vec{u} \cdot (\vec{j} \times \vec{B})}{j} dl = \int \frac{\alpha n \vec{u} \cdot (\vec{j} \times \vec{B})}{j/e \quad n_e e} dl \quad (7-13)$$

where we again note that \vec{u} is parallel to $\vec{j} \times \vec{B}$. Then, continuing our approximate analysis, we write:

$$\begin{aligned} \int \frac{\alpha n u j B}{j/e \quad n_e e} &\approx \left(\frac{n u}{j/e} \right) \frac{\alpha j B}{n_e e} L_{\parallel} \\ &\approx u B L \end{aligned} \quad (7-14)$$

from the previous form of the back emf integral. ($L \rightarrow L_{\parallel}$ in association with L_{\perp}). Thus, we have:

$$\mathcal{E}_f \approx \left(\frac{j/e}{n u} \right) \left(\frac{L_{\perp}}{L_{\parallel}} \right) u B L \quad (7-15)$$

Now, $j/e \approx [(J/e)/(2\pi R L_{\perp})]$ and $\dot{m}/m \approx nu(2\pi R L_{\parallel})$, where we use the lateral surface area of a truncated cone of mean radius R , and slope length L_{\perp} and L_{\parallel} , respectively. So

$$\mathcal{E}_f \approx \left(\frac{J/e}{\dot{m}/m} \right) u B L \quad (7-16)$$

But we have already seen that $u B L \approx \bar{R}_m \gamma j L \approx \frac{(V_{\text{TOT}} - V_F) \bar{R}_m}{1 + \bar{R}_m}$. We, therefore, obtain a relationship between the final heavy-particle energy and the voltage drop across the plasma:

$$\mathcal{E}_f = \left(\frac{J/e}{\dot{m}/m} \right) \left(\frac{\bar{R}_m}{1 + \bar{R}_m} \right) (V_{\text{TOT}} - V_F) \quad (7-17)$$

We see that, with $[(J/e)/(\dot{m}/m)] \sim 1$, heavy-particle energies in the arcjet exhaust should be comparable to the arc voltage. We note that electrothermal contributions to the plasma kinetic energy have not been included. A major portion of this input occurs near the cathode surface and is associated with the cathode fall voltage. Thus, we may be able to add a fraction of this voltage to the plasma kinetic energy, bringing \mathcal{E}_f closer to the total arc voltage. We consider this possibility in a later section.

MPD Arcjet Exhaust Velocity

We may relate the final kinetic energy of the heavy particles to the exhaust velocity of the arcjet as:

$$\frac{1}{2} \frac{m_i u_f^2}{e} = \mathcal{E}_f \quad (7-18)$$

From the electromagnetic thrust equation we have in the high-current limit (where we neglect gasdynamic contributions):

$$\dot{m} u_f = \frac{\mu_0 J^2}{4\pi} \left[\ln(r_A/r_c) + 3/4 \right] \quad (7-19)$$

so,

$$\frac{1}{2} \left[\frac{\mu_0}{4\pi} \left(\ln(r_A/r_c) + 3/4 \right) \right]^2 \frac{m_i J^4}{e \dot{m}^2} = \left(\frac{J/e}{\dot{m}/m} \right) \frac{\bar{R}_m}{1 + \bar{R}_m} (V_{TOT} - V_F) \quad (7-20)$$

But,

$$(V_{TOT} - V_F) = \left(\frac{\eta}{2\pi R} \right) (1 + \bar{R}_m) J \quad (7-21)$$

so

$$\frac{1}{2} \left[\frac{\mu_0}{4\pi} \left[\ln(r_A/r_c) + 3/4 \right] \right]^2 \frac{J^4}{\dot{m}^2} = \frac{J^2}{\dot{m}} \frac{\eta \bar{R}_m}{2\pi R} \quad (7-22)$$

Thus, we see that in a self-field plasma thruster J^2/\dot{m} is a constant depending only on geometry and plasma conductivity:

$$\frac{J^2}{\dot{m}} = \frac{\bar{\eta} \bar{R}_m}{\pi R} \left[\frac{\mu_0}{4\pi} \left(\ln v_A/v_c + 3/4 \right) \right]^{-2} \quad (7-23)$$

This indicates that the exhaust velocity of an MPD arcjet should become constant as the current level is increased and/or the mass flow rate is decreased, insofar as the gasdynamic and electrothermal contributions to performance may be neglected in this limit. Experimental observations in several MPD arcjets confirm this result. (We note that u_f is proportional to Z , the characteristic impedance of the arcjet which is also rather constant for different experiments.)

In our own case, $v_A/v_c \approx 5.6$, $R = 2.5 \times 10^{-2}$ m, $\bar{\eta} \approx 2 \times 10^{-4}$, and $\bar{R}_m \approx 4$, so

$$\frac{J^2}{\dot{m}} = 1.6 \times 10^{11} \left[\frac{A^2 - SEC}{Kg} \right] \quad (7-24)$$

Also, in this particular case $J = 17.5$ kA and $\dot{m} = 5.5 \times 10^{-3}$ kg/s, for which $J^2/\dot{m} = 5.6 \times 10^{10}$. These results are in fair quantitative agreement, considering the approximate nature of the analysis and our rather rough estimate of \bar{R}_m .

Electromagnetic Thrust Efficiency of a Self-Field MPD Arcjet

We may define the thrust efficiency of the electromagnetic acceleration process in a self-field MPD arcjet as:

$$\epsilon_{EM} = \frac{1/2 \dot{m} u_f^2}{(V_{TOT} - V_F) J} = \frac{1/2 m u_f^2 / e}{(V_{TOT} - V_F)} \left(\frac{\dot{m}/m}{J/e} \right) \quad (7-25)$$

where u_f is computed from the electromagnetic thrust equation.
But

$$\frac{1}{2} m u_f^2 / e = E_f = \left(\frac{J/e}{m/m} \right) \frac{\bar{R}_m}{1 + \bar{R}_m} (V_{TOT} - V_F) \quad (7-26)$$

so

$$\epsilon_{EM} = \frac{\bar{R}_m}{1 + \bar{R}_m} \quad (7-27)$$

We see that this efficiency is also a constant determined by the geometry of the accelerator. The relationship to \bar{R}_m is rather natural, since \bar{R}_m is the ratio of energy associated with motion in the magnetic field to energy dissipated by conduction in a resistive plasma.

\bar{R}_m Revisited

Having seen that arcjet performance depends primarily on \bar{R}_m , we return to the discussion of the previous chapter to examine more closely the influence of accelerator geometry on this factor. We again work with the simpler rectangular situation. The essential construction is that the current conduction pattern is completed when the conduction boundary layers of the electrodes overlap. In particular, the last element of the current flow, connecting the trailing edges of the electrodes, must diffuse across the fully accelerated plasma flow. By analogy with viscous boundary layer flow, the penetration of this current into the plasma flow is given by:

$$\delta(x - x_0) = \frac{x - x_0}{\sqrt{\bar{R}_m(x - x_0; u_f)}} \quad (7-28)$$

where x_0 is the streamwise position of the trailing edge of the electrode. Thus, if D is the interelectrode separation,

the current pattern is completed when

$$D = \delta_c (L - x_c) + \delta_A (L - x_A) \quad (7-29)$$

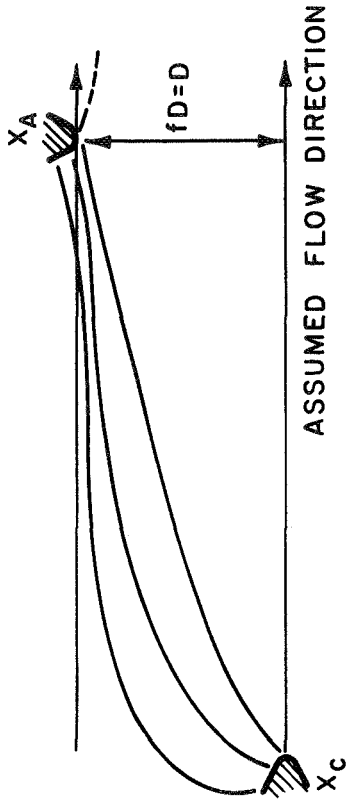
where L defines the streamwise distension of the current pattern, and the subscripts refer to the cathode and anode, respectively.

If the intersection occurs a distance fD into the flow from one electrode, then the magnetic Reynolds number may be obtained as previously and equals:

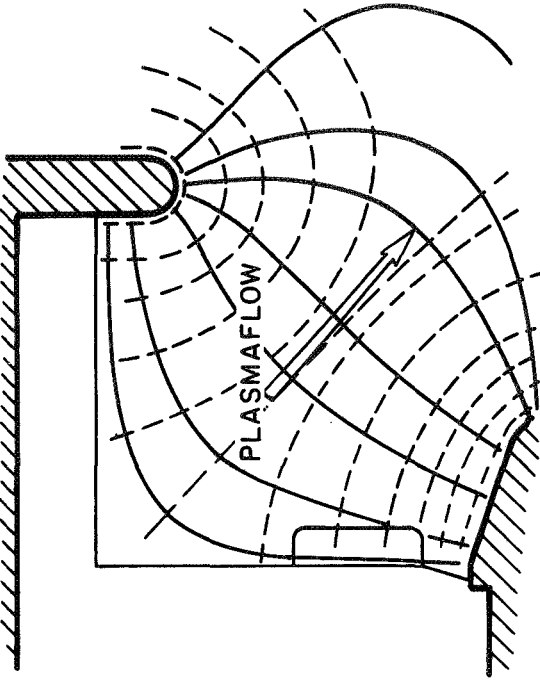
$$\overline{R}_m = \frac{1}{f^2} \quad (7-30)$$

where we have again assumed a linear velocity profile, $u(x) = u_f x/L$, through the discharge (appropriate to a diffuse current distribution).

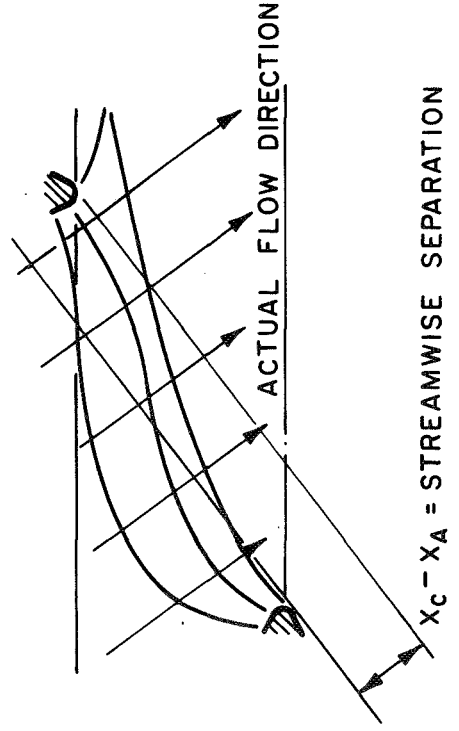
The limitations on f are determined schematically in Fig. 7-1. If we assume a one-dimensional plasma flow, parallel to the boundaries as shown, then we may use the analogy with viscous flow over a flat plate to sketch the growth of the conduction boundary layers. For $x_A - x_C = 0$, Fig. 7-1a, the boundary layers intersect in the middle of the flow; while at some point $(x_A - x_C) > 0$, Fig. 7-1b, one layer completes the current pattern before the other develops. Thus, we find $\frac{1}{2} \leq f \leq 1$. We observe, however, that since the plasma flow and current flow should tend to be orthogonal, the assumption of a one-dimensional flow fails badly for $x_A - x_C > 0$. In Fig. 7-1c, we note that the net result of this coupling is to rotate our assumed streamwise direction so as to reduce the effective value of $(x_A - x_C)$. The actual direction of the flow may be estimated from the current pattern of the scalar situation, since ions will be accelerated normal to the current streamlines. Simple sketches, such as Fig. 7-1d, suggest that the effective value of $(x_A - x_C)$ is never large compared to the electrode separation (normal to the flow). Thus, the influence of geometry on the value of \overline{R}_m is rather weak, and $\overline{R}_m \approx 4$ should be typical of



a) $f = 1/2$



b) $f = 1$



c) $f = 1/2$

d) SKETCH OF CURRENT PATTERN SCALAR SITUATION

CURRENT PATTERNS IN SELF-FIELD PLASMA THRUSTERS

FIGURE 7-1

steady, self-field plasma thrusters. (The situation is essentially this: In an MPD arcjet a high speed flow normal to the current pattern is created by the $\vec{j} \times \vec{B}$ force. Since the flow is initially low speed, the direction of this flow, defined by the direction of current flow, is determined approximately from the scalar ($R_m \rightarrow 0$) limit. In a scalar situation, the average direction of current flow is about parallel to the line of minimum distance between the electrodes. If the plasma flow is normal to this line, the streamwise electrode separation will be small compared to the minimum electrode gap.)

Electrothermal Contributions to MPD Arcjet Performance

The primary complication in evaluating the electrothermal processes in an MPD arcjet is due to the nonequilibrium nature of the plasma flow. In Chap. 3 we indicated that the plasma flow continues to ionize through the arc chamber so that even a two-temperature formulation of the state of the plasma is inadequate (except, perhaps, in the high density layer at the cathode surface). It was also noted that the electron temperature remains rather uniform throughout the arcjet and exhaust plume because of cooling due to inelastic collisions with ions and atoms. That is, the energy received by the electrons from the electric field (ohmic heating) or from collisions with higher temperature ions in the cathode surface layer, jet, and plume is lost to the activation and population of excited states of the atoms and ions. Since such inelastic processes are much more efficient in transferring energy from the electrons to heavy particles than elastic encounters, the major effect of ohmic heating in an MPD arcjet is the creation of an ionized gas of high electrical conductivity and large specific heat. The first property limits the energy dissipated by conduction through the plasma. The second result allows the heat generated within the discharge to be absorbed into the working fluid, thereby permitting operation at rather moderate temperatures.

In the cathode surface layer, the situation resembles that behind a strong shock wave in an ionized gas. The heavy-

particle temperature increases greatly from its initial value as does the particle density. Heavy particles then heat the electrons which, in turn, ionize and excite the gas. Only a small increase in electron temperature is needed to increase vastly the rate of inelastic cooling. The electron fluid acts as a heat conductor between the high (kinetic) temperature heavy particles and the low-temperature reservoir formed by their excited states. (Note that "temperature" is ill-defined in this situation and is used here in analogy with more familiar equilibrium concepts.) Thus, the heat generated in the cathode surface layer, by the heavy-particle collisions associated with flow deflection and by electronic acceleration and collision processes in the cathode fall, is lost to ionization and excitation of the plasma flow. Measurements of ion and electron temperature in the exhaust plume (Chap. 2) indicate that the nonequilibrium character of the flow persists far downstream of the arc chamber suggesting that this heat energy is never recovered. It appears, therefore, that the same inelastic processes, permitting the cathode region to operate at moderate heavy-particle temperatures, are associated with the frozen flow loss of electrothermal contributions to thruster performance.

Losses at the Cathode

The cathode fall voltage represents the cost of conducting current across the cathode-plasma interface. From Chap. 5 we have that the heat generated near the cathode surface is:

$$q_c + q_p = j(V_{cF} - \phi_w) \quad (7-31)$$

As indicated in the previous section, this heat does not contribute to the acceleration processes of the arc. Furthermore, the energy involved in removing electrons from the cathode, $j\phi_w$, is later deposited in the anode as heat, so that this term also represents a loss of energy from the system.

Thus, we may consider the ratio V_{CF}/V_{tot} as a measure of arc-jet inefficiency associated with the cathode conduction process.

Again, from Chap. 5, we obtain that the cathode fall voltage is:

$$V_{CF} = \frac{q_c(\tau_w, t) + j\phi_w}{\frac{n_c m_i u_c^2}{R T_e / e} \left(\frac{R T_w}{2\pi m_i} \right)^{1/2}} - \epsilon_i \quad (7-32)$$

where $n_c m_i u_c^2 / k T_e = n_w$ the particle density at the edge of the emission layer.

Regardless of the heat transfer to the cathode (on the surface temperature), we see that V_{CF} is inversely proportional to n_w . This is because the required energy transfer to the surface by ion bombardment may be obtained with a lower voltage, if more particles are involved; the conduction process becomes more efficient.

Thus, to achieve better arcjet performance, we should operate with high particle densities at the cathode surface. Since the value of the electron temperature is determined by a balance between acceleration in the cathode fall and inelastic cooling, this requires high pressures at the cathode. Such a condition may be obtained by increasing the arc current since $n_c m_i u_c^2$ is proportional to the electromagnetic thrust of the arcjet ($\sim J^2$), and/or by increasing the mass flow rate to the cathode surface (this may be accomplished by altering the accelerator geometry so that the current pattern provides ion acceleration paths that intercept a larger portion of the input mass flow). In the first approach, arcjet performance improves because the total arc voltage increases while the cathode fall voltage is diminished. Application of the second approach requires a design trade-off between energy losses associated with the cathode fall and those involved in flow deflection.

Review and Concluding Discussion

We have applied our understanding of the electromagnetic and mechanical structure of an MPD discharge in the cathode region to obtain relationships between arcjet properties. The three principal elements of this structure are that (a) in an MPD discharge electron current predominates so that the current and plasma flows are orthogonal. (b) Conduction of current by electrons in the presence of a strong magnetic field requires a component of electric field normal to the current flow to balance the Lorentz force on the electrons; this electric field then transmits the $\vec{j} \times \vec{B}$ force in the discharge to the heavy particles of the plasma. (c) The resulting plasma flow provides a back emf which distorts the current pattern, causing it to distend downstream, since the plasma flow is created by current conduction the back emf cannot everywhere dominate the conduction process so in steady, self-field plasma accelerators interaction of the flow with the current pattern must be moderate ($\bar{R}_m \sim 4$). Analysis of the experimentally determined distributions of electric and magnetic field and current density led us to the first two results. All three were established on more fundamental foundations in the previous chapter.

Recognizing that the back emf and resistive voltage drop must be commensurate by (c), we found that the voltage across the plasma is proportional to the arc current:

$$(V_{TOR} - V_F) = Z J \quad (7-33)$$

where the effective impedance:

$$Z \cong \frac{Z}{2\pi R} (1 + \bar{R}_m) \quad (7-34)$$

is determined by plasma resistivity and accelerator geometry. From (a) and (b) we have that the kinetic energy of a heavy particle in the exhaust flow is:

$$\epsilon_f = \frac{1}{2} m u_f^2 \approx \left(\frac{J/e}{m/m} \right) \frac{\bar{R}_m}{1 + \bar{R}_m} (V_{TOR} - V_F) \quad (7-35)$$

so that energies comparable to the arc voltage should be obtained. This relation also provides the electromagnetic efficiency of the arcjet:

$$\epsilon_{EM} = \frac{\bar{R}_m}{1 + \bar{R}_m} \quad (7-36)$$

which reflects (c) in that current conduction, with the associated dissipation of energy, is necessary to obtain the plasma flow from an MPD arcjet.

Furthermore, we have that the final kinetic energy \mathcal{E}_f is proportional to J^2/\dot{m} . But, since it is also proportional to $(J^2/\dot{m})^2$ through u_f , in the high-current, low mass flow limit we find that:

$$\frac{J^2}{\dot{m}} \approx \frac{\gamma \bar{R}_m}{\pi R} \left[\frac{\mu_0}{4\pi} \left(l_w r_A/r_c + 3/4 \right) \right]^{-2} \quad (7-37)$$

$\propto u_f$

so u_f is determined by geometry and plasma resistivity.

All this has been achieved by approximating the actual structural details of the discharge flow with mean quantities and characteristic distances. We have essentially linearized the MPD situation, depositing all the inherent nonlinearity and coupling in the overall structural parameter, \bar{R}_m . Having argued that the magnetic Reynolds number which characterizes the interaction between the plasma and current flows is relatively independent of the arcjet inputs J and \dot{m} , relationships involving changes in properties with J and \dot{m} were obtained. By the details of this argument, we are limited to the high current, low mass flow situation for which gasdynamic contributions to plasma acceleration can be neglected and where the magnetic Reynolds number based on the exhaust velocity is large ($\sigma \mu u_f R > 4$).

We have also assumed that γ could be treated as a parameter determined by processes independent of the discharge flow interaction. In this case, specification of γ prescribes

the ratio J^2/\dot{m} . If we supply a certain current level, then the mass flow required will be obtained either from the input gas or by ablation of insulator and electrode material. (Note that the overfed situation will not be accessible to our analysis if $\sigma \mu u \rightarrow R$ becomes small.) Additional mass flow from ablation may not be readily available to the arc if the proper insulator and electrode materials are used. We then have that J^2/\dot{m} determines ζ . That is, if the proper level of mass flow cannot be supplied by gas input or ablation, the plasma resistivity is coupled to the discharge flow situation. If the mass flow is sufficient, however, ζ will depend on other aspects of arc operation. We note that if J^2 is given and \dot{m} is lower than required with ζ determined by these latter processes, the plasma resistivity will increase. This results in greater heating in the arc chamber (and higher temperatures since fewer particles are involved), so that the possibility of ablation is enhanced. Recalling our expression for the arc-jet impedance, we see that impedance (and therefore voltage at a given current level) should increase inversely with mass flow rate below the mass flow required with ζ otherwise determined.

The prescription of ζ by arc processes is intimately coupled to the determination of the ionization level. Higher ionization levels provide lower resistivities until near $\alpha = 1$, the production of multiply-charged ions causes the resistivity to increase (assuming that the electron temperature remains limited by these and other inelastic processes). From our analysis, we may obtain an expression for α . We have:

$$\left(\frac{\mu u}{j/e}\right) \frac{\alpha jB}{m_e e} L_{11} \approx uBL \quad (7-38)$$

so that:

$$\alpha \approx \left(\frac{J/e}{\dot{m}/m}\right) \frac{uB}{jB/m_e e} \approx \left(\frac{J/e}{\dot{m}/m}\right) \frac{R_m}{R_e} \quad (7-39)$$

But from Chap. 6 we have:

$$\Omega_e \approx R_{me} \approx R_m \left[\frac{1}{\alpha^2} \left(\frac{J/e}{\dot{m}/m} \right)^2 + 1 \right]^{1/2} \quad (7-40)$$

so

$$\alpha \approx \frac{(J/e / \dot{m}/m)}{\left[\left(\frac{J/e}{\alpha \dot{m}/m} \right)^2 + 1 \right]^{1/2}} \quad (7-41)$$

Thus, if we fix the current level and lower the particle flow rate, we obtain higher ionization levels and higher conductivities. The velocity of the plasma flow also increases so that we attain the high-current, low mass flow operation in which the electromagnetic contribution to the arcjet thrust dominates and to which the results of our approximate analysis apply. Above an ionization level of a few percent, ζ will be about constant, decreasing only slightly with higher α (insofar as T_e is about constant). As we go to still lower particle flow rates, $\alpha \rightarrow 1$, in which case we expect multiple ionization to be important so that ζ will increase. Thus, we may associate the situation wherein ζ is independent of J^2/\dot{m} with $[(J/e)/(\dot{m}/m)] \leq 1$; while the case of ζ increasing with lower mass flow rate obtains for $[(J/e)/(\dot{m}/m)] > 1$. The critical particle flow rate is thus given by $[(J/e)/(\dot{m}/m)] = 1$. We note that at this condition the arc operates with about the minimum resistivity, so that heat dissipation (and thus entropy production) occurs at the minimum rate.

We expect that there will be two classes of MPD arcjet: ablative and nonablative. In the first, lower mass flow rates will be compensated by higher ablation rates so that the plasma resistivity, arc impedance, and arcjet exhaust velocity will all attain constant values at high-current, low mass flow conditions. The particle flow rate required is given by:

$$\dot{m} \geq J/e \quad (7-42)$$

while the mass flow rate will be proportional to the square of the current:

$$\dot{m} = \dot{m}_{\text{INPUT}} + \dot{m}_{\text{ABLATED}} \propto J^2 \quad (7-43)$$

We note that insulators, such as Plexiglas used in our experiment, can significantly contribute to the particle flow rate without affecting the mass flow appreciably (see Chap. 2 on insulator erosion).

In the second case of an ideal, nonablative thruster, the plasma resistivity, arc impedance, and arcjet exhaust velocity all increase inversely with mass flow for high-current, low mass flow operation. Higher heavy-particle temperatures and multiple ionization should be observed here at low mass flow rates.

In neither case will electrothermal effects contribute to arcjet performance because of the high effective specific heat of an ionizing gas. As we have indicated, however, this nonequilibrium situation allows operation at moderate temperatures (\leq few eV). In particular, the heat generated near the cathode surface can be absorbed by internal states of the plasma and carried away by the surface flow. This convective heat transfer process is assisted by the strong $\vec{j} \times \vec{B}$ force parallel to the surface which accelerates the flow to hypersonic Mach numbers. We note that if such acceleration occurs further out in the discharge, the mass flow to the cathode surface would be less and higher cathode falls would be needed to maintain the cathode conduction process. Protection of the cathode surface by a high density, low (heavy-particle) temperature plasma would also be less efficient. This situation would obtain in the case of little magnetic interaction in the convective zone, since the current pattern would then resemble the scalar solution, with $\vec{j} \times \vec{B}$ there directed parallel, rather than toward, the cathode surface. Thus, cathode operation and survivability improve with high plasma conductivity and flow speed in the cathode region, such conditions provided by appropriate particle and mass flows at high-current levels.

The results of our analytical formulation await confirmation by experiments currently in progress. Preliminary evidence²⁸ indicates that the arcjet exhaust velocity increases linearly with decreasing input mass flow rate until $[(J/e)/(\dot{m}/m)] \approx 1$, after which it remains constant. In terms of our discussion, this suggests that insulator ablation becomes important when the input mass flow is fully ionized by the arc. Since the back emf and the resistive voltage drop across the plasma flow must be commensurate, lower input mass flow rates and higher exhaust speeds predicate greater heating in the arc chamber, thereby providing the mechanism for mass addition by insulator and/or electrode ablation. Any effort to compare arcjet impedance, exhaust velocity, and mass flow rate over a range of operating conditions must include an accurate appraisal of the ablated mass and particle flow rates and the influence of ablated material on the mechanical, chemical, and thermodynamic properties of the plasma.

REFERENCES

- ¹Noeske, H. O., "The Coaxial MPD Engine, A State-of-the Art Review," AIAA Paper 66-242 (1966).
- ²Nerheim, N. M. and Kelly, A. J., "A Critical Review of the State-of-the-Art of the MPD Thrustor," AIAA Paper 67-688 (1967).
- ³Clark, K. E. and Jahn, R. G., "The Magnetoplasmadynamic Arc-jet," *Astronautica Acta* 13, 315-325 (1967).
- ⁴Jahn, R. G., Physics of Electric Propulsion, McGraw-Hill Book Company, New York, 1968, Chap. 8.
- ⁵Clark, K. E., "Quasi-Steady Plasma Acceleration," Ph.D. Thesis, Dept. of Aerospace and Mechanical Sciences, Rept. No. 859, May 1969, Princeton Univ., Princeton, N. J.
- ⁶Stratton, T. F., "High-Current Steady-State Coaxial Plasma Accelerators," *AIAA J.* 3, 1961-1963 (1965).
- ⁷Jahn, R. G., "An Electron's View of the MPD Arcjet," Giannini Scientific Corp. Technical Rept. 5QS085-968 (Aug. 1965).
- ⁸Malliaris, A. C. and Libby, D. R., "Velocities of Neutral and Ionic Species in an MPD Flow," AIAA Paper 69-109 (1969).
- ⁹Kogelschatz, U., "Doppler-Shift Measurements of Axial and Rotational Velocities in an MPD Arc," *AIAA J.* 8, 150-154 (1970).
- ¹⁰Clark, K. E., DiCapua, M. S., Jahn, R. G., and Von Jaskowsky, W. F., "Quasi-Steady Magnetoplasmadynamic Arc Characteristics," AIAA Paper 70-1095 (1970).
- ¹¹Von Jaskowsky, W. F., private communication.
- ¹²Chen, F. F., "Electric Probes," Chap. 4 in Plasma Diagnostic Techniques, Huddleston, R. H. and Leonard, S. L. (Eds.), Academic Press, New York, 1965.
- ¹³Kirchhoff, R. H., Peterson, E. W. and Talbot, L., "An Experimental Study of the Cylindrical Langmuir Probe Response in the Transition Regime," AIAA Paper 70-85 (1970).
- ¹⁴Jahn, R. G., Clark, K. E., Oberth, R. C., and Turchi, P. J., "Acceleration Patterns in Quasi-Steady MPD Arcs," AIAA Paper 70-165 (1970).
- ¹⁵Burton, R. L., "Structure of the Current Sheet in a Pinch Discharge," Ph.D. Thesis, Dept. of Aerospace and Mechanical Sciences, Rept. No. 783, Princeton Univ., Princeton, N. J., p. A-9.

REFERENCES

- 16 Spitzer, Jr., L., Physics of Fully Ionized Gases, Interscience Publishers, New York, 1962, Chap. 5.
- 17 Nighan, W. L., "Electrical Conductivity of Partially Ionized Noble Gases," Phys. Fluids 12, 1, 162-171 (1969).
- 18 Cann, G. L. and Ducati, A. C., Argon Mollier Chart, Plasma-dyne Rept. PLR-55 AFOSR TN 59-247, Feb. 1959.
- 19 Schaaf, S. A. and Chambré, P. L., Flow of Rarefied Gases, Princeton Univ. Press, Princeton, N. J., 1961, Chap. 1.
- 20 McCarthy, Jr., J. F. and Kubota, T., "A Study of Wakes Behind a Circular Cylinder at $M = 5.7$," AIAA J. 2, 4, 629-636 (1964).
- 21 Reeves, B. L. and Lees, L., "Theory of Laminar Near Wakes of Blunt Bodies in Hypersonic Flow," AIAA J. 3, 11, 2061-2074 (1965).
- 22 Cobine, J. D., Gaseous Conductors, Dover Publications, New York, 1958, Chap. IX.
- 23 Carslaw, H. S. and Jaeger, J. C., Conduction of Heat in Solids, Oxford Clarendon Press, 1959.
- 24 Ecker, G., "Electrode Components of the Arc Discharge," Ergebnisse der exakten Naturwissenschaften, Vol. 33, Springer-Verlag, 1961.
- 25 Aisenberg, S., Hu, P., Rohatgi, V., and Ziering, S., "Plasma Boundary Interactions," Space Sciences, Inc., NASA CR-868 (1967).
- 26 Lee, T. H., Greenwood, A., Breingan, W. D., Fullerton, H. P., "An Analytical Study of the Physical Processes in the Cathode Region of an Arc," General Electric Co., OAR Rept. ARL 66-0065 (1966).
- 27 Lam, S. H., private communication.
- 28 Jahn, R. G., Clark, K. E., Oberth, R. C., and Turchi, P. J., "Acceleration Patterns in Quasi-Steady MPD Arcs," AIAA J. (to be published).